Fall 12-2020

In the Margins: Reconsidering the Range and Contribution of Diazotrophs in Nearshore Environments

Corday R. Selden
Old Dominion University, crselden@gmail.com

IN THE MARGINS:
RECONSIDERING THE RANGE AND CONTRIBUTION OF MARINE DIAZOTROPHS IN NEARSHORE ENVIRONMENTS

by

Corday R. Selden
B.S., 2014, Eckerd College
M.S., 2017, Old Dominion University

A Dissertation Submitted to the Faculty of
Old Dominion University in Partial Fulfillment of the
Requirements for the Degree of

DOCTOR OF PHILOSOPHY

OCEANOGRAPHY

OLD DOMINION UNIVERSITY
December 2020

Approved by:

Margaret R. Mulholland (Co-Director)

P. Dreux Chappell (Co-Director)

Angela Knapp (Member)

John Whiteman (Member)

ABSTRACT

IN THE MARGINS:
RECONSIDERING THE RANGE AND CONTRIBUTION OF MARINE DIAZOTROPHS IN NEARSHORE ENVIRONMENTS

Corday R. Selden
Old Dominion University, 2020
Co-Directors: Drs. Margaret R. Mulholland and P. Dreux Chappell

Dinitrogen (N_2) fixation enables primary production and, consequently, carbon dioxide drawdown in nitrogen (N) limited marine systems, exerting a powerful influence over the coupled carbon and N cycles. Our understanding of the environmental factors regulating its distribution and magnitude are largely based on the range and sensitivity of one genus, *Trichodesmium*. However, recent work suggests that the niche preferences of distinct diazotrophic (N_2 fixing) clades differ due to their metabolic and ecological diversity, hampering efforts to close the N budget and model N_2 fixation accurately. Here, I explore the range of N_2 fixation across physico-chemical gradients (e.g., light, nutrients, oxygen) in nearshore environments of significance in global biogeochemical cycling: the major pelagic oxygen deficient zones (ODZs) in the Eastern Tropical South (ETSP) and North (ETNP) Pacific Ocean, and the broad continental shelf of the Western North Atlantic Ocean (WNA). The ODZs are hypothesized to play an important role in N cycle homeostasis by generating conditions thought to promote diazotrophy; recent work suggests that broad continental shelf environments may contribute substantially to new reactive N inputs globally. N_2 fixation rates were measured using a robust ^{15}N tracer method that accounts for the slow dissolution of N_2 gas. To explore niche partitioning and better characterize spatial heterogeneity on the WNA shelf, I built an empirical model of N_2 fixation and investigated diazotroph identity using amplicon sequencing and qPCR. In the ETSP, N_2 fixation was only detected in a subset of low-oxygen samples. N_2 fixation within the ETNP ODZ was patchy and

driven by organic carbon availability; however, significant rates were observed at coastal stations near the Gulf of California. Frontal mixing on the WNA shelf resulted in exceptionally high rates of N_2 fixation, associated with high UCYN-A activity. My findings suggest that (1) diazotrophy is more energetically favorable (relative to dissolved inorganic N) in low-oxygen waters but may be carbon-limited, and (2) continental inputs and dynamic conditions at coastal margins can favor significant N inputs via diazotrophy.

An edited version of Chapter III was submitted for publication in *Limnology and Oceanography*, August 3 2020.

An edited version of Chapter IV was submitted for publication in *Limnology and Oceanography*, August 17 2020.

This dissertation is dedicated to my partner, Alfonso, my calm in the storm, and to my family, who inspired and supported my development as a scientist.

ACKNOWLEDGMENTS

I am profoundly grateful for the guidance and support that I have received during my tenure as a graduate student. I thank my advisors and committee for their intellectual and financial support. I thank Margie Mulholland for inspiring me with her enduring enthusiasm, Dreux Chappell for grounding me with her pragmatism, Angie Knapp for her sound judgment, and John Whiteman for offering an external perspective. I consider myself deeply fortunate to have had many strong role models, mentors, and teachers along my way. In addition to my advisors, these include Brittany Widner, whose footsteps have guided me, Greg Cutter, whose counsel has helped me shape my own path, Sophie Clayton, who showed me how to be an awesome hacker, Fred Dobbs, whose prowess at scientific communication I aim to emulate, and Alexander Bochdansky, who taught me to teach and offered me the space to practice. I am thankful for the support that I have received from my community at ODU over the years, including from the faculty who leave their doors ajar, the unflappable administrators who work tirelessly to make everything run smoothly, and the graduate students with whom I've learned, grown and weathered the trials of graduate life.

While many hands helped to build the presented work, I would like to express my particular gratitude to Pete Bernhardt for greasing the gears. None of the work presented here would have been possible without his strong stomach at sea and deft skills in mass spectrometry. Many members of the Mulholland and Chappell labs participated in the production of the datasets presented here, including Brittany Widner, who facilitated sample collection and analysis on all cruises. I thank Kim Powell for offering her expertise and aid in sequencing, and Zuzanna Abdala and Katherine Crider for their respective roles in collecting, processing and analyzing samples for diazotroph quantification presented in Chapter IV. I also thank David Shelley, Chanel Flores-

Vargas and the other wonderful undergraduates who have come through the Mulholland lab for assisting with processing particulate nitrogen samples, and making the lab run smoothly. For their role in the machine learning aspects of this study, I thank Sophie Clayton, whose instruction enabled its execution, and Alfonso Macías-Tapia, Denni Einarsson, Michael Echevarria, and Austin Abbott for offering their perspectives.

I thank the captains and crews of the *R/V Atlantis,* the NOAA vessel *Ronald H. Brown* and the *R/V Hugh R. Sharp* for enabling the field work in the Eastern Tropical South Pacific (ETSP), Eastern Tropical North Pacific (ETNP), and Western North Atlantic, respectively, as well as the scientists who participated in sample collection and analysis on these cruises—particularly Shannon Cofield, Steve Stone, Wei Yan, Nicole Travis and Matt Forbes. I thank Amal Jayakumar and Bonnie Chang their role in planning and executing the Pacific cruises, Bess Ward for the use of her facilities, and Bonnie Chang, Qixing Ji and Alfonso Macías-Tapia for analyzing $^{15}N_2$ samples. Additionally, I would like to thank Osvaldo Ulloa and Gadiel Alarcón, respectively, for contributing and operating the pump profiling system on the ETSP cruise. On the ETNP cruise, I extend thanks to the Monterey Bay Aquatic Research Institute and Margeurite Blum for the same.

I would never have arrived here without the support of my family, who fostered my curiosity and pointed it at the natural world. I thank my father for his guidance in navigating the world professionally and psycho-emotionally, my sister for inspiring me to always put my best foot forward, and my mother, my dear friend, for making me a strong woman. Finally, I would like to express my deep gratitude to my partner in science and life, Alfonso Macías-Tapia, who supported my journey as a graduate student and the development of the work presented here in every conceivable way. He was there on my first cruise as a PhD student, racing me to remove bubbles from incubation bottles; and he was there on my last PhD cruise, lugging ice buckets

across the ship's deck to cool my incubators when they started over-heating. Along the way, Alfonso has been my sounding board, my code-debugging buddy, my counselor, my biggest critic, and my biggest supporter. I would not be where I am or who I am without him.

This work, its presentation/dissemination, and my time were funded by the National Science Foundation (grants OCE-1356056 and OCE-1459698 awarded to Mulholland/Jaykumar and Mulholland, respectively), the Jeffress Trust Awards Program in Interdisciplinary Research (awarded to Chappell), and the ODU Department of Ocean, Earth and Atmospheric Science. Analyses presented from the North Atlantic were funded in part by the Jacques S. Zaneveld and Neil and Susan Kelley Endowed Scholarships. The Dorothy Brown Scholarship enabled me to present portions of this work at several conferences over the years.

NOMENCLATURE

A_{PN}	^{15}N isotopic enrichment of the particulate nitrogen pool (atom-%); subscripts "t=0" and "t=f" indicate A_{PN} at the initial and final incubation time points, respectively
A_{N2}	^{15}N isotopic enrichment of the N_2 pool (atom-%)
BDL	Below the analytical detection limit
C	Carbon
Chl-a	Chlorophyll *a*
CO_2	Carbon dioxide
DIN	Dissolved inorganic nitrogen, operationally defined as the sum of nitrate, nitrite and ammonium (µM)
DNQ	Detectable but not quantifiable i.e., above the detection limit but below the limit of quantification
ETNP	Eastern Tropical North Pacific
ETSP	Eastern Tropical South Pacific
GS	Gulf Stream
LOD	Limit of detection
LOQ	Limit of quantification
MAB	Mid-Atlantic Bight (Western North Atlantic)
N	Nitrogen
N_2	Dinitrogen gas
N+N	Nitrate plus nitrite (µM)
NFR	Dinitrogen fixation rate (nmol N L^{-1} d^{-1} unless otherwise specified; see Eqn. 1 on p. 13)

NH_4^+ Ammonium (µM)

NO_2^- Nitrite (µM)

NO_3^- Nitrate (µM)

N_r Reactive nitrogen i.e., nitrogen forms prone to biological, photochemical, or radiative transformation

ODZ Oxygen deficient zone[1] i.e., region where dissolved oxygen is sufficiently low for anaerobic microbial processes to occur

OMZ Oxygen minimum zone i.e., where the lowest dissolved oxygen concentrations are observed at a given latitude/longitude

PC Particulate carbon

PN Particulate nitrogen (µg)

[PN] Particulate nitrogen concentration (µM)

$[\overline{PN}]$ Mean particulate nitrogen concentration over incubation period (µM)

SAB South Atlantic Bight (Western North Atlantic)

SUR Specific N_2 uptake rate (d^{-1}; see Eqn. 2 on p. 55)

SRP Soluble reactive phosphorus (µM)

[1] In Chapter II, this term is operationally defined as the volume of water where dissolved oxygen concentrations are too low to be detected via convention sensors (Seabird, ~3 µmol kg^{-1}) and nitrite concentrations exceed 0.5 µM (Thamdrup et al. 2012).

TABLE OF CONTENTS

LIST OF TABLES

LIST OF FIGURES

CHAPTER 1

BACKGROUND AND RATIONALE

As a key component of nucleic and amino acids, the building blocks of genetic material and proteins respectively, nitrogen (N) is fundamental to all known life. Consequently, N availability imposes an upper limit on ecosystem productivity. The predominant N form on Earth is dinitrogen (N_2), a ubiquitous but relatively inert gas. N_2 can be 'fixed', i.e., reduced to reactive N (N_r) compounds, biologically (by microbes), abiotically (e.g., by lightning), or industrially (by humans via the Haber-Bosch process). On a global scale, N_2 fixation is the only true source of "new" N_r to the Earth's reserve. Once fixed, a single atom of N may be continuously transformed between various reactive species and transferred between the geosphere, hydrosphere, biosphere and atmosphere. N_r inputs due to N_2 fixation are counterbalanced by losses, primarily through microbial processes that occur under anoxic conditions (Devol 2008).

In the ocean, N availability tends to limit phytoplankton growth in surface waters, particularly at low latitudes where N_r resupply from deep waters is sluggish (Moore et al. 2013). Organisms capable of biological N_2 fixaiton (diazotrophs) can thus stimulate production in such systems. By exerting a powerful influence over carbon dioxide (CO_2) drawdown via photosynthesis, the distribution and amount of N_r in the ocean plays a critical role in regulating global climate (Gruber 2004). Understanding the factors controlling the distribution and magnitude of marine N_2 fixation is, thus, paramount to unraveling Earth's biogeochemical history and future.

The genetic capacity for N_2 fixation is widely distributed throughout aquatic Bacteria and Archaea and has been identified in organisms with diverse metabolic strategies (e.g., photo/chemoautotrophs and heterotrophs, aerobes and anaerobes) and lifestyles (e.g., symbiotic, colonial, free-living) (Zehr and Paerl 2008). Focus has, however, historically been drawn to

Trichodesmium, a filamentous cyanobacterium that fixes N_2 at significant rates in oligotrophic (sub)tropical surface waters (e.g., Capone et al. 1997; Dugdale et al. 1964; Goering et al. 1966). N_2 fixation has thus been ascribed primarily to systems bearing conditions known to support the proliferation of *Trichodesmium* i.e., high temperatures and low concentrations of dissolved inorganic N (DIN). This paradigm has been reinforced by the belief that significant DIN concentrations preclude N_2 fixation because the energetic cost of N_2 fixation is generally higher than that of assimilating nitrate (NO_3^-), the major component of DIN (Falkowski 1983), as well as observations that DIN additions reduce rates of N_2 fixation in cultures (e.g., Mulholland and Capone 1999; Mulholland et al. 2001) though the subject of this work has largely been *Trichodesmium* (Knapp 2012 and references therein).

While *Trichodesmium* is certainly a major player in the marine N cycle (Capone et al. 2005; Capone et al. 1997), a plethora of diazotrophic groups with differing tolerances, sensitivities and relations to the pelagic food web are now recognized as well. These include eukaryote-symbionts and non-cyanobacterial diazotrophs, whose responses to ambient DIN appear to diverge from that of *Trichodesmium* (e.g., Bombar et al. 2016; Mills et al. 2020). Elucidating the range of these organisms is challenging because most are not, presently, culturable. However, recent observations of N_2 fixation in a myriad of marine systems, including in N_r-replete waters (Knapp 2012), has significantly expanded the known range of diazotrophs (Zehr and Capone 2020). This research suggests that a reappraisal of the contributions of diazotrophs in non-paradigmatic ocean realms is presently warranted. Two types of systems along ocean margins have received particular attention—pelagic oxygen deficient zones (ODZs) and broad continental shelf environments.

Pelagic ODZs, which can result near ocean margins from the combined effects of high surface productivity and poor ventilation (Fiedler and Talley 2006), foster conditions that should,

theoretically, favor N_2 fixation: they deplete N_r relative to other essential nutrients (Deutsch et al. 2007) and provide havens from O_2-inhibition of the N_2 fixation enzyme (nitrogenase) at depth (Großkopf and LaRoche 2012). These hypotheses are examined in Chapters II and III, which focus on the world's largest pelagic ODZs in the Eastern Tropical North (ETNP) and South (ETSP). Prior work from the ETSP has suggested that N_2 fixation rates (NFRs) are low but persist throughout deep waters (e.g., Bonnet et al. 2013). This important finding is refuted in Chapter III.

Chapter IV focuses on N_2 fixation across the Western North Atlantic continental shelf. Recent work suggests that a significant proportion of N_2 fixation in the North Atlantic occurs on the shelf (Mulholland et al. 2019). Such systems are subject to dynamic physical structures (e.g., eddies, frontal systems) that profoundly affect microbial metabolism and biogeochemical cycling. However, NFR measurements are labor-intensive and expensive, meaning that their coverage is typically insufficient to resolve fine-scale variability. To overcome this hurdle and elucidate the role of coastal water mass interactions on diazotroph activity and niche partitioning, I applied a supervised machine learning approach.

As the totality of the work presented here has been submitted for or undergone publication in peer-reviewed journals, each chapter is written such that it may stand alone. Consequently, some background material is repeated in each chapter's Introduction.

By examining the range and sensitivity of diazotrophs existing beyond the paradigmatic niche for marine N_2 fixation, the research presented here will support development of more accurate conceptual and quantitative N_2 fixation models. This, in turn, will facilitate resolution of several important outstanding questions, including: (1) Is the modern N cycle balanced? (2) What homeostatic feedback mechanisms maintain Earth's modern N_r reservoir? Additionally, resolving controls on marine N_2 fixation will enable greater accuracy in climate models.

CHAPTER II

N_2 FIXATION ACROSS PHYSICO-CHEMICAL GRADIENTS OF THE EASTERN TROPICAL NORTH PACIFIC OXYGEN DEFICIENT ZONE

PREFACE

The content of this Chapter was previously published by the American Geophysical Union (Copyright 2019 AGU): Selden, C. Mulholland, M., Bernhardt, P., Widner, B., Macías-Tapia, A., Qi, J., and A. Jayakumar. 2019. Dinitrogen fixation across physico-chemical gradients of the Eastern Tropical North Pacific oxygen deficient zone. Global Biogeochem. Cycles 33. doi: 10.1029/2019GB006242.

INTRODUCTION

One of the major sources of N_r to the global ocean is N_2 fixation (Gruber and Galloway, 2008), the assimilation of N_2 gas into biomass. Despite the abundance of N_2 in marine systems, only select prokaryotes have the genetic capacity to mediate its intracellular reduction to ammonia, which can then be assimilated via common metabolic pathways (Berges and Mulholland, 2008). Where present, these organisms can increase the N_r pool and consequently stimulate primary production in N-limited ocean regions, thereby enhancing atmospheric drawdown of CO_2 and, potentially, export of this carbon (C) through the biological pump (e.g., Karl et al. 2012). Understanding the factors regulating N_r inputs and losses is essential to predicting how oceanic N_r inventories vary under changing climatic conditions and affect the ocean's capacity to take up CO_2.

Historically, N_2 fixation has been ascribed primarily to filamentous cyanobacteria that thrive in nutrient-deplete tropical and subtropical waters where warm temperatures and low DIN concentrations are thought to promote diazotrophy (Carpenter and Capone 2008; Flores and Herrero 2005; Mulholland et al. 2001). Recent work has challenged this paradigm, expanding the range of N_2 fixation to include cooler (Blais et al. 2012; Harding et al. 2018; Moisander et al. 2010; Sipler et al. 2017), aphotic (Benavides et al. 2015, 2016; Bonnet et al. 2013; Rahav et al. 2013, 2015) and mesotrophic (Knapp 2012; see also Bentzon-Tilia et al. 2015; Bonnet et al. 2013; Farnelid et al. 2013; Grosse et al. 2010; Mulholland et al. 2012; Rees et al. 2009; Sohm et al. 2011) waters. Concomitantly, appreciation has grown for the importance of diverse and broadly-distributed diazotrophic clades, including eukaryote-symbionts (e.g., Martinez-Perez et al. 2016; Moisander et al. 2010) and non-cyanobacterial diazotrophs (Bombar et al. 2016; Moisander et al. 2017 and references therein), to the global N cycle. The sensitivities and physiological ranges of these groups likely differ from those of long-cultured and well-studied cyanobacterial diazotrophs like *Trichodesmium*, complicating our understanding of the environmental factors that regulate the magnitude and distribution of NFRs in the ocean.

Based on early studies of freshwater and tropical cyanobacterial diazotrophs, it was determined that significant concentrations (i.e., ≥ 1 μM) of ambient DIN should preclude N_2 fixation, an energetically costly means of acquiring N (Falkowski 1983; Knapp 2012); yet, recent work suggest this paradigm must be revisited (Knapp 2012; see also Bentzon-Tilia et al. 2015; Bonnet et al. 2013; Farnelid et al. 2013; Grosse et al. 2010; Mulholland et al. 2012, 2019; Rees et al. 2009; Sohm et al. 2011). There are a variety of reasons organisms may fix N_2 despite its energetic costs. Certain organisms, including some eukaryote-symbionts, lack the genetic ability to reduce NO_3^- (Caputo et al. 2018); investing in NO_3^- assimilation machinery may be unfavorable

for diazotrophs already growing on N_2 (Karl et al. 2002); and some diazotrophs may use N_2 fixation as a mechanism for regulating intracellular state (Bombar et al. 2016), potentially decoupling its activity from N demand satiety. One energetic complication is that nitrogenase, the enzyme that mediates N_2 fixation, is permanently inhibited by O_2 (Postgate 1998), and oxygenic diazotrophs as well as those inhabiting oxic environments must invest in O_2-avoidance strategies to minimize nitrogenase turnover (Vitousek 2002). Diazotrophs in anoxic environments could evade this cost, potentially making N_2 fixation more favorable (Groβkopf and LaRoche 2012). Active N_2 fixation has now been observed in low-O_2 waters despite ambient DIN concentrations in excess of 1 μM (Bonnet et al. 2013; Dekaezemacker et al. 2013; Farnelid et al. 2013; Fernandez et al. 2011; Hamersley et al. 2011; Jayakumar et al. 2017; Losher et al. 2014), as well as in ammonium (NH_4^+)-rich anoxic sediments (e.g., Andersson et al. 2014; McGlathery et al. 1998).

There are three major O_2-deplete regions of the pelagic ocean, which arise in the ETNP, ETSP and Arabian Sea (DeVries et al. 2012). The O_2 minimum zones (OMZ), i.e., the low-O_2 depth horizon, and ODZs, where O_2 is undetectable using common sensors, are predominantly below the euphotic zone (Paulmier and Ruiz-Pino 2008). The majority of N_2 fixation within such waters is consequently mediated by non-cyanobacterial diazotrophs (Chang et al. 2019; Jayakumar et al. 2012; 2017), some portion of which are presumably heterotrophic. Heterotrophic diazotrophs can become organic C-limited, particularly in deep waters, and organic C availability may therefore constrain their NFRs (Bombar et al. 2016). Indeed, dissolved organic C additions has enhanced NFRs in both mesopelagic (Benavides et al. 2015; Bonnet et al. 2013; Rahav et al. 2013) and epipelagic waters (Losher et al. 2014; Rahav et al. 2015).

Pelagic ODZs account for roughly one-third of N_r loss from the ocean (DeVries et al. 2012). Significant N_r deficits are observed in these regions relative to the concentrations of other

dissolved constituents including phosphate (soluble reactive phosphate, SRP) and iron (Fe), an essential co-factor in the nitrogenase enzyme (Dixon and Kahn 2004). As such, these waters are hypothesized to favor diazotrophic activity once advected into the euphotic zone, where the remaining DIN is rapidly depleted, by limiting the growth of competitors who cannot fix N_2 (Deutsch et al. 2007; Monteiro et al. 2011). In so doing, these geochemical signals (e.g., low DIN:SRP) are believed to play a critical role in the feedback mechanism between N_2 fixation and N_r losses regulating the ocean's N_r inventory (Weber and Deutsch 2014); however, Fe limitation of N_2 fixation may spatially decouple N_r inputs from losses (Weber and Deutsch 2014), as hypothesized for the South Pacific basin (Bonnet et al. 2017; Dekaezemacker et al. 2013; Knapp et al. 2016, 2018; Weber and Deutsch 2014). The North Pacific receives higher aeolian Fe inputs than the South Pacific Ocean (Jickells et al. 2005), but N_2 fixation measurements in the ETNP ODZ region remain sparse despite local observations of diazotrophs (Jayakumar et al. 2017; White et al. 2013).

This study leveraged naturally occurring light, nutrient, and O_2 gradients in the ETNP to characterize N_2 fixation by mixed diazotroph communities with respect to these variables. The influence of dissolved organic C availability on N_2 fixation below the euphotic zone was investigated by amending whole water incubations with either glucose or a mixed amino acid solution. By furthering understanding of the physico-chemical factors regulating diazotroph activity, this study contributes to our evolving view of N_2 fixation in the marine environment and the feedback mechanisms maintaining the ocean's N_r inventory.

METHODS

I measured NFRs, nutrient concentrations and hydrographic characteristics within and adjacent to the ETNP ODZ aboard the NOAA vessel *Ronald H. Brown* in April, 2016, during an ENSO event (Climate Prediction Center). The cruise track extended southeast along the Mexican coastline from the Rosa Seamount (25°N, 115°W) off the Baja peninsula to 15°N and 99°W, proximal to the Guerrero-Oaxaca border, then offshore in a northwesterly direction to 18°N and 113°W (Fig. 1a). 'Inshore' was defined here as being within 200 km of the coastline; however, all stations were beyond the shelf break and were at least 2000 m deep. Our sampling strategy was optimized for high resolution data collection along vertical gradients of light, dissolved nutrients, and O_2.

Hydrographic and nutrient measurements

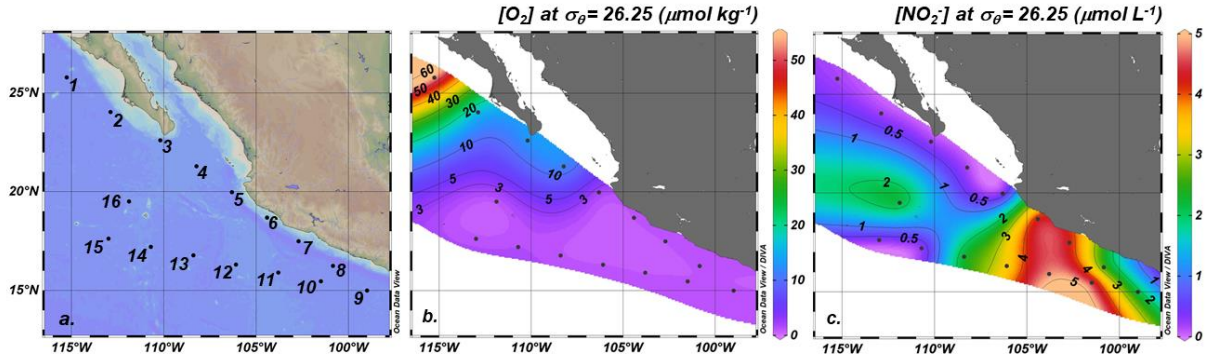

Figure 1. Bathymetry overlain by station numbers (a), and dissolved O_2 (μmol kg^{-1}) and NO_2^- (μM) concentrations, collected using the Sea-Bird CTD and Pump Profiling System respectively, along an isopycnal surface σ_θ = 26.25 (b-c), illustrating the extent of the study region and oxygen deficient zone. Oxygen deficiency was defined by O_2 concentrations below detection (3 μmol kg^{-1}) and NO_2^- concentrations exceeding 0.5 μM.

Vertical profiles of temperature, salinity, O_2 and chlorophyll *a* (chl-a) fluorescence were obtained at 16 stations using a Sea-Bird SBE 11plus CTD, equipped with a model 43 dissolved oxygen sensor (detection limit ~3 μmol kg^{-1} O_2), a LI-COR Biospherical Photosynthetically Available Radiation (PAR) Sensor and a Seapoint Chlorophyll Fluorometer. These instruments were mounted to a sampling rosette holding twenty-four 12 L Niskin bottles from which water samples were collected at select depths to measure chl-a and dissolved nutrient concentrations. Water for N_2 fixation incubations in the euphotic zone and below the ODZ were also collected from Niskin bottles (see below). Chl-a concentrations were determined via the non-acidification method (Welschmeyer 1994). NO_3^- plus nitrite (NO_2^-) and SRP concentrations were measured onboard using an Astoria-Pacific nutrient autoanalyzer following standard colorimetric methods (Parsons et al. 1984) and according to the manufacturer's specifications. A Biosciences Ultrospec 2100 *pro* spectrophotometer was used for NO_2^- analysis (Parsons et al. 1984) and NO_3^- concentrations were calculated by difference. NH_4^+ concentrations were determined fluorometrically using the orthophthaldialdehyde (OPA) method (Holmes et al. 1999). DIN was calculated as the sum of NO_3^-+NO_2^- and NH_4^+ concentration. Further details of these analyses are available in Suppl. Text 1.

In addition to discrete measurements, a Pump Profiling System, developed and built by the Monterey Bay Aquarium and Research Institute (Sakamoto et al. 1990), was used to generate near-continuous nutrient profiles in real-time to approximately 350 m and to collect low-oxygen water. This system was comprised of a cable, hose and a small rosette to which a submersible water pump, a Sea-Bird SBE 19 SeaCAT CTD, WetStar Fluorometer, Sea Tech Beam Transmissometer and a LI-COR Biospherical PAR Sensor were mounted. The Pump Profiling System was deployed to a maximum depth of 400 m. Water was pumped directly from depth to the laboratory to generate *in*

situ nutrient profiles and to an on-deck station where samples from the O_2 minimum depth horizon were collected for incubation experiments (see below). In the laboratory, this flow ran first through an MBARI-modified Durafet pH sensor before being shunted to an Alpkem Astoria-Pacific Rapid Flow Analysis System which determined concentrations of NO_3^- plus NO_2^-, NO_2^-, and NH_4^+ at a rate of 1 measurement per second. NO_3^- and NO_2^- measurements were made following manufacturer's instructions (Sakamoto et al. 1990). The OPA method (Holmes et al. 1999) was adapted for the Rapid Flow Analysis System and used to determine *in situ* NH_4^+ concentrations. A Fast Repetition Rate Fluorometer collected chl-a fluorescence profiles at a rate of 1 sample per 30 seconds.

N_2 fixation incubation experiments

Whole water was collected from the Niskin bottles or pumped from depth anoxically using the Pump Profiling System for N_2 fixation incubation experiments carried out above, below or within the OMZ, respectively (Table 1). I define the OMZ as the region of the water column in which the lowest O_2 concentrations were observed at a site. This is distinct from the ODZ, operationally defined by O_2 concentrations below the limit of detection of the Seabird O_2 sensor (3 μmol kg^{-1}) and NO_2^- concentrations exceeding 0.5 μM which has been deemed indicative of functionally-anoxic conditions (Thamdrup et al. 2012).

Table 1. Summary of NFR measurement incubation protocols.

Depth horizon[a]	Bottle type	Collection protocol	Incubation conditions	Duration
EUPH	Clear PETG bottles (1L)	Collected in shaded 10 L carboys from Niskin bottles	Incubated in appropriately-shaded on-deck tanks with continuously flowing surface seawater	~24 hrs
OMZ	Amber glass bottles (4L)	Collected anoxically and directly from depth using pump	Incubated in the dark in a walk-in cold van at ~12°C	~24 hrs
DEEP	Amber glass bottles (4L)	Collected in shaded 10 L carboys from Niskin bottles	Incubated in the dark in either ~12°C cold van or 4°C walk-in refrigerator	~48 hrs

[a]EUPH, OMZ, and DEEP indicate waters collected from above, within and below the O_2 minimum layer (typically ~150 – 400 m), respectively. Note that not all 'OMZ' samples exhibit suboxia (<20 μmol kg^{-1}). See Supplemental Materials and Methods for a detailed description of sample handling.

NFR measurements were made using a modified version of the traditional $^{15}N_2$ bubble method (Montoya et al. 1996). In the traditional $^{15}N_2$ bubble method, $^{15}N_2$ gas is injected into a filled sample bottle and ^{15}N enrichment of the particulate N (PN) pool is measured following an incubation period. The assimilation rate of the ^{15}N tracer into biomass (i.e., NFR) can then be calculated using a mixing model as shown below (eqn. 1; Montoya et al. 1996). N_2 gas is, however, slow to equilibrate, causing source pool enrichment (i.e., dissolved N_2 enrichment) to change over the course of the incubation which may result in an underestimation of NFRs (Böttjer et al. 2017; Großkopf et al. 2012; Mohr et al. 2010).

To address this issue, the dissolution of highly enriched $^{15}N_2$ gas (~99%, Cambridge Isotopes, Tewksbury, MA) was hastened following injection by slowly inverting sample bottles on a large see-saw for 15 minutes. The see-saw consisted of a flat panel affixed to a central axis with baskets on either side in which incubation bottles were secured laterally. In this configuration, the $^{15}N_2$ gas bubble travelled the full length of each bottle as the panel was gently rocked. Cambridge Isotope $^{15}N_2$ gas was selected because, while significant ^{15}N-NH_4^+ and -NO_3^-

concentrations have been observed in other brand stocks, these contaminants have only been reported from Cambridge Isotope stocks at tracer-level concentrations (Dabundo et al. 2014). The remaining gas bubble was then removed using a syringe prior to the incubation period and ^{15}N enrichment of the N_2 pool was measured directly (see below). $^{15}N_2$ uptake experiments were carried out in triplicate. A detailed description of sample collection and incubation procedures is available in Suppl. Text 1.

Euphotic samples were incubated on-deck in tanks equipped with neutral density screens to approximate light levels at the depth of sample collection, which was determined using the PAR sensor mounted to the CTD rosette. Continuously flowing surface seawater maintained near-ambient surface temperatures in the deck incubators. Sub-euphotic waters (below the 0.1% light level) were incubated in the dark, in either a ~12°C cold van or a 4°C walk-in refrigerator, depending on the temperature at the depth of sample collection. Due to a cold van malfunction, incubations from within the OMZ at stations 8, 9, and 10 were carried out in a darkened room retrofitted with air conditioners, capable of maintaining temperatures at ~16°C. While warmer temperatures may increase metabolic activity (Price and Sowers 2004), the effect of this slight increase in temperature on N_2 fixation was likely minimal as rates from the affected bottles were largely undetectable (Suppl. Table 2). For samples above and within the OMZ or ODZ, uptake experiments were 24 hours. Water samples collected below the OMZ or ODZ, where biomass is lower and cooler temperatures reduce metabolic rates (Price and Sowers 2004), were incubated for 48 hours. Incubations were terminated by filtration of the sample onto pre-combusted (450 °C for 2 hours) Whatman GF-75 filters (nominal pore size of 0.3 μm). Immediately prior to filtration, an aliquot of each sample to measure $^{15}N_2$ enrichment in each bottle was transferred to a helium-flushed exetainer using a gas-tight syringe and preserved by adding 50 μL of a helium-flushed zinc

chloride or mercuric chloride solution (50% w/v $ZnCl_2$ and $HgCl_2$, Thermo Fisher Scientific, Waltham, MA).

To establish the initial isotopic composition and concentration of PN in water samples, water from each depth sampled was collected separately. Triplicate samples were filtered at the time of collection in a designated laboratory space isolated from where experiments using ^{15}N tracer were being conducted to avoid isotope contamination. Filters for both initial and final PN analysis were placed in sterile microcentrifuge tubes and frozen until analysis at Old Dominion University. Filters were dried for 48 hours at 50°C, then pelletized in tin discs. Particulate N and C concentrations and isotopic enrichment were measured using an Europa 20-20 isotope ratio mass spectrometer (IRMS) equipped with an automated N and C analyzer. Isotopic enrichment of dissolved N_2 was measured using a Europa 20-22 continuous flow IRMS, as described in Jayakumar et al. (2017).

NFR calculations and error analysis

Volumetric NFRs were calculated following Montoya et al. (1996):

$$\text{NFR} = \frac{A_{PN_{t=f}} - A_{PN_{t=0}}}{A_{N_2} - A_{PN_{t=0}}} \times \frac{[\overline{PN}]}{\Delta t} \qquad \textit{Equation 1.}$$

where $A_{PN_{t=0}}$, $A_{PN_{t=f}}$, A_{N_2}, and $[\overline{PN}]$ represent the average initial and mean PN isotopic composition, isotopic composition of the N_2 pool, and PN concentration of three replicate samples. Here, initial PN mass was used rather than the mean because final PN mass was measured with less accuracy (based on bottle volume). The standard deviation of these replicates was propagated to calculate NFR error following Montoya et al. (1996) and Gradoville et al. (2017). The incubation time is denoted as Δt and the uncertainty of this value was estimated based on the average time required to filter the given volume of seawater relative to the length of the incubation. A sensitivity

analysis of the relative contributions of each measurement to total error is presented in Suppl. Table 1. See Suppl. Text 1 for further details on rate and error calculations.

A change in the atom-% enrichment of the PN pool was considered detectable if it exceeded three times the standard deviation of eight 12.5 μg N replicate standards which were run daily (Ripp 1996). A limit of detection (LOD was calculated for each volumetric rate by substituting this value for $A_{PN_f} - A_{PN_0}$. A limit of quantification (LOQ) was similarly calculated by taking 10 times the standard deviation of the replicate standards (Ripp 1996). The average limit of detection for PN mass, calculated based on blanks (3σ, n=4), among all IRMS runs for this study was 0.83 μg N. This value, however, should not be confused with the minimum mass deemed acceptable for determination of isotope ratios. The accuracy of enrichment measurements decreases with decreasing mass (Sharp 2017), and so a lower limit of acceptable mass was established per instrument run based on the linearity of the atom-% measured during each standard run; on average this was 3.0 μg N for this study. The mass of standards ranged from 1.17 to 100 μg N.

Areal (depth-integrated) rates were calculated for the euphotic zone (defined as the region extending from the surface to the 0.1% light level) by averaging volumetric rates measured for the surface mixed layer, from the bottom of the surface mixed layer to the 1% light level, and from the 1% to 0.1% light level, then depth-integrating over each layer and summing the respective contributions. If the volumetric rate at a given depth was below the LOD, then it was assigned a value of 0 nmol N L^{-1} d^{-1} for the purpose of calculating the areal rate. If the calculated NFR was above the LOD but below the LOQ (i.e., it was detectable but not quantifiable), then the LOD was used in the areal rate calculation. The error associated with both non-detectable and non-quantifiable rates was propagated along with that of all quantifiable rates. NFRs were not depth-integrated in sub-euphotic waters because quantifiable rates were sparse and accurate estimation

of sub-euphotic areal NFRs consequently untenable. Areal NFRs from the euphotic zone were compared between inshore (1 to 9) and offshore (10 to 16) stations using a two-tailed Mann-Whitney *U* test.

Carbon addition bioassays

Carbon addition bioassays were carried out at stations 6, 9, 12, 15 and 16 at depths within and below the core ODZ to determine whether the supply of organic C limited NFRs. For these experiments, samples were collected as described above. Once sealed, but prior to $^{15}N_2$ additions, one set of triplicate bottles was amended with glucose (Cambridge Isotopes, Tewksbury, MA) and another with a mixture of 20 amino acids (Cambridge Isotopes, Tewksbury, MA), resulting in a final addition of 40 μmol organic C L^{-1} to both sets of incubations. This addition approximately doubled the availability of dissolved organic C (Hansell and Carlson 1998; Loh and Bauer 2000), although much of the ambient dissolved organic C pool is thought to be very old and likely refractory (Druffel et al. 1992) thereby augmenting the significance of these C amendments to microbial communities present. Un-amended triplicate incubations served as controls. Experimental treatments were compared to controls using a Wilcoxon signed-rank test. Where N_2 fixation was not detected or quantified, the lower limit of these values, zero or the LOD respectively, was used in statistical calculations. This approach increases our ability to detect significant differences (Lori Type II error risk) but increases the probability of a false positive (higher Type I error risk).

RESULTS AND DISCUSSION

Regional hydrography

Surface waters of the ETNP are characterized by high productivity, a strong pycnocline that prevents local ventilation of deep waters, and a thermal front where the cool California Current meets the eastern Pacific warm pool (Fiedler and Talley 2006). Our study area crossed this frontal region. Alongshore surface waters were cool to the north (<25°C at stations 1 to 4) and warmer south of the Gulf of California (Table 2, Fig. 2a). Surface waters at stations 9 to 13 exceeded 27.5°C, characteristic of the eastern Pacific warm pool (Fiedler and Talley 2006) and salinity was low, below 34 (Table 2, Fig. 2b), suggestive of Tropical Surface Waters (T>25, S<34) (Fiedler and Talley 2006).

Table 2. Surface hydrographic characteristics and depth-integrated NFRs within euphotic zone.

Station	Latitude (°N)	Longitude (°W)	Surface temperature (°C)	Surface salinity	Euphotic zone depth (m)	Areal euphotic NFR (μmol N m^{-2} d^{-1})[a]
1	25.791	-115.261	19.5	34.4	99	814 (396)
2	24.041	-112.891	21.0	34.6	114	6226 (5493)
3	22.608	-110.202	21.9	34.6	88	102 (30)
4	21.292	-108.242	24.3	34.5	107	14 (17)
5	19.985	-106.313	25.2	34.6	81	588 (108)
6	18.688	-104.416	25.3	34.4	65	250 (66)
7	17.500	-102.700	26.6	34.3	89	99 (29)
8	16.250	-100.845	27.0	34.2	69	257 (95)
9	15.000	-98.999	28.7	33.7	74	Not detected
10	15.469	-101.502	29.2	33.6	94	85 (41)
11	15.901	-103.799	29.1	33.6	110	7 (21)
12	16.315	-106.091	28.0	33.5	107	Not detected
13	16.778	-108.398	27.7	33.9	108	Not detected
14	17.204	-110.712	25.9	34.1	111	Not detected
15	17.625	-113.001	27.0	33.7	117	Not detected
16	19.508	-111.895	24.0	34.6	118	Not detected

[a]Rate measurement propagated error, calculated as described in Materials and Methods, is given in parentheses.

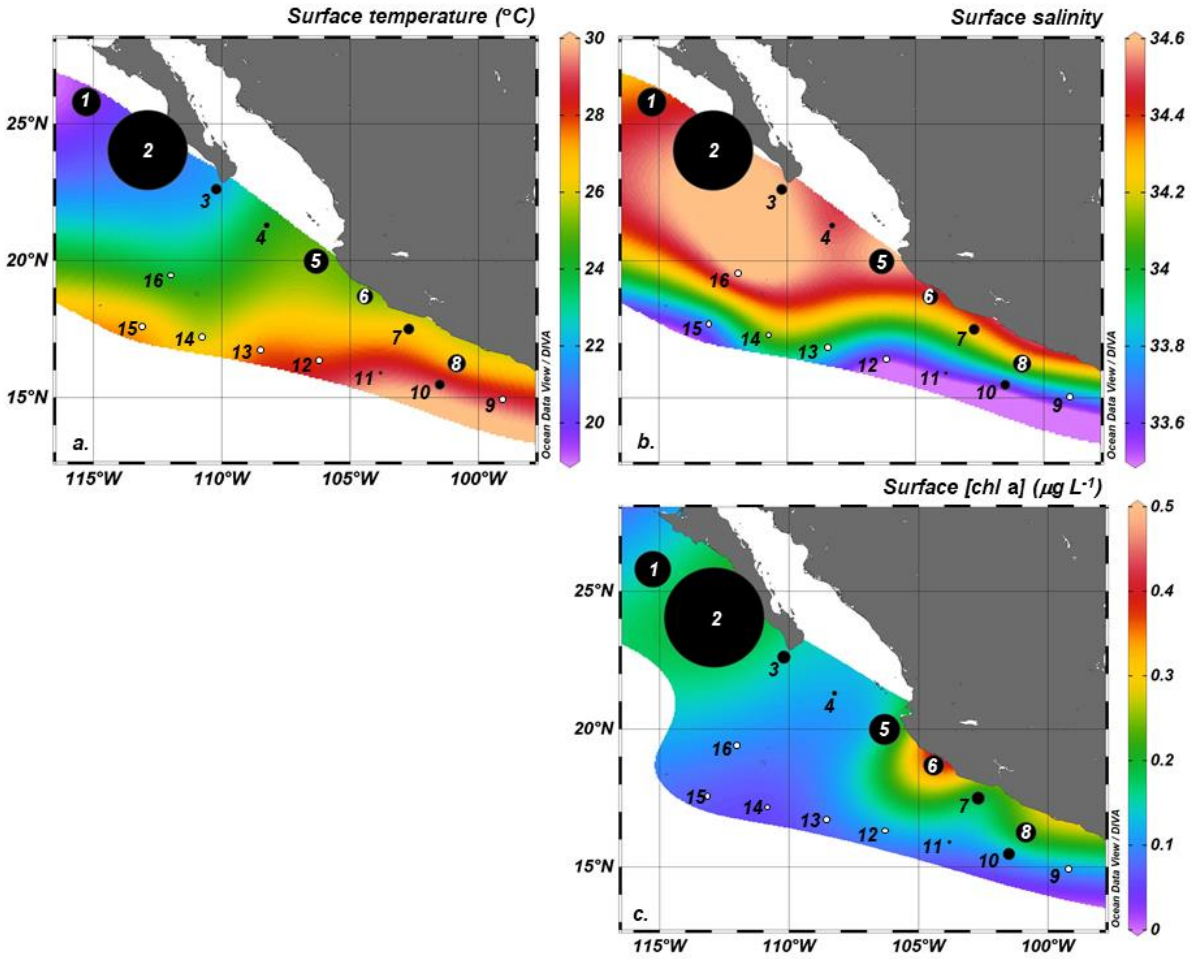

Figure 2. Surface temperature (°C, a), salinity (b) and chl-a concentration (μg L^{-1}, c) overlain by black dots sized to represent NFRs depth-integrated throughout the euphotic zone (see Table 2 for values). White dots depict locations where N_2 fixation was undetectable throughout the euphotic zone.

These waters typically exhibit little seasonal and ENSO variability in sea surface temperature and salinity; however, ENSO events are associated with a local deepening of the thermocline (Fiedler and Talley 2006). In the present study, the thermocline shoaled and strengthened alongshore to the southeast (Fig. 3i-j), following regional trends observed previously (Fiedler and Talley 2006). The nitracline and primary chl-a fluorescence maximum also shoaled to the southeast, accompanied by an increase in chl-a fluorescence (Fig. 3e-h). A secondary chl-a fluorescence maximum was evident at stations 5 to 13, where the core ODZ was thickest and NO_2^- concentrations highest.

O_2-deficient waters, defined as those in which O_2 concentrations were below detection by the Seabird O_2 sensor (<3 μmol kg^{-1}) and NO_2^- concentrations were above 0.5 μM (Thamdrup et al. 2012), were observed at all offshore stations (10 to 16) and inshore stations 5 to 9 along the west coast of Mexico (Fig. 1b-c). The thickness of the ODZ increased towards the southeastern-most station, expanding from 200 to 400 m at northerly stations 15, 16 and 5, to a thickness of 100 to 600 m at station 9. Stations 1 to 4 were north of the ODZ but exhibited suboxic (<20 μmol kg^{-1} O_2) conditions below the euphotic zone (Fig. 3a-d). The OMZ, the low-O_2 depth horizon present throughout the region, was characterized by slightly higher salinity (~34.7 – 34.8) and warmer temperatures (10 – 16°C) relative to underlying waters (S ≈ 24.6 – 34.5, T ≤ 10°C) and higher salinity (Suppl. Table 2) than the California Current water intruding from the north (Fiedler and Talley 2006). DIN:SRP ratios remained within a narrow range (8.5 to 12) from below the thermocline to approximately 400 m then gradually increased, stabilizing near 14 after 1000 m. In the North Pacific Ocean, DIN:SRP ratios are typically ~14.1, averaging 14.6 below 1000 m (Tyrrell and Law 1997).

Figure 3. Hydrography (a-j) and NFRs (k-l) in upper 350 m of inshore (left) and offshore (right) transects. Black lines and dots represent continuous or near-continuous profiles collected from the Pump Profiling System and discrete sampling points, respectively.

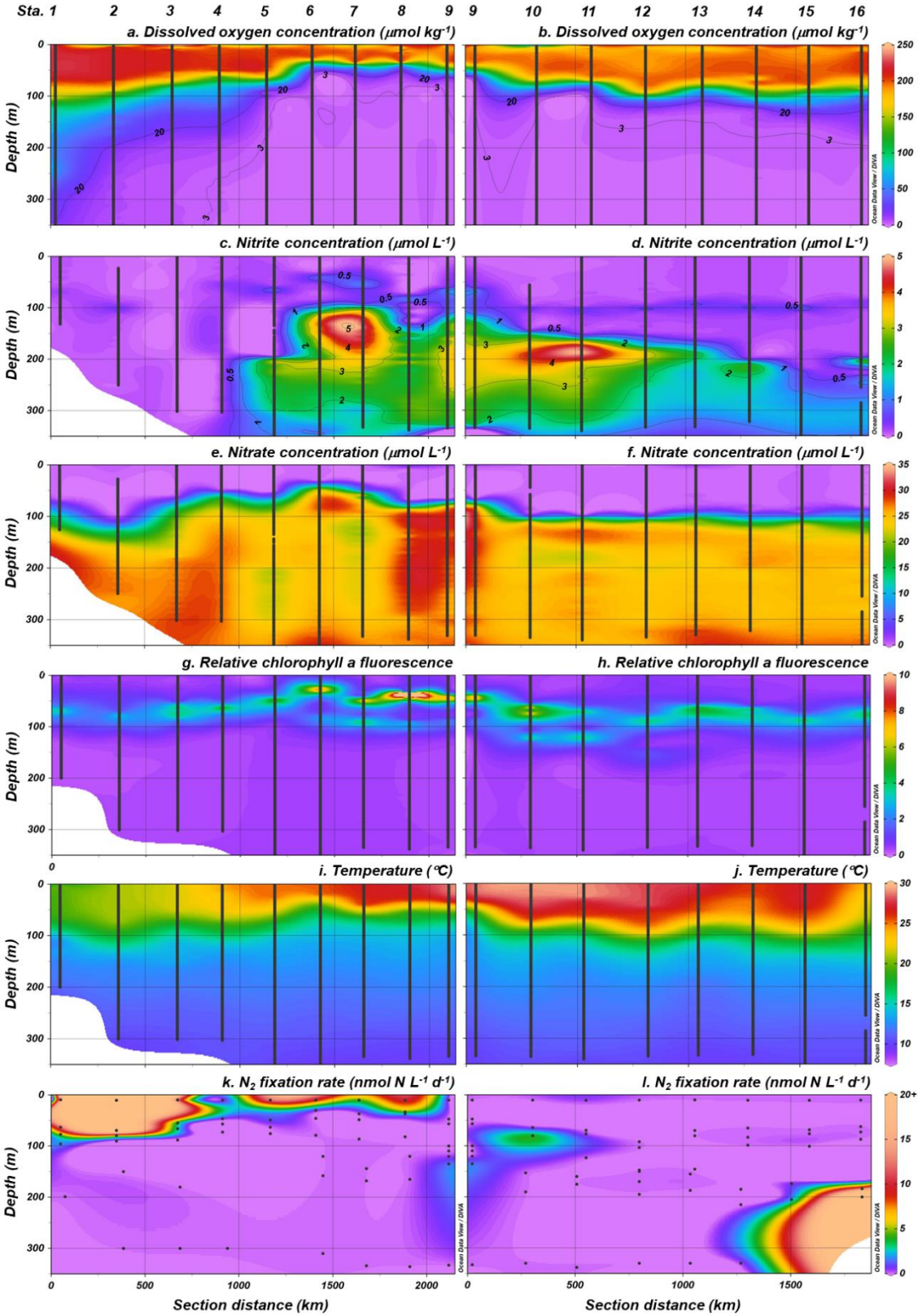

See figure legend on preceding page.

N_2 fixation in the euphotic zone

NFRs were relatively high in the warm, sunlit, oxic waters (Fig. 3k-l), where NO_3^- and SRP concentrations were low (Figs. 3e-f, S1a-b) and DIN:SRP was consistently below 3 (Suppl. Fig. 1c-d), suggestive of N_r limitation. N_2 fixation was detected in euphotic waters at 10 of the 16 stations, in 17 of 62 samples collected (Suppl. Table 2). Most of these samples came from stations 1 to 8 where surface salinity and concentrations of chl-a and SRP were comparatively high (Figs. 2b-c, S1a-b). NFRs were highest and extended deeper into the water column where the thermocline was weakest, constricting towards the southeast as the underlying ODZ shoaled (Fig. 3a-b, k-l; Suppl. Table 2). Depth-integrated euphotic NFRs among inshore stations (1 to 9) were significantly greater than at offshore stations (10 to 16) (Mann Whitney U, n_1=7, n_2=9, U=93, p=0.003), ranging from below detection to 6230 ±5500 μmol N m^{-2} d^{-1} (Table 2) with a median value among all measurable areal rates of 176 μmol N m^{-2} d^{-1}.

Recent work has focused on the potential for enhanced N_2 fixation along productive ocean margins, particularly those in which low DIN:SRP waters are upwelled (e.g., Bonnet et al. 2013; Chang et al. 2019; Deutsch et al. 2007; Dekaezemacker et al. 2013; Fernandez et al. 2011; Jayakumar et al. 2017; Knapp et al. 2016; Losher et al. 2014; Sohm et al. 2011; White et al. 2013). Comparison of these systems to N_r-deplete ocean gyres, where the bulk of global N_2 fixation has historically been ascribed, is, however, complicated by methodological biases—chiefly, the potential underestimation of the classic $^{15}N_2$ bubble method due to the slow dissolution of $^{15}N_2$ (Böttjer et al. 2017; Großkopf et al. 2012; Mohr et al. 2010), as well as under- or overestimation of N_2 fixation when measured indirectly via the acetylene reduction assay (Mulholland et al. 2004). Luo et al. (2012) calculated an arithmetic mean areal NFR for North Pacific (0 to 55°N) euphotic zone of 120 ±22 μmol N m^{-2} d^{-1} based on studies applying these methods primarily in the basin's

interior. Böttjer et al. (2017) accounted for the approximately two-fold underestimation of the $^{15}N_2$ bubble method in time series data from station ALOHA (North Pacific subtropical gyre) and calculated an average rate of 230 ±136 μmol N m^{-2} d^{-1}. These values are in relatively good agreement if a correction factor of two (Böttjer et al. 2017; Großkopf et al. 2012) is also applied to Luo and colleague's basin-wide estimate.

Of the ten stations where N_2 fixation was detected in surface waters for this study, areal rates exceeded the station ALOHA mean (Böttjer et al. 2017) at five—all located near the coastline (Table 2). If, however, I account for the error inherent to the areal rates presented in this study and variation from the mean at station ALOHA, only rates at stations 1, 2 and 5 clearly exceed mean N_2 fixation at station ALOHA, and only at stations 1 and 2 does N_2 fixation exceed the maximum rate at ALOHA where NFRs range from 21 to 676 μmol N m^{-2} d^{-1} (Böttjer et al. 2017). Nevertheless, the observed distribution of euphotic zone N_2 fixation in this study and the elevation of these rates above the regional average suggests that conditions in the cooler, saltier, more productive water mass near the continent favored the growth and activity of local diazotroph communities relative to those in the central North Pacific basin. This finding supports the observation of Jayakumar and colleagues (2017) that euphotic, inshore NFRs in the ETNP ODZ region exceeded those offshore.

Euphotic NFRs reported here (with a median value of 176 μmol N m^{-2} d^{-1}) were also high relative to waters overlying the ETSP ODZ, where Bonnet et al. (2013) and Fernandez et al. (2011) estimate average areal rates of 43 ±6 and 48 ±68 μmol N m^{-2} d^{-1}, respectively, using the classic $^{15}N_2$ bubble method. These values are in relatively good agreement with other incubation-based estimates from the ETSP euphotic zone (Dekaezemacker et al. 2013; Knapp et al. 2016) and are comparable to those observed in the central South Pacific gyre (94 ±61 μmol N m^{-2} d^{-1}; Halm et

al. 2012), indicating that surface waters of the ETSP ODZ do not support elevated NFRs as predicted by Deutsch et al. (2007). Despite these low regional means, Losher et al. (2014) observed N_2 fixation to exceed 800 μmol N m^{-2} d^{-1} at one coastal sulfidic station in the ETSP, suggesting that sulfidic events may sporadically enhance rates. Nevertheless, N_2 fixation is thought to be only a minor contributor of N_r to export production in the ETSP (Chang et al. 2019; Knapp et al. 2016).

N_2 fixation may be greater in ETNP surface waters relative to those of the ETSP because the North Pacific receives higher aeolian Fe inputs (Jickells et al. 2005). Indeed, Fe amendments have been observed to increase NFRs in ETSP surface waters (Dekaezemacker et al. 2013). It must be noted, however, that the present study occurred during an ENSO event, which has been associated with enhanced NFRs in the ETSP (Dekaezemacker et al. 2013). Further work is therefore necessary to elucidate whether this event affected N_2 fixation in the ETNP, and consequently whether these regional differences are truly significant.

High rates of N_2 fixation—on par with those observed here at stations 1, 2, and 5 (Table 2)—have also been observed along other ocean margins (e.g., Carpenter et al. 1999; Mulholland et al. 2012, 2014; Rees et al. 2009; Shiozaki et al. 2015; Wen et al. 2017) including areas characterized by low concentrations of DIN relative to SRP and other essential elements (e.g., Fe, silicon for diatom-diazotroph symbioses) resulting from riverine inputs (Grosse et al. 2010; Subramaniam et al. 2008) and advection of ODZ-generated N_r-deplete waters into marginal seas (White et al. 2013). In the Amazon River plume and Gulf of California, the latter of which receives N_r-deplete waters from the ETNP ODZ via the California Undercurrent, areal NFRs as high as ~8000 μmol N m^{-2} d^{-1} (Subramaniam et al. 2008) and ~900 μmol N m^{-2} d^{-1} (White et al. 2013) have been reported, respectively. Along the Southern New England shelf, NFRs reached 4106 μmol N m^{-2} d^{-1} in Fall (Mulholland et al. 2019). In euphotic waters of the Benguela Upwelling System,

another eastern boundary upwelling system predicted by Deutsch and colleagues (2007) to support elevated N_2 fixation, rates were far lower but increased inshore (Sohm et al. 2011) as observed in this study. These findings, along with the present study, suggest that diazotroph activity is heightened along ocean margins, particularly where N_r is drawn down relative to SRP and other nutrients as occurs in the ETNP (Table 2).

Proximity to the continent likely offers advantages to some diazotrophic groups relative to others, depending on the physical and chemical properties of the water column, their metabolic requirements and genetic capabilities. Enhanced availability of organic C in productive inshore waters may provide energy to heterotrophic diazotrophs and low-oxygen/anoxic microzones for non-cyanobacterial diazotrophs fixing N_2 in fully oxic waters (Bombar et al. 2016), such as those observed in the ETNP and ETSP ODZs (Chang et al. 2019; Jayakumar et al. 2017). Indeed, sinking particles have been identified as loci of both cyanobacterial and non-cyanobacterial diazotrophs in the North Pacific subtropical gyre (Farnelid et al. 2019). Additionally, Fe can be delivered to the ocean from the continents via aeolian transport and riverine inputs (Hunter and Boyd 2007), the latter of which may also serve as a source of Fe-binding ligands (e.g., Bundy et al. 2015; Laglera and van den Berg 2009) that maintain dissolved Fe in solution (Rue and Bruland 1995; van den Berg 1995).

Sub-euphotic N_2 fixation and carbon limitation

Within OMZ waters, NFRs were detected at three of the 16 stations (Sta. 9, 15 and 16), within five of the 39 samples collected at this depth horizon—all of which were from suboxic (<20 μmol kg^{-1} O_2) waters (Suppl. Table 2). Within the OMZ at stations 9 and 15, the highest volumetric rates were 1.55 ±0.41 nmol N $L^{-1}d^{-1}$ (Sta. 9 at 135 m, n=3) and 1.01 ±1.34 nmol N $L^{-1}d^{-1}$ (Sta. 15

at 174 m, n=3), respectively. Of the four stations (6, 9, 12 and 16) where NFRs were measured in samples collected below the ODZ (≥500 m), rates were only detected at stations 9 and 16, and were lower than measurable rates within the ODZ at these sites (Fig. 4). O_2 concentrations at these stations remained low, below 150 μmol kg^{-1}, even in deep waters (Suppl. Table 2). At station 9, a NFR of 0.87 ±0.99 nmol N $L^{-1}d^{-1}$ (n=3) was measured at 1000 m; N_2 fixation was detectable but not quantifiable at 2000 m. Rates at station 16 exceeded those measured elsewhere by about an order of magnitude (9.88 ±3.85 nmol N $L^{-1}d^{-1}$ at 184 m and 35.9 ±12.0 nmol N $L^{-1}d^{-1}$ at 200 m, n=3), peaking at the top of the ODZ but remaining quantifiable to 3000 m (0.36 ±0.15 nmol N $L^{-1}d^{-1}$, n=3) (Fig. 4).

If low-O_2 conditions within the water column favor N_2 fixation, then one would expect NFRs to be commensurately higher within and around the ODZ than in other oceanic environments. Both within and below the OMZ at all sites, however, NFRs appeared patchy. Of the 51 sub-euphotic samples collected, N_2 fixation was only detected in 10 (Suppl. Table 2), and five of these were from one station, 16, located near the inner Revillagigedo Islands. NFRs previously reported in oxygenated, aphotic marine waters are typically on the order of 1 nmol N L^{-1} d^{-1} or lower (Moisander et al. 2017 and references therein). This rate is comparable with measurements presented here from within and below the ETNP OMZ including in ODZ waters, except for at station 16 (Suppl. Table 2; Fig. 4), suggesting that suboxic/anoxic conditions alone do not result in elevated sub-euphotic N_2 fixation in this region. This appraisal is consistent with work from Jayakumar et al. (2017) who previously observed few low rates (<1 nmol N L^{-1} d^{-1}) of N_2 fixation within the upper ETNP ODZ.

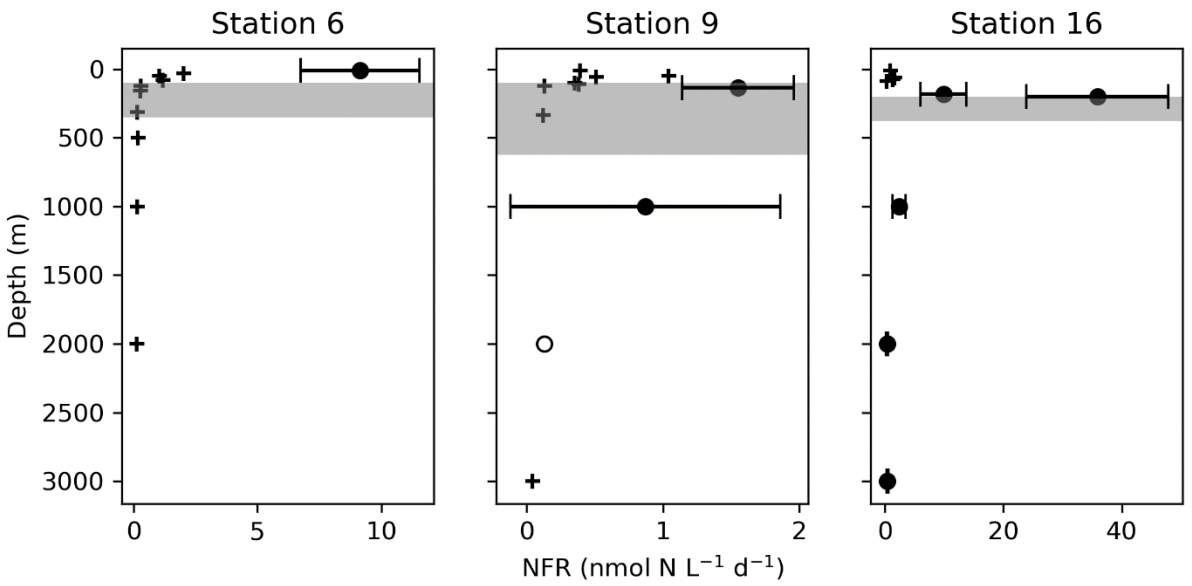

Figure 4. NFR profiles at stations 6 (inshore), 9 (southerly), and 16 (northerly, offshore). Black crosses, open circles, and filled circles represent rates that were below detection, detectable but not quantifiable, and quantifiable. For rate measurements below detection, the LOD was plotted; for non-quantifiable rates, the LOQ was plotted. Error bars for quantifiable rates represent the propagated error. The shaded region represents where core ODZ conditions (O_2 concentrations below detection and >0.5 μM NO_2^-) occurred. A deep profile of NFRs was also produced at station 12 (offshore), however, no N_2 fixation was detected at this site (Suppl. Table 2).

The patchy distribution of sub-euphotic N_2 fixation presented here contrasts with some observations from the ETSP ODZ. In the ETSP, Bonnet et al. (2013) reported that low (<1 nmol N L^{-1} d^{-1}) but persistent rates below the euphotic zone account for ~90% of total N_2 fixation. Similarly, Fernandez et al. (2011) estimated that the ODZ contributed about five times as much newly fixed N as oxic, euphotic waters. More recent work from Chang et al. (2019), which applied the same $^{15}N_2$ bubble removal method as this study, diverges from these accounts. Chang and

colleagues (2019) found no detectable NFRs below the euphotic zone. This stark difference may be partially the result of methodological disparities, including the erroneous assumption in earlier ODZ work (e.g., Fernandez et al. 2011) that atom-% ^{15}N of the initial PN pool is equivalent to atmospheric values which may inflate reported rate measurements (Chang et al. 2019; Voss et al. 2001). Whether the sub-euphotic environment contributes significantly to total regional N_r inputs also depends upon the manner in which detection limits are calculated given that even very small rates may be substantive when depth-integrated through a deep water column. Regardless, NFR measurements in sub-euphotic ETSP waters are largely within the range of those observed elsewhere in the ocean's interior (≤1 nmol N L^{-1} d^{-1}; Moisander et al. 2017 and references therein) and generally appear less patchy than those reported here from the ETNP.

Though NFRs were undetectable throughout most of the ETNP OMZ, dissolved organic C additions of either glucose or dissolved free amino acids (DFAA) stimulated N_2 fixation within all OMZ waters surveyed, including within the ODZ at stations 6 and 12 where NFRs were otherwise undetectable (Fig. 5a). This finding indicates that the ETNP OMZ hosts populations of diazotrophs capable of fixing N_2 in suboxic and anoxic waters, despite significant concentrations of ambient DIN. Additions largely failed to stimulate N_2 fixation below the OMZ (Fig. 5b). As energy-rich molecules, DFAA and glucose may enter both catabolic and anabolic pathways. Consequently, our findings could indicate that diazotrophic activity within the OMZ is limited by either energy or assimilable C.

DFAA additions stimulated NFRs at five of seven sampling locations within the OMZ, although this lacked statistical significance when compared across all sites (Wilcoxon signed rank,

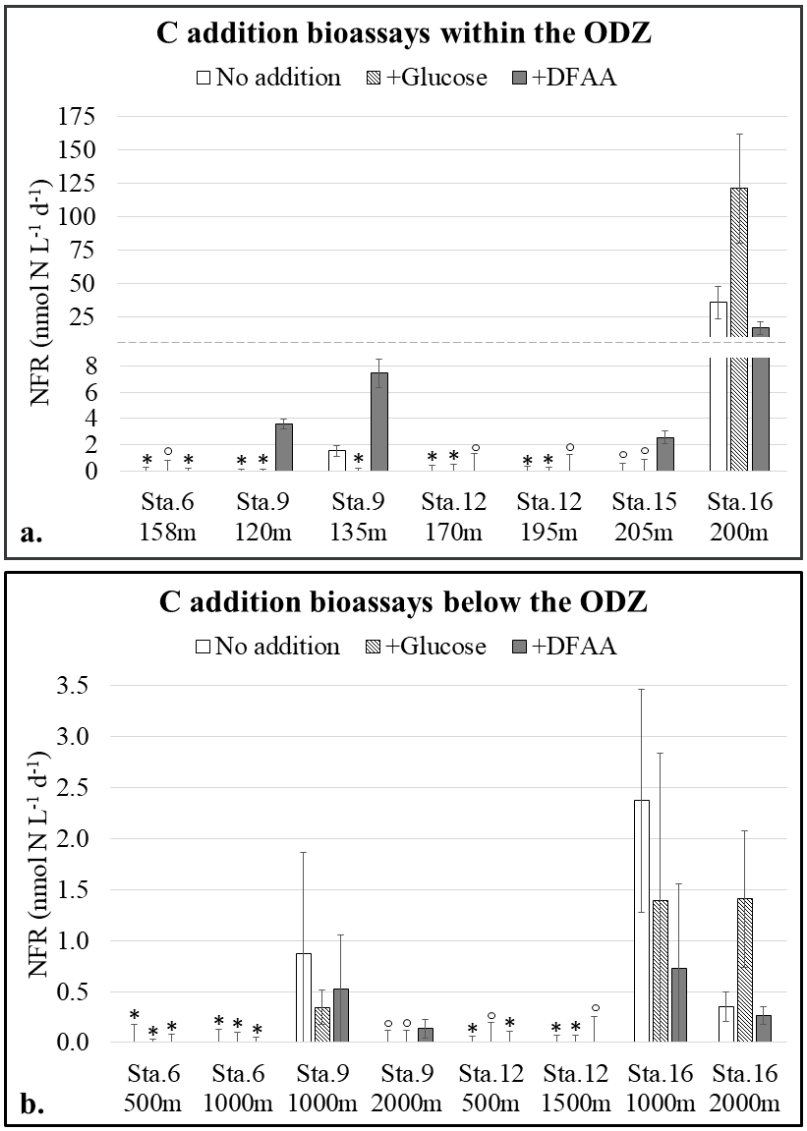

Figure 5. Results of carbon addition bioassay experiments within (a) and below (b) the OMZ. NFRs marked with an open circle were detectable but not quantifiable (DNQ). Stars indicate rates that were below the detection limit (BDL). For quantifiable rates, error bars express the propagated error. For DNQ rates, error bars express the limit of quantification calculated for that sample. Where no N_2 fixation was detected, the error bar marks the limit of detection. Neither additions of glucose nor dissolved free amino acids (DFAA) increased rates within ($n_1=n_2=7$) or below ($n_1=n_2=8$) the OMZ significantly when compared across all sites (Wilcoxon signed rank, $p>0.05$).

while glucose additions stimulated rates at certain depths at station 16 (Fig. 5). Within the ETSP ODZ, Bonnet et al. (2013) found that DFAA additions stimulated N_2 fixation in all ODZ waters surveyed while mixed carbohydrate or glucose additions only stimulated N_2 fixation at one-third of the stations surveyed. DFAA additions also enhanced N_2 fixation in the Red Sea (Rahav et al. 2013; 2015) and mesopelagic waters of the southwest Pacific Ocean (Benavides et al. 2015). These observations are perhaps surprising given that DFAA offer a source of N as well as C for heterotrophs and might thus be expected to suppress NFRs. If, however, DFAA were used in catabolic rather than anabolic (assimilatory) processes, organic N might be excreted in the form of a waste product. I hypothesize that site-specific differences in microbial response to DFAA and glucose additions are due to population-specific substrate preferences, variability in energy/C limitation, or both. Regarding the response of diazotrophic communities below the OMZ, lower temperatures can slow bacterial metabolic rates (Price and Sowers 2004) and decrease affinity for organic substrates (Nedwell 1999). The response of any diazotrophs present in deep waters may consequently have been dampened within the timeframe of incubations, or there are no diazotrophs present and active at this depth.

Our findings suggest that diazotrophs inhabit the ETNP region and fix N_2 at elevated rates in euphotic waters near the coast, but are largely inactive in OMZ and ODZ waters, as well as in the water column below, likely due to energy or C limitation at the OMZ depth horizon. In sub-euphotic waters, detectable NFRs were mostly on par with previous reports from oxygenated aphotic ocean waters (Moisander et al. 2017 and references therein). High NFRs were, however, observed within suboxic waters at one station, 16, located near volcanic islands, suggesting that non-cyanobacterial diazotrophs may thrive in DIN-replete waters given the right conditions. Here, NFRs were highest in suboxic waters and decreased below the ODZ (Fig. 4) following increased

O_2 concentrations (Suppl. Table 2) and decreased provision of organic C given that particulate C fluxes decrease with depth (Martin et al. 1987). High-carbon/low-oxygen conditions have previously been associated with increased activity of non-cyanobacterial diazotrophs (Severin et al. 2015) and further investigation into how these factors may affect the range and magnitude of non-cyanobacterial N_2 fixation is warranted.

CONCLUSIONS

Here, I present the most extensive dataset to date of N_2 fixation above, within, and below the ETNP ODZ. Our observation of high rates (>500 μmol N m^{-2} d^{-1}) at inshore stations supports the growing body of evidence that ocean margins contribute a greater amount of newly-fixed N than previously thought (Mulholland et al. 2019; Tang et al. 2019b). I hypothesize that continental inputs, inshore upwelling, or both alleviate growth limitation by an essential factor and play a key role in shaping the distribution of diazotrophs in N_r-deplete waters regionally. Furthermore, I speculate that diazotrophs residing near the coast (this study) and in marginal seas (White et al. 2013) where N_r-deplete waters upwell are important to basin-scale compensation of N_r-deficits generated in the ETNP ODZ and merit further investigation.

This study also demonstrates that sub-euphotic, suboxic waters in the region harbor diazotrophs capable of fixing N_2 despite high (>20 μmol N L^{-1} d^{-1}) ambient DIN concentrations, but their activity is highly patchy and appears C-limited. While it is known that ambient DIN does not necessarily preclude N_2 fixation (Knapp 2012), the observation of relatively high NFRs (>9 nmol N L^{-1} d^{-1}) in DIN-replete deep waters challenges the prevailing hypothesis that N cycle homeostasis is maintained, in part, by the occurrence of N_2 fixation where N_r is drawn down (Deutsch et al. 2007; Weber and Deutsch 2014). Further work is needed to elucidate the response

of diverse diazotrophic communities to DIN. Despite observation of patchy but high rates within and around the ETNP ODZ, N_2 fixation throughout the region appears too low to compensate for local N_r losses. This finding adds to the mounting evidence that N_r inputs and losses are spatially decoupled (Bonnet et al. 2013, 2017; Knapp et al. 2016, 2018; Weber and Deutsch 2014). By elucidating the distribution of N_2 fixation across physico-chemical gradients in an under-sampled but biogeochemically-important region, this study contributes to our evolving understanding of the factors that regulate marine N_2 fixation and the ocean's N_r inventory.

CHAPTER III

NFRS IN THE EASTERN TROPICAL SOUTH PACIFIC OXYGEN DEFICIENT ZONE: IMPLICATION FOR THE RANGE AND SENSITIVITY OF MARINE DIAZOTROPHS

PREFACE

A slightly edited version of this Chapter was submitted to *Limnology and Oceanography* for publication on August 17, 2020. The supplemental materials have been refined here for clarity. Please note that the approach applied here for estimating analytical error in NFR calculations differs from that used in Chapter II. A rational for this switch is offered in Suppl. Text 2.

INTRODUCTION

Nitrogen (N) limits productivity across a vast expanse of the ocean's surface (Moore et al. 2013). Consequently, N availability plays an important role in regulating ocean C cycling and global climate (Deutsch et al. 2004; Falkowski 1997; Karl et al. 2002). Unlike other important macronutrients such as SRP, N_r has biological sources and sinks capable of modulating the N_r pool in response to environmental forcings. N_r losses occur primarily in anoxic sediments and pelagic ODZs where NO_3^- respiration (denitrification) and anaerobic ammonium oxidation (anammox) are energetically favorable (Devol 2008). In contrast, the distribution and magnitude of oceanic N_2 fixation, the prokaryote-mediated conversion of relatively unreactive N_2 gas to N_r, remain poorly constrained because diazotrophic groups are ecologically diverse and can be metabolically flexible (Zehr and Capone 2020).

The ocean's largest pelagic ODZs occur in the ETNP and ETSP, and together account for roughly one-quarter of marine N_r loss (DeVries et al. 2012). When denitrified waters surface, DIN

is exhausted in advance of SRP, creating conditions thought to favor N_2 fixation (Deutsch et al. 2007; Weber and Deutsch 2014) because assimilation of NH_4^+ and NO_3^-, the primary forms of DIN available in the ocean, are typically less energetically-costly means of acquiring N (Falkowski 1983). The degree to which N_r inputs and losses are spatially coupled is hypothesized to be a function of the availability of dissolved iron (dFe), a key co-factor in the N_2 fixation enzyme nitrogenase (Bonnet et al. 2017; Weber and Deutsch 2014). This mechanism is believed to play a major role in balancing the ocean's N_r inventory (e.g., Weber and Deutsch 2014).

Direct observations of N_2 fixation (e.g., Knapp et al. 2018; Knapp et al. 2016) suggest that N_r inputs and losses are relatively decoupled due to dFe limitation in the ETSP (Dekaezemacker et al. 2013; Kondo and Moffett 2015; Weber and Deutsch 2014). Nevertheless, and despite significant concentrations of DIN (> 1 μM), ETSP waters harbor a diverse assemblage of predominantly non-cyanobacterial diazotrophs (Bonnet et al. 2013; Chang et al. 2019; Fernandez et al. 2011; Löescher et al. 2014) reported to actively fix N_2 at low, but persistent, rates throughout the water column (e.g., Bonnet et al. 2013; Fernandez et al. 2011). If this pattern held true throughout the ocean's interior, it would mean that sub-euphotic diazotrophs contribute a significant fraction (~6 – 32%) of the ocean's N_r inputs (Benavides et al. 2018). Moreover, the widespread occurrence of N_2 fixation under DIN-replete conditions would suggest that new N_r inputs (via diazotrophy) are either less sensitive to changes in the N_r inventory (via denitrification/anammox) than hypothesized (e.g., Weber and Deutsch 2014), or that our conception of the feedback process between them is incomplete.

Interpretation of NFR data from the ETSP and other mesopelagic systems has, however, been hampered by methodological issues associated with implementation of the $^{15}N_2$ tracer incubation approach (Montoya et al. 1996) where diazotroph activity is low (see discussion in

White et al. 2020). Using a more conservative approach to quantifying NFRs, I present a comprehensive examination of NFRs in the ETSP within the context of past work.

METHODS

Hydrographic data and sample collection

Samples were collected in January 2015, while aboard the R/V *Atlantis*. Vertical profiles of temperature, salinity, PAR, dissolved oxygen (O_2) and chl-a fluorescence were obtained using a Sea-Bird SBE 11plus CTD, equipped with a model 43 dissolved O_2 sensor, a QSP200L Biospherical PAR sensor, and a IT Labs ECO-AFL chlorophyll fluorometer. Samples for nutrient analysis were collected from Niskin bottles affixed to the CTD rosette and, within the ODZ, from a pump profiling system. Samples for NO_3^-+NO_2^- and SRP were syringe-filtered through a Sterivex filter (0.2 µm). Filtrate was collected and stored upright in acid-washed polyethylene bottles at -20°C until analysis at Old Dominion University using an Astoria-Pacific autoanalyzer and standard colorimetric protocols (Parsons et al. 1984). NO_2^- samples were filtered by gravity through a 0.2 µm Millipore filter directly from the Niskin bottles into acid-washed Falcon tubes. These samples were analyzed immediately using a manual colorimetric method on a Shimadzu (UV-1800) spectrophotometer (Pai et al. 1990). The LODs for NO_2^-, NO_3^-+NO_2^- and SRP analyses were 0.02, 0.14 and 0.03 µM (3σ, n = 7), respectively.

Oxic water samples for N_2 fixation incubations and PN enrichment and mass were collected in 10 L carboys from Niskin bottles mounted to the CTD rosette. Incubations from the shallow oxic zone were conducted in clear, 1.2 L PETG bottles in triplicate. Duplicate water samples were also filtered at the initial time point onto pre-combusted (450°C, 2 hrs) 0.3 µm glass fiber filters (GF-75, Advantec MFS Inc, Dublin CA, USA) to measure particulate C (PC)/PN concentration

and initial PN ^{15}N enrichment. These samples were frozen and stored at -20°C until analysis at Old Dominion University (see below).

Incubation samples from below the suboxic layer were collected directly from Niskin bottles into 4.3 L amber glass bottles. PC/PN samples were collected as described above. Within the suboxic layer, samples were pumped directly from depth into He-flushed 4.3 L amber glass bottles using a submersible water pump affixed to a small CTD as described by Selden et al. (2019). To limit O_2 contamination, bottles were first filled with sample then submerged in a ~50 L tub of ODZ water. Sample bottles were flushed continuously from the bottom to avoid back-flow from the tub until they had been filled three times over. With this set-up, a roughly 0.5 m thick layer of continuously replenished low-O_2 water covered the bottles as they flushed, preventing atmospheric O_2 contamination and maintaining *in situ* temperature as samples were collected.

NFR measurements

Incubation set-up. NFRs were determined using the bubble removal technique (e.g., Jayakumar et al. 2017), a modified version of the $^{15}N_2$ incubation-based assay of Montoya et al. (1996) that accounts for the slow dissolution time of N_2 gas (Mohr et al. 2010). In brief, approximately 1 or 4 mL additions (to 1.2 and 4.3 L incubation bottles, respectively) of pressurized, highly enriched (~99%, Cambridge Isotopes, Tewksbury MA, USA) $^{15}N_2$ was added to PETG or glass incubation bottles. Prior to these additions, incubation bottles were filled completely and any air bubbles were removed. Additions were made using a gas-tight syringe (VICI Valco Instruments Co., Houston TX, USA) through a silicon septa cap that allowed for small changes in volume. Sample bottles were gently inverted for 15 minutes using a seesaw, as described by Selden et al. (2019), to increase

the rate of gas dissolution. After mixing, the remaining gas bubble was removed using a syringe so that the $^{15}N_2$ enrichment of the seawater remained constant throughout the incubation period. Sample bottles were then incubated under approximate *in situ* light and temperature conditions.

For euphotic zone samples, incubation bottles were placed in on-deck incubators that were continuously flushed with surface seawater to maintain temperature. Appropriate light conditions, as determined using the CTD-mounted PAR sensor, were approximated using neutral-density screens. Samples collected below the euphotic zone were maintained in the dark, either in a walk-in cold van (~12°C) or refrigerator (~4°C), whichever more closely simulated ambient environmental conditions at the depths samples were collected. For samples collected below the suboxic zone, incubation bottles were placed in a dark, walk-in refrigerator (~4°C), where they were incubated for ~48 hours. All other samples were incubated for ~24 hours.

Contamination (^{15}N-labelled DIN) has been previously been reported for some commercially available $^{15}N_2$ stocks (Dabundo et al. 2014; White et al. 2020). While the purity of the tracer stocks used here were not directly tested, I note that this issue has never been reported for $^{15}N_2$ gas from Cambridge Isotope Laboratories. Additionally, after 24 and 48 hour incubations, generally little ^{15}N enrichment was detected in the particulate N pool (i.e., rates of N_2 fixation were largely undetectable, see Results and Discussion; Suppl. Table 3). It is thus highly unlikely that our stocks were contaminated.

At the end of the incubation, aliquots (6 ml) were transferred to He-flushed 12 ml Exetainers^{TM} using a gas-tight syringe (Hamilton 1000 series, Reno NV, USA) to determine the ^{15}N enrichment of the N_2 pool. To these samples, 50 µl of 50% w/v $ZnCl_2$ (Thermo Fisher Scientific, Waltham, MA) was added to ensure the termination of microbial activity. The remaining sample was immediately filtered on 0.3 µm glass fiber filters (GF-75, Advantec MFS

Inc, Dublin CA, USA). Filters were frozen and stored in sterile microcentrifuge tubes at -20°C until analysis at Old Dominion University. Exetainer samples were stored at room temperature until analysis at Princeton University. They did not undergo any significant pressure changes (e.g., from air shipping) during storage.

Sample analysis. $^{15}N_2$ gas samples were analyzed at Princeton University using a Europa 20-20 isotope ratio mass spectrometer (IRMS), following Jayakumar et al. (2017). $^{15}N_2$ enrichment in sample incubations ranged from 2.22 – 8.57 atom-% (mean = 3.64 ±0.04 atom-%, n = 159). Particulate samples, collected both from the environment (t=0) and from incubation bottles (t=f), were dried (50°C for ~2 days) and then pelletized in tin discs at Old Dominion University. ^{15}N enrichment of the PN pool and its mass were subsequently determined using a Europa 20-20 IRMS equipped with an automated N and C analyzer. Samples from initial (non-enriched) and final (potentially ^{15}N tracer-enriched) time points were pelletized separately, stored in separate desiccators, and analyzed separately to avoid carry-over contamination.

The LOD for PN mass was calculated separately for each run using 12.5 µg N standards (3σ, n = 7). The mean LOD among natural abundance instrument runs (n = 8) in this study was 2.06 µg N. Since the accuracy of enrichment analysis diminishes at lower mass (White et al. 2020) and low NFRs are sensitive to small variations in ^{15}N enrichment, I assumed a conservative lower linearity limit of 10 µg N based on instrument performance during the time samples were analyzed (Suppl. Fig. 2). This value is consistent with current "best practice" recommendations from the scientific community (White et al. 2020). If sample mass was below 10 µg N, ^{15}N enrichment data from that sample was discarded. A standard curve (1.17 – 100 µg N) was also run each day to verify measurement linearity.

NFR calculations. NFRs were calculated as described by Montoya et al. (1996; see Eqn. 1). If an $A_{PN_{t=0}}$ measurement was not available from the exact location of the incubation water, then the final PN concentration and the mean $A_{PN_{t=0}}$ within either oxic or suboxic waters (whichever was appropriate) were used in the calculation in place of the $[\overline{PN}]$ and direct $A_{PN_{t=0}}$ measurement.

N_2 fixation was considered detectable if $(A_{PN_{t=f}} - A_{PN_{t=0}})$ was greater than three times the standard deviation of seven 12.5 µg standards run daily with enriched ($A_{PN_{t=f}}$) samples (Ripp 1996). To calculate minimum detectable rates i.e., LODs, this minimum detectable enrichment value (mean = 0.0054 ±0.0026 atom-% across 11 IRMS runs) was substituted for $(A_{PN_{t=f}} - A_{PN_{t=0}})$ in Eqn. 1 (Jayakumar et al. 2017; White et al. 2020). Consequently, LODs scale with PN concentration. In this study, the mean and median NFR LOD were 3.00 and 1.09 nmol N L^{-1} d^{-1}, respectively.

NFRs were considered detectable at a given location if ^{15}N enrichment was detected in at least two replicate incubations. Where two replicates were deemed detectable but the third was not, a mean NFR was calculated by forcing the undetectable rate to zero (Bonnet et al. 2013; Chang et al. 2019). NFR error was assessed by taking the standard deviation of rates from replicate incubations (Suppl. Text 2). These values are provided in Suppl. Table 3. To ensure that detectable changes in $A_{PN_{t=f}}$ were due to diazotrophy, control incubations were conducted at a subset of stations (Suppl. Text 3; Suppl. Table 4).

RESULTS AND DISCUSSION

Regional hydrography

Our study area encompassed both offshore and nearshore waters. Upwelling, visible as a decrease in sea surface temperature (Fig. 6A), was apparent near the Peruvian coast during the

study period (January 2015). These cooler waters were associated with elevated surface chl-a (Fig. 6B) and high surface nutrient concentrations. At the shallowest (<750 m depth) and most nearshore stations, the concentrations of DIN and SRP exceeded 14 and 1 µM, respectively, in the upper 10 m (stations 13, 16 and 19; Suppl. Fig. 3A-B). Surface DIN and SRP concentrations were slightly lower at other nearshore stations (stations 12, 14, 15, and 18), and decreased to <4 and <0.7 µM, respectively, at most offshore stations.

Suboxia (<20 µmol O_2 kg^{-1}) was detected at all stations. The suboxic layer shoaled to an average depth of 80 m among nearshore stations (12-19; Suppl. Fig. 3D). Here, the thermocline was shallower and stronger (Suppl. Fig. 3E). At offshore stations to the south (>16.5°S, stations 1-5), the suboxic layer was generally thinner particularly at stations 4 and 5, the latter of which

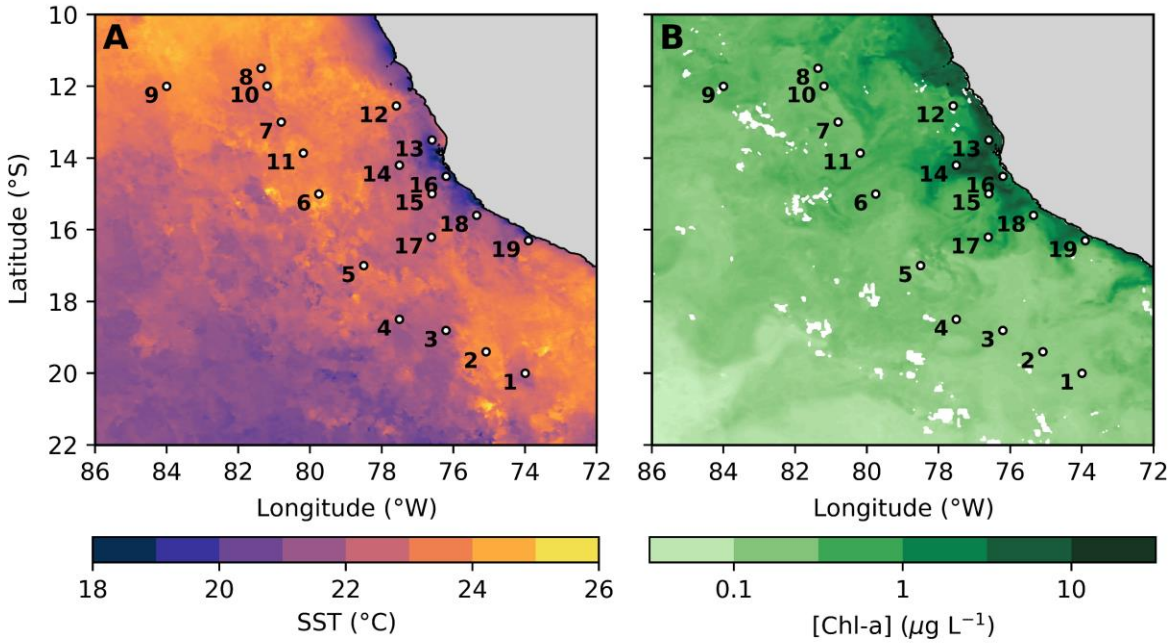

Figure 6. Mean MODIS (NASA Goddard Space Flight Center 2018 Reprocessing) sea surface temperature (A) and chl-a concentration (B) for January 2015 overlain by stations.

was atop the Nazca Ridge. The average suboxic layer thickness at the southern stations was 360 m compared to averages of 640 and 540 m among northern offshore (<16.5°S, stations 6-11) and nearshore stations, respectively. Functionally anoxic conditions were observed in the upper suboxic layer at all stations except station 5, as indicated by NO_2^- concentrations in excess of 0.5 µM (Thamdrup et al. 2012). For offshore stations (stations 1-11), these conditions occurred between ~100 and 380 m depth.

Distribution of N_2 fixation in the ETSP ODZ

I assessed NFRs in 61 samples collected within the oxic (> 20 µmol kg^{-1} O_2), euphotic waters, 59 samples collected within suboxic waters, and five samples collected in oxic waters beneath the ODZ. Of these, N_2 fixation was detected in only eight samples (Fig. 7, Suppl. Table 3), five from two stations at the southern end of our study site (stations 18 and 19, 5 depths), one from a particularly productive site (depth-integrated chl-a: 36.7 mg m^{-2}, particulate C: 20 – 65 µM) slightly offshore (station 14, 1 depth), and two from an offshore site (station 1). Where detectable, NFRs were low (Suppl. Table 3). By applying a conservative LOQ (Selden et al. 2019), calculated by propagating a minimum quantifiable change in A_{PN} (10σ, n = 7 12.5 µg standards; Ripp 1996) through Eqn. 1, I assert that even the detectable NFRs reported here cannot be accurately quantified. The LOQs where N_2 fixation was detected ranged from 0.4 to 1.4 nmol N L^{-1} d^{-1} (Suppl. Table 3), representing an upper bound on NFRs. In contrast, LODs, i.e., the lower bounds for these rate measurements, ranged from 0.09 to 0.3 nmol N L^{-1} d^{-1} (Suppl. Table 3).

Seven of the locations where NFRs were detected were within suboxic waters. At all but one of these (station 18, 100 m), NO_2^- concentrations exceeded 0.5 µM suggesting functional anoxia (Thamdrup et al. 2012). The eighth and final detectable rate occurred along a shallow

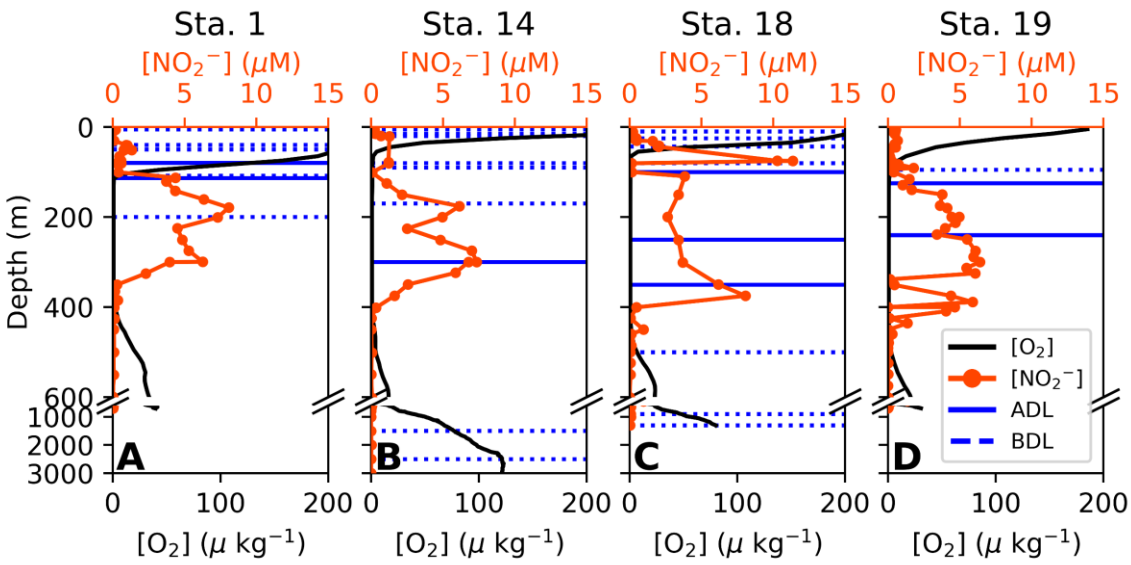

Figure 7. Sites at which N_2 fixation was detected. Solid and dashed blue lines indicate the depths at which N_2 fixation rates were above (ADL) and below the detection limit (BDL), respectively. NO_2^- (red line) and dissolved oxygen (O_2; black line) profiles indicate the extent of the ODZ at each station.

oxycline (station 1, 80 m). Our observation that N_2 fixation is restricted to the upper oxycline/ODZ is consistent with prior reporting of a broad NFR peak (<0.4 nmol N L^{-1} d^{-1}) across the oxycline and upper ODZ at nearshore stations (Löescher et al. 2014). Similarly, Chang et al. (2019) observed an increase in *nifH* concentrations within the ODZ, and Löescher et al. (2014) noted that the majority of the *nifH* sequences that they recovered were from within ODZ waters. Theoretical calculations suggest that N_2 fixation may offer a slight energetic advantage over NO_3^- assimilation in anoxic zones where the cost of shielding nitrogenase from oxidative damage is minimized (Großkopf and LaRoche 2012). However, given the limited range and low levels of N_2 fixation reported here, I proffer that diazotrophs active in the ETSP ODZ are unlikely to represent a significant source of N_r locally.

In contrast to our findings, Chang et al. (2019), whose experimental approach was most similar to that employed here, did not detect N_2 fixation within the ODZ. NFRs may have been affected by differences in organic matter availability to heterotrophic diazotrophs during austral winter (Chang et al. 2019) versus austral summer (Bonnet et al. 2013; this study; Löescher et al. 2014). Organic C additions have been observed to increase NFRs in sub-euphotic O_2-deplete waters (Bonnet et al. 2013; Löescher et al. 2014; Selden et al. 2019). During austral winter, surface productivity is lower (Pennington et al. 2006) due to reduced upwelling (Fiedler and Talley 2006) and the supply of organic C to heterotrophic diazotrophs is consequently diminished. Additionally, Chang et al. (2019) collected low-O_2 incubation water from Niskin bottles, rather than via pumping, as I did in this study, which could have resulted in O_2 contamination and consequent changes in microbial community structure and metabolism (see discussion below).

I observed elevated NFRs at two nearshore stations, as has been noted in other eastern boundary upwelling environments (Selden et al. 2019; Sohm et al. 2011). This finding may reflect alleviation of growth limitation by elements such as Fe due to continental inputs. While aeolian Fe inputs to the ETSP are low (Albani et al. 2014), Fe-limitation of N_2 fixation may be relieved by remobilization of sedimentary Fe(II) (Cutter et al. 2018; Scholz et al. 2016) and subsequent regeneration/recycling (Hutchins et al. 1993). Löescher et al. (2014) observed very high NFRs at one nearshore station (between stations 12 and 13 in this study) where the sulfide/NO_2^- transition was remarkably shallow (~30 m) and dFe concentrations exceeded 150 nmol kg^{-1} at the surface. Similarly, Selden et al. (2019) observed high NFRs (>9 nmol N L^{-1} d^{-1}) in the ETNP ODZ associated with a subsurface dFe plume (J. Moffett, personal communications). N_2 fixation within the ETSP ODZ may thus be tied to temporal variability affecting Fe cycling.

Interpretation of low NFRs

Overestimation. The potential for low NFRs in deep, sub-euphotic environments (Benavides et al. 2018; Moisander et al. 2017) has instigated reconsideration of how to apply the $^{15}N_2$ tracer assay in pelagic environments (White et al. 2020). NFR methodology in the ETSP ODZ has therefore varied (Table 3), complicating comparisons between studies. NFRs may be overestimated when the natural abundance of ^{15}N in the PN pool (i.e., $A_{PN_{t=0}}$) is assumed rather than measured, when the mass of PN on the filter is too low (e.g., < 10 μg N), and/or NFR LODs are not calculated based on instrument performance (see White et al. 2020 for comprehensive discussion).

Some studies assume that $A_{PN_{t=0}}$ is in equilibrium with atmospheric N_2 (0.3663 atom-%). This is a poor assumption within and around denitrified waters and in many environments where the dissolved N_r pool is highly dynamic; I observed a mean $A_{PN_{t=0}}$ of 0.3692 ±0.0018 atom-% (n = 146) throughout all surveyed waters at the time of our study. The difference between these values would have constituted detectable enrichment in about one-third of our IRMS runs in this study. Moreover, the mean natural abundance of ^{15}N in PN is typically greater in suboxic waters than in the overlying waters (Chang et al. 2019; this study; Voss et al. 2001). Consequently, the use of surface $A_{PN_{t=0}}$ measurements for NFR incubations conducted with suboxic water may result in the over-estimation of rates from deeper waters. In January 2015, $A_{PN_{t=0}}$ was significantly different between suboxic (0.3700 ±0.0016 atom-%, n=44) and oxic waters (0.3690 ±0.0017 atom-%, n=94; one-way ANOVA, df = 136, F = 11.85, p = 0.0002 based on 10,000 random permutations). These values are consistent with those reported by Chang et al. (2019) in July 2011, suggesting low seasonal/inter-annual variability.

The mass of PN collected on the filter at the end of the incubation is also crucial for accurate instrument detection. When sample mass is too low, typically below ~10 μg N, isotope ratio

measurements often drift (Suppl. Fig. 2; White et al. 2020). Either positive drift in $A_{PN_{t=f}}$ or negative drift in $A_{PN_{t=0}}$ may falsely inflate NFRs. Even when mass is sufficiently high, analytical variability may affect the relative difference between $A_{PN_{t=0}}$ and $A_{PN_{t=f}}$, necessitating the determination of a minimum detectable difference in A_{PN} based on instrument variability (e.g., 3σ of standards) from which a NFR LOD can be calculated (White et al. 2020). As variability is a function of mass (Suppl. Fig. 2; White et al. 2020), a conservative minimum detectable difference would be one based on the variability of standards at the lower end of the sample mass range. Where reported, minimum detectable differences in enrichment for ETSP studies vary by ~10x (Table 3). I note that calculating NFR uncertainty as the standard deviation of rates from replicate incubations does not constrain variability in $A_{PN_{t=0}}$, complicating inter-comparisons of low rates (Suppl. Text 2).

Underestimation. NFRs may be underestimated because of slow $^{15}N_2$ equilibration (Mohr et al. 2010) when employing the traditional bubble method (Montoya et al. 1996), inappropriately large filter pore-size in systems with small diazotrophs (Bombar et al. 2018), drift in A_{PN} measurements at low mass (see above), and/or inhibition of low O_2-adapted organisms by O_2 contamination during sampling. Löescher et al. (2014) found that O_2 exposure (10 µM) in ODZ incubations reduced the abundance of *nifH* associated with some non-cyanobacterial diazotrophs. While O_2 exposure is minimized by collecting samples using a submersible pump (as deployed in this study), even minor shifts in O_2 and substrate availability, temperature and pressure can alter the activity of ODZ microbial communities (Stewart et al. 2012). Most studies from the ETSP have attempted to address the issue of O_2 contamination (Table 3); however, the efficacy of different approaches and the effect of O_2 intrusion on NFRs in suboxic waters, has not been assessed.

Table 3. Volumetric NFRs reported from the ETSP ODZ region.[a]

Reference	Date	Depth range	Mean NFR or range (nmol N L^{-1} d^{-1})	Sample collection	Method[b]	Filter size	Incub. volume (L)	Minimum filter mass (µg N)	Minimum detectable enrichment	$A_{PN_{t=0}}$[c] measured directly?
Fernandez et al. 2011	Oct./Nov. 2005	Surface	0.89 ±0.08 (n = 17)	Niskin[f]	TBM	0.7 GF/F	2	Not reported[i]	Not reported	Not reported
		Upper oxycline	0.075 ±0.07 (n = 8)							
	Feb. 2007 (ENSO)	Surface	0.66 ±0.7 (n = 10)							
		Upper oxycline	1.71 ±1.03 (n = 17)							
		Upper ODZ (<400 m)	1.27 ±1.2 (n = 13)							
Bonnet et al. 2013	Feb./March 2010 (ENSO)	Surface – 2000 m	BDL – 0.80 (n = 40)	Niskin[g]	TBM[h]	0.7 GF/F	4.5	3.8[j]	0.0005 atom-%, (3σ, n = 10 IAEA reference samples)	No[m]
	March/April 2011 (La Nina)	Surface – 2000 m	BDL – 0.26 ±0.12 (n = 216)							Yes
		Below ODZ (400 – 2000 m)	0.00 ±0.01 – 0.21 ±0.13							
Dekaezemacker et al. 2013	Feb./March 2010 (ENSO)	Surface – 200 m	<0.06 – 0.88	Niskin[g]	TBM[h]	0.7 GF/F	4.5	2.9[j]	0.0005 atom-%, (3σ, n = 10 IAEA reference samples)	Surface only
	March/April 2011 (La Nina)	Surface – 200 m	BDL – 0.87							Yes
Löscher et al. 2014	Jan./Feb. 2009	Surface	<24.8 ±8.4	Niskin	TBM	0.7 GF/F	2	~3[k]	Not reported	Yes
		Oxycline to ODZ (~40 – 350 m)	<0.4	Pump[g]						

[a]Geographic distribution of studies displayed in Fig. 8.
[b]TBM and BRM refer to the traditional bubble method (Montoya et al. 1996) and the bubble removal method (Jayakumar et al. 2017), respectively.

Table 3. *Continued.*

Reference	Date	Depth range	Mean NFR or range (nmol N L^{-1} d^{-1})	Sample collection	Method[b]	Filter size	Incub. volume (L)	Minimum filter mass (µg N)	Minimum detectable enrichment	$A_{PN_{t=0}}$[c] measured directly?
Knapp et al. 2016	Feb./March 2010 (ENSO)	Surface – 180 m	0.25 ±0.11 – 0.54 ±0.72[d]	Niskin	TBM	0.7 GF/F	4	10	Not reported[l]	Yes[n]
	March/April 2011 (La Nina)	Surface – 150 m	0.15 ±0.16 – 0.41 ±0.15[d]							
Chang et al. 2019	July 2011	Euphotic zone	BDL – 3.9	Niskin[f]	BRM	0.7 GF/F	2.5	2	0.0025 (3σ, n = 7 12 µg N standards)	Yes
		Upper ODZ (<400 m)	BDL				5			
This study	Jan. 2015	Upper oxic waters	BDL	Niskin	BRM	0.3 GF75	1.2	10	Mean = 0.0054 ±0.0026 atom-% (3σ, n = 7 12.5 µg N standards)	Yes[o]
		ODZ (~100 - 700 m)	BDL – 0.8[e]	Pump[g]	BRM		4.3			Yes[p]
		Below ODZ	BDL	Niskin[g]	BRM		4.3			Yes[o]

[c]$A_{PN_{t=0}}$ refers to ^{15}N-PN atom-% enrichment.
[d]Average volumetric rates per station; these values were calculated by dividing reported areal rates (µmol N m^{-2} d^{-1}) for each station by the integration depth.
[e]If a limit of quantification (10σ, n = 7 12.5 ug standards) is applied, then all detectable rates would be considered too low to quantify (<0.4 - 1.4 nmol N L^{-1} d^{-1})
[f]Care taken to avoid O_2 contamination in low-O_2 samples by filling evacuated gas-tight bags.
[g]Care taken to avoid O_2 contamination in low-O_2 samples by flushing and filling bottles from the bottom.
[h]Bottles shaken after $^{15}N_2$ addition to increase rate of gas dissolution.
[i]In order to achieve a minimum mass of 10 µg N, ambient PN concentration would need to be >0.36 µM given a filtration volume of 2 L. While mean PN concentrations in the region within the upper 400 m typically exceed this threshold, lower values are often observed, particularly < ~150 m.
[j]IRMS linearity verified via Fisher test ($p < 0.01$).
[k]Authors reported that most samples exceeded 10 µg N.
[l]Authors reported "reproducibility" (σ) as equal to 0.0001 atom-%.
[m]$A_{PN_{t=0}}$ assumed to be in equilibrium with atmospheric N_2 (0.3663 atom-%).
[n]The mean ^{15}N-PN enrichment in the upper water column was used as $A_{PN_{t=0}}$ for NFR calculations.
[o]Mean ^{15}N-PN enrichment within oxic waters was used as $A_{PN_{t=0}}$ when direct measurement was not available (e.g., when mass of collected sample was insufficient).
[p]Mean ^{15}N-PN enrichment within suboxic (<20 µmol kg^{-1}) waters used as $A_{PN_{t=0}}$ when direct measurement was not available.

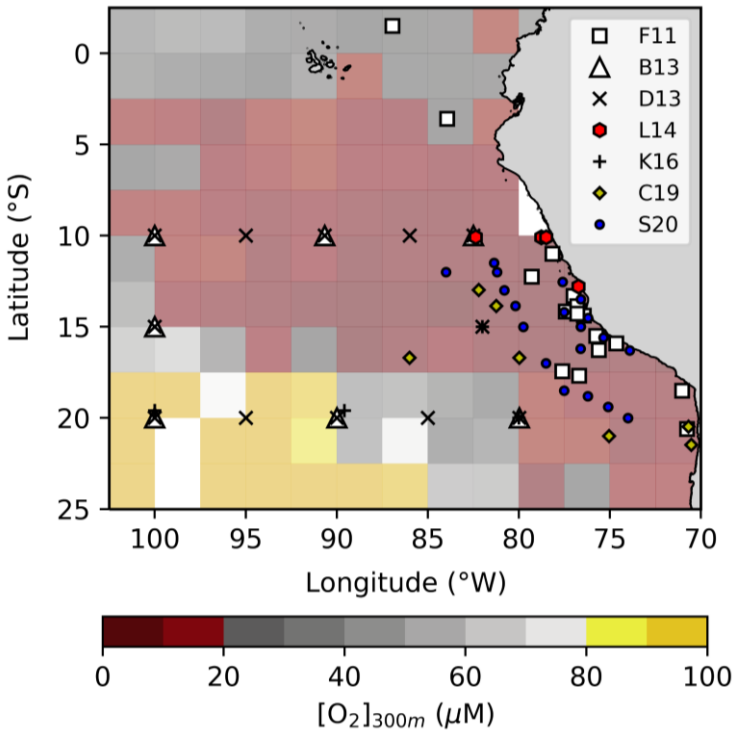

Figure 8. Sites where NFRs have been measured overlying World Ocean Atlas mean dissolved oxygen concentration ($[O_2]$) at 300 m (Garcia et al. 2018), binned per 2.5°. F11 = Fernandez et al. 2011; B13 = Bonnet et al. 2013; D13 = Dekaezemacker et al. 2013; L14 = Loescher et al. 2014; K16 = Knapp et al. 2016; C19 = Chang et al. 2019; S20 = this study.

Summary. Given the issues outlined here, I proffer that some previous studies in the ETSP may have over-estimated NFRs there. Further, depth-integration of rates near the analytical LOD can result in high areal estimates of N_2 fixation, making it essential that NFR error is accurately calculated and propagated (Suppl. Text 2). In addition to the methodological differences outlined above (Table 3), discrepancies among NFRs in surface waters between this and previous studies may also be attributable to the differences in the geographic ranges among studies; Bonnet et al. (2013), Dekaezemacker et al. (2013) and Knapp et al. (2016) all focused on the periphery of the

South Pacific Subtropical Gyre, further offshore than this study (Fig. 8). However, given that sub-euphotic diazotrophs typically respond to organic matter inputs suggestive of heterotrophic C limitation (Bonnet et al. 2013; Löescher et al. 2014), I consider it unlikely that sub-euphotic NFRs would be higher further offshore than beneath relatively more productive upwelling waters. Ultimately, differentiating detectable and undetectable NFRs with sensitivity has far-ranging implications for our understanding of oceanic N budgets and N_2 fixation in marine systems.

CONCLUSIONS

Our conservative evaluation of NFRs in the ETSP ODZ contradicts previous reports of low but persistent NFRs throughout the region (Table 3), which are often cited in support of the hypothesis that N_2 fixation is widespread in the ocean's interior (Benavides et al. 2018). Instead, our work suggests that N_2 fixation in this region is sparse and restricted to low O_2 waters in the upper ODZ. Our findings support the idea (Bombar et al. 2016; Großkopf and LaRoche 2012) that ODZs may favor N_2 fixation by non-cyanobacterial diazotrophs despite significant concentrations of ambient DIN.

CHAPTER IV

A COASTAL N_2 FIXATION HOTSPOT AT THE CAPE HATTERAS FRONT: ELUCIDATING SPATIAL HETEROGENEITY IN DIAZOTROPH ACTIVITY VIA SUPERVISED MACHINE LEARNING

PREFACE

A slightly edited version of this Chapter is currently undergoing peer-review for publication in *Limnology and Oceanography* (submitted August 3 2020).

INTRODUCTION

An essential element for life, N is often the nutrient limiting biological productivity in the surface ocean (Moore et al. 2013). The predominant form of N on Earth is N_2 gas, which is highly abundant but thermodynamically stable. Consequently, it is not readily accessible to organisms as a source of N. However, a select group of organisms, diazotrophs, can enzymatically mediate its reduction to an assimilable form of N. N_2 fixation may subvert N limitation and thus significantly contribute to new production by supplying biological systems with bioavailable N (e.g., Capone et al. 2005).

Marine N_2 fixation has historically been ascribed to the warm, well-lit surface waters of subtropical and tropical ocean basins where concentrations of dissolved inorganic N (e.g., NO_3^- plus NO_2^- (N+N) and ammonium) are at or near the limits of analytical detection (Carpenter and Capone 2008). Such conditions foster the growth of *Trichodesmium*, a well-studied and globally significant filamentous cyanobacterial diazotroph (Capone et al. 2005). *Trichodesmium* forms macroscopic colonies in the surface ocean that are easy to identify and manipulate. Consequently,

Trichodesmium was one of the first marine diazotrophs to be established in stable culture (Prufert-Bebout et al. 1993). Bias towards *Trichodesmium* in the study of marine N_2 fixation and diazotroph physiology has inadvertently led to the conflation of its niche preferences with those of other pelagic diazotrophs (e.g., Knapp 2012). However, recent work (Zehr and Capone 2020 and references therein) suggests that the ecophysiology of diverse diazotrophic clades is not so generalizable.

Aided by methodological advances in molecular biology, research in the past decade has expanded the known range of pelagic N_2 fixers to include temperate (e.g., Moisander et al. 2010) and Arctic ocean basins (e.g., Blais et al. 2012), dark and N-rich mesopelagic waters (e.g., Rahav et al. 2013), and eastern boundary upwelling systems (e.g., Selden et al. 2019). Moreover, high NFRs have been observed in tropical (e.g., Grosse et al. 2010) and temperate (e.g., Mulholland et al. 2012; Fonseca-Batista et al. 2019) coastal systems where they can drive productivity (e.g., Hunt et al. 2016). In the North Atlantic Ocean, the magnitude of NFR tends to increase with proximity to the North American continent (Tang et al. 2019b), flouting the historical paradigm that significant NFRs are restricted to the oligotrophic ocean. Indeed, direct NFR measurements indicate that these coastal waters can contribute significantly to basin-wide fixed N inputs. Recently, Mulholland et al. (2019) estimated that the continental shelf extending from the Mid-Atlantic Bight (MAB) to the Gulf of Maine alone adds 0.02 Tmol N yr^{-1} to the North Atlantic Ocean. Though this region represents only 6.4% of the total North Atlantic continental shelf, this N input is equivalent to previous estimates for the entire shelf area (Nixon et al. 1996).

High NFRs (>100 nmol N L^{-1} d^{-1} or >1000 µmol N m^{-2} d^{-1}) in cooler, temperate North Atlantic coastal waters have been associated primarily with the haptophyte-symbiont UCYN-A and diatom-diazotroph assemblages (DDAs) (Fonseca-Batista et al. 2019; Mulholland et al. 2019;

Tang et al. 2019b). Non-cyanobacterial diazotrophs may also be active in these waters, although they have not been associated with high NFRs (Fonseca-Batista et al. 2019; Mulholland et al. 2019). *Trichodesmium* has also long been observed in the MAB and South Atlantic Bight (SAB), which are subject to inputs from the warm and oligotrophic Gulf Stream (GS; e.g., Mulholland et al. 2012; Mulholland et al. 2019; Tang et al. 2019b). Delimiting the distribution and magnitude of N_2 fixation on regional to global scales will require insight into the range and sensitivity of distinct diazotrophic assemblages in disparate but connected marine environments. Moreover, understanding the factors regulating marine diazotrophy on local to regional scales will require more sophisticated characterization of the spatial and temporal heterogeneity of N_2 fixation than can be gleaned from direct rate measurements alone.

This study sought to characterize the distribution of N_2 fixation and diazotrophic populations across the western North Atlantic Ocean margin, where warm SAB shelf and GS waters interact with cooler MAB shelf waters. As NFR measurements are highly labor-intensive, a supervised machine learning algorithm was applied to augment their spatial coverage throughout the region at the time of the study. This approach facilitates examination of N_2 fixation spatial heterogeneity and offers insight into the physical and chemical factors affecting its distribution and magnitude in a coastal frontal regime.

METHODS

Sample collection

Samples were collected aboard the research vessel (*R/V*) *Hugh R. Sharp* in August, 2016, along eight transects (Fig. 9) extending across the northwestern mid-Atlantic continental shelf (33.3 to 37.7°N). The study area crossed the continental shelf and slope to the north (MAB) and

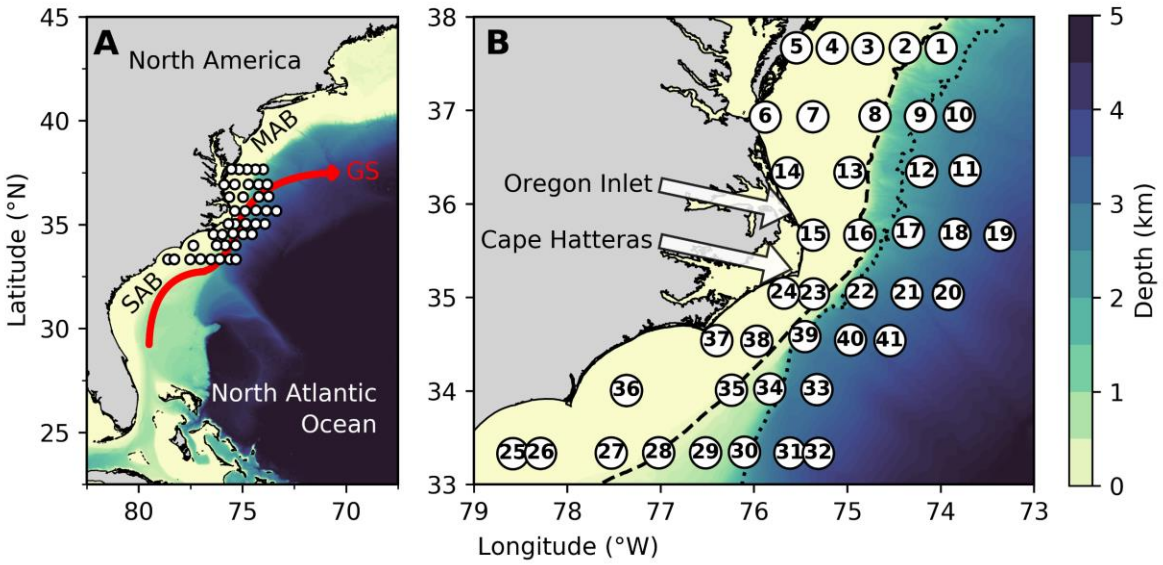

Figure 9. Study region (A) and labelled station map (B) overlying ETOPO1 1 Arc-Minute Model bathymetry (Amante and Eakins 2009). In Panel A, the solid red line indicates the approximate path of the Gulf Stream (GS). In B, the dashed and dotted lines indicate the 200 and 2000 m isobaths, representing the edges of the shelf and slope, respectively.

south (SAB) of Cape Hatteras, NC (Fig. 9B), where the GS separates from the shelfbreak. Water samples were collected from Niskin bottles mounted to a rosette, which was equipped with a SeaBird Electronics 911plus conductivity, temperature and depth (CTD) sensor package and a chl-a (chl-a) fluorometer (ECO-AFL/FL, IT Labs).

Nutrient determination

Samples for nutrient analyses were filtered directly from the Niskin bottles using a 0.2 μm Supor membrane cartridge filter (AcroPak 1500^{TM}, PALL corp.) into sterile 15 ml Falcon^{TM} tubes and analyzed on-board. N+N, NO_2^- and soluble reactive phosphorus (SRP) concentrations were determined colorimetrically using an Astoria Pacific nutrient autoanalyzer, according to

manufacturer specifications (Parsons et al. 1984). The detection limits for N+N and SRP were 0.14 and 0.04 μM (3σ, $n = 7$), respectively.

NFR measurements

NFRs were quantified using a modified version of the $^{15}N_2$ tracer method (Montoya et al. 1996) known as the bubble removal or bubble release technique (Selden et al. 2019; White et al. 2020). This approach addresses the issue of slow N_2 gas dissolution (White et al. 2020)—which may result in rate underestimation—by removing undissolved N_2 after a mixing period. The $^{15}N_2$ enrichment of the dissolved N_2 pool is then measured directly. White et al. (2020) provide a thorough description and discussion of this approach.

N_2 fixation incubations. Whole water was collected from Niskin bottles directly into 10 L LDPE carboys. Carboys were covered with mesh screens during daytime sample collection to avoid light-shocking microbes. To measure rates of NFR, triplicate PETG bottles (0.5 – 2 L) were rinsed and filled completely from carboys. Incubations were initiated by injecting tracer-level (~10% by vol.) $^{15}N_2$ gas (~99% ^{15}N, Cambridge Isotope Laboratories, Inc., Tewksbury, MA, USA) through a silicon septa using a gas-tight syringe (VICI Precision Sampling, Baton Rough, LA, USA). Samples were mixed gently for 15 minutes to aid gas dissolution as described in Selden et al. (2019). At the end of mixing, any remaining bubble was removed using a syringe. Incubation bottles were then transferred to on-deck incubators equipped with flow-through seawater and screens to maintain approximate temperature and light conditions.

While concerns have been raised regarding contamination by some commercially available $^{15}N_2$ stocks leading to false positives (Dabundo et al. 2014; White et al. 2020), this issue has never

been reported for $^{15}N_2$ gas from Cambridge Isotope Laboratories. Furthermore, for each $^{15}N_2$ gas tank used in this study, ^{15}N enrichment of the PN pool was undetectable in some samples despite significant plankton biomass, which would not have been possible if ^{15}N-labelled DIN were present. I are therefore confident that the rates presented here did not result from ^{15}N contamination of gas stocks. All incubations lasted approximately 24 hours and so represent daily rates.

Sample processing, storage and analysis. After the ~24 hour incubation period, a 6 ml aliquot from each incubation bottle was transferred to a 12 ml He-purged Exetainer™ using a gas-tight syringe (Hamilton Co., Reno, NV, USA). To prevent microbial activity in exetainers, 50 µl $ZnCl_2$ (50% w/v) was also injected. Samples were stored upside-down, such that the liquid rather than the gas was in contact with the septum, and ground-shipped to Princeton University for analysis. The isotopic enrichment of the N_2 gas was measured on a Europa 20/20 Isotope Ratio Mass Spectrometer (IRMS) in continuous flow mode within 2.5 months of sample collection. The remaining sample was filtered onto pre-combusted (450 ºC for 2 hours) 0.3 µm GF75 glass fiber filters (Advantec MFC, Inc., Dublin, CA, USA) and stored frozen (4°C) until analysis at Old Dominion University (ODU).

Analyte can be lost from gas samples stored in Exetainer™ vials due to leakage on monthly timescales (Laughlin and Stevens 2003). Absolute N_2 mass in the exetainers is not pertinent to Eqn. 1. However, the intrusion of isotopically light atmospheric N_2 into vials can dilute the isotopic enrichment of sample N_2 (White et al. 2020). While $^{15}N_2$ samples in this study were not stored submerged, as is advisable (White et al. 2020), exetainers were over-pressurized relative to the atmosphere. Consequently, gas intrusion was likely minor.

Triplicate samples were collected to measure the ambient ^{15}N enrichment and mass of PN. These samples were filtered onto pre-combusted (450 ºC for 2 hours) 0.3 μm GF75 glass fiber filters and stored frozen (4°C) until analysis at ODU. Ambient PN sample were processed and analyzed separately from isotopically-enriched samples in order to avoid contamination.

Samples for initial and final PN enrichment and mass were analyzed at ODU on a Europa 20/20 IRMS equipped with an automated nitrogen and carbon (ANCA) preparation module. The linearity of the IRMS response was evaluated daily using standards ranging from 1.17 to 100 μg N. Samples with filter mass below the lowest standard in the linear range on the day they were run were discarded.

Rate calculation. NFRs were calculated using Eqn. 1 (Montoya et al. 1996). Here, I used the initial PN mass to calculate [PN] rather than the mean value across time because initial PN volume was measured with greater accuracy and precision than that at the final time point. If the $^{15}N_2$ sample enrichment was < 2.0 atom-% for a given incubation, no rate was calculated. If the $^{15}N_2$ sample for a given incubation was lost or damaged, the mean enrichment achieved across the study (5.14 ±2.03 atom-%) was used to calculate NFR.

As shown in Eqn. 1, NFRs are a function of both the relative importance of N_2 to PN turnover and the absolute amount of PN in a given sample. To facilitate intersystem comparison of diazotroph activity, the specific uptake rate (SUR) of N_2 by particles in the incubation bottle is therefore also reported (Eqn. 2).

$$SUR = \frac{A_{PN_{t=f}} - A_{PN_{t=0}}}{A_{N_2} - A_{PN_{t=0}}} \times \frac{1}{time} \qquad \textit{Equation 2.}$$

This value can be conceptualized as the relative activity of diazotrophs within a water parcel, or as the inverse of PN turnover time if, hypothetically, all PN were diazotroph-derived (Glibert and Capone 1993).

The error reported is the standard deviation of three replicate incubations. LODs were calculated for each individual rate following Eqn. 3. The minimum detectable difference between initial and final PN ^{15}N atom-% ($\mathrm{min}\Delta A_{PN}$) is assumed to be equal to three times the standard deviation of eight 12.5 µg N standards measured daily alongside samples (White et al. 2020).

$$LOD = \frac{min\Delta A_{PN}}{(A_{N_2} - A_{PN_{t=0}})} \times \frac{[PN]}{time} \qquad \textit{Equation 3.}$$

Statistics

Replicated rate measurements were grouped by locality and compared via one-way ANOVA. Significance was determined by comparing the computed test statistics (F values) to those derived from 10,000 random permutations of the data. This approach is robust regardless of whether the residuals of the data are normally distributed (Manly 2006).

***nifH* sequencing and quantification**

The diazotroph communities present during the study period were investigated by sequencing and quantifying the abundance of *nifH*, a structural gene of the enzyme that mediates N_2 fixation. For *nifH* quantification, water was collected from Niskin bottles into acid-cleaned 4 L Cubitainers® (Qorpak, Clinton, PA, USA) and filtered onto 1.2 µm polyethersufone membrane filters (Sterlitech, Kent, WA, USA) using acid-cleaned tubing. Filters were immediately transferred to sterile 2 ml tubes and submerged in RLT Plus buffer (Qiagen). Samples were frozen in liquid nitrogen immediately after filtering and, once ashore, stored at -

80°C until analysis. As many non-colonial and non-symbiotic diazotrophs are smaller than 1.2 µm, *nifH* was sequenced from smaller size-fraction samples (0.03 µm) collected at a subset of stations. The sampling protocol was as described above except that water was collected from Niskin bottles into acid-cleaned 10 L LDPE carboys and samples were flash-frozen dry.

DNA and RNA were co-extracted from samples using the AllPrep DNA/RNA Mini Kit (Qiagen) following manufacturer's instructions with the addition of a bead-beater step. To quantify the abundance of *nifH* transcripts, indicative of diazotrophic activity, RNA was treated with amplification-grade DNase I (Invitrogen, Carlsbad, CA, USA) and reverse-transcribed using SuperScript IV First-Strand Synthesis System (Invitrogen, Carlsbad, CA, USA). For small size-fraction samples, reverse-transcription was performed using the SuperScript III First-Strand Synthesis System (Invitrogen, Carlsbad, CA, USA) and the nifH3 primer (Zehr and Turner 2001) in place of random hexamers.

To assess diazotroph community diversity, DNA and the product of RNA reverse-transcription (cDNA) were amplified via nested PCR using degenerate primers (Zehr and Turner 2001), with the adjustment that Illumina overhang adapter sequences for two-step amplicon sequencing (http://www.wellumina.com/content/dam/wellumina-support/documents/documentation/ chemistry_documentation/16s/16s-metagenomic-library-prep-guide-15044223-b.pdf) were added to the second round PCR primers (nifH1 and nifH2). PCR products were then gel-purified using a QIAquick Gel Extraction Kit (Qiagen, Germany), subject to index PCR (http://www.wellumina.com/content/dam/wellumina-support/documents/documentation/ chemistry_documentation/16s/16s-metagenomic-library-prep-guide-15044223-b.pdf), and sequenced on an Illumina MiSeq platform using a 2x300 bp kit. Sequences were subsequently de-multiplexed, imported into CLC Genomics Workbench

(Qiagen, Germany) as pairs, trimmed, and merged. To standardize the number of reads per sample, 11,000 random reads were extracted from each prior to *nifH* community composition analysis using the minimum entropy decomposition (MED) pipeline (Eren et al. 2015). The nucleotide sequences for MED-defined operational taxonomic units (OTUs) were identified by BLAST (Altschul et al. 1990) against an in-house *nifH* sequence database.

The abundances of dominant diazotrophic phylotypes were quantified in surface waters via quantitative PCR (qPCR) using 2x TaqMan Fast Advanced Master Mix (Applied Biosystems, USA) and custom primer/probe sets (Suppl. Table 5). These targeted *nifH* sequences specific to *Trichodesmium* spp., *Richelia intracellularis* (Het-1, a symbiont of the diatom *Rhizosolenia* sp.) and two UCYN-A sublineages, UCYN-A1 (Church et al. 2005a) and UCYN-A2 (Thompson et al. 2014). The abundance of *Braarudosphaera bigelowii*, a known host for UCYN-A, was also quantified using an 18S rRNA sequence (Thompson et al. 2014). Primer/probe sets for *Trichodesmium* spp. and Het-1 were redesigned for this study based on previously published gene sequences (Suppl. Table 5).

DNA samples were diluted 1:10 with nuclease-free DEPC-treated water (Millipore, Germany) before qPCR. Reactions (20 µl total volume) were prepared by combining the following: 10 µl 2x TaqMan Fast Advanced Master Mix, 4 µl nuclease-free water, 1.6 µl 5 µM forward and reverse primers, 0.8 µl 5 µM probe, and 2 µl 1:10 DNA or cDNA. Serially-diluted ($5 \times 10^{-2} – 10^{-9}$ ng DNA reaction^{-1}) synthetic plasmids (GeneWiz, USA) and no-template controls were run in triplicate alongside samples. Reactions proceeded using a StepOnePlus Real-Time PCR System and StepOne Software v. 2.2.2 (Applied Biosystems, USA) following manufacturer's specifications. Effective LODs (ELODs) and limits of quantification (ELOQs) were determined for qPCR data by assuming that the minimum detectable (MDC) and

quantifiable concentrations (MQC) are 3 and 10 copies reaction^{-1}, respectively (Bustin et al. 2020), as follows:

$$ELOD = \frac{MDC}{V_t} \times \frac{V_d}{V_f} \quad \textit{Equation 4.}$$

$$ELOQ = \frac{MQC}{V_t} \times \frac{V_d}{V_f} \quad \textit{Equation 5.}$$

where V_t, V_d, and V_f represent the volume of the DNA template (µl extract reaction^{-1}), the DNA extract (µl), and the total seawater filtered to obtain the extract (L).

Supervised machine learning approach

Empirical models of NFR, as a function of a varied suite of hydrographic predictors, were derived via random forest regression (Breiman 2001) using the scikit-learn package (Pedregosa et al. 2011) in Python. Random forest regression is an ensemble machine learning approach. Briefly, the training data are iteratively sub-sampled (with replacements) and each sub-sample is used to fit a decision tree. Their predicted values are then averaged, improving model accuracy and reducing over-fitting (Breiman 2001). The environmental predictors applied included sample depth, seafloor depth, temperature, salinity, chl-a concentration derived from in situ fluorescence, and N+N and SRP concentrations. These parameters were chosen based on the depth of their coverage and theoretical applicability to predicting NFRs. With this approach, NFRs are predicted from multi-dimensional trends in the input parameters, and thus accounts for relationships among input variables (e.g., N+N:SRP). Seafloor depth at each sampling point was taken as the mean depth within 0.1° from the ETOPO 1-Arc Minute Relief Model (Amante and Eakins 2009).

A model trained on temperature, chl-a concentration and seafloor depth was used to predict sea surface NFRs from an independent, external dataset composed of MODIS satellite sea surface temperature and chl-a concentrations (NASA Goddard Space Flight Center 2018 Reprocessing)

and ETOPO 1-Arc Minute Global Relief Model seafloor depth (Amante and Eakins 2009). Salinity was not included here because it did not significantly augment model performance and available satellite salinity data (e.g., Meissner et al. 2019) were at significantly lower resolution than the other data. To estimate NFR from CTD depth profiles, the model was trained on depth, seafloor depth, temperature, salinity and chl-a concentration. The relative importance of N+N and SRP in predicting NFRs was assessed by adding these parameters into the latter model and predicting NFR from Niskin bottle files where nutrient concentrations were measured.

Data accession and transformation. Models were trained on NFRs calculated for each individual incubation. This ensured that the model incorporated rate measurement variability and served to maximize training data volume. Each rate was associated with the mean hydrographic parameters of all Niskin bottles from which sample water was collected. NFRs were logarithm-transformed (base 10), following Sammartino et al. (2018), to balance the importance of extreme values among the training data. All rates below the LOD were assumed to be equal to the median LOD (0.54 nmol N L^{-1} d^{-1}). The median value was used rather than the individual LODs for each rate measurement to avoid scaling undetectable rates with PN concentration. As some detectable values in the training set were below the median LOD, trends among low NFRs (on the order of 10^{-1} nmol N L^{-1} d^{-1}) may have been obscured. Data were subsequently split at random into training/testing (80%) and validation (20%) subsets. Validation data were withheld from model construction. All predictive data were scaled based on the training/testing data.

To reduce noise in the depth profile predictor dataset, hydrographic parameters were binned at 1 m intervals. NFR profiles were predicted from the average water column profile at each station, calculated as the average of all binned casts (n = 1-3). Casts at each station were

collected within ~3 hours of one another. To reduce the computational expense of running the model, NFRs were predicted for every other depth bin (e.g., every 2 m).

Processed MODIS satellite data were accessed from https://oceandata.sci.gsfc.nasa.gov on March 19, 2020. Data are mean values from August 12 to 19, 2016. This time period was selected because it is the 8-day mean available from NASA Goddard Space Flight Center (2018 Reprocessing) that most closely aligned with the study period (August 7 to 16, 2016). Satellite data and bathymetry model (Amante and Eakins 2009) output were associated based on latitude/longitude and binned at 0.05° resolution.

Random forest regression. For each model variant, hyperparameters (e.g., total number of decision tree estimators, maximum tree depth) were tuned using a grid search approach with K-fold cross validation (Pedregosa et al. 2011). With this approach, the data are divided into equal "folds" (n = 9) and each is used in turn to test the performance of a model built on the other n–1 folds. Here, 9 folds were used to ensure that each represented >20 rate measurements. For each run, model hyperparameters were varied. The best combination of hyperparameters was selected as that with the highest coefficient of determination (R^2). This process was repeated n times such that each fold was used to test the model and obtain optimized hyperparameters once (Suppl. Table 6). The final model was then refit using the best hyperparameters for the entire dataset. Model performance was assessed using the validation dataset withheld at the beginning via linear regression.

Areal (depth-integrated) NFR calculations

Areal NFRs were calculated using (1) measured NFRs and (2) predicted NFRs from Model 1. Rates were trapezoidally depth-integrated through the upper 100 m of the water column or to the seafloor depth, whichever was shallower. Areal rates were only calculated from direct measurements if at least two replicated NFRs were available within the integration depth range. The 100 m threshold was chosen because the density of direct measurements made below 100 m was relatively low. While areal rates are often calculated to a given isolume rather than a given depth, I deemed this approach to be inappropriate here due to the presence of non-cyanobacterial (potentially non-phototrophic) diazotrophs (see below).

The following assumptions were made to calculate areal NFRs: (a) N_2 fixation was assumed to be constant from the surface (0 m) to the depth of the shallowest rate, which was always within the surface mixed layer. (b) At very shallow stations (seafloor depth < 50 m), which were typically well-mixed, N_2 fixation was assumed to be constant from the depth of the deepest rate to the seafloor. At all other stations, NFR was assumed to be equal to 0 nmol N L^{-1} d^{-1} at the bottom of the integration depth range if there were no rates at or below this depth. I note that detectable NFRs were often observed below this depth at deep stations, particularly those within the GS. At these stations, rates were available below 100 m and this assumption was consequently unnecessary. (c) To avoid over-estimation, any measured or predicted NFRs below the detection limit or the mean measured rate LOD (1 nmol N L^{-1} d^{-1}), respectively, were assumed to be equal to 0 nmol N L^{-1} d^{-1}.

RESULTS AND DISCUSSION

Regional hydrography

Three water masses converge near Cape Hatteras, NC, USA (Fig. 9B), which is designated as the boundary between the SAB and MAB. Cool (surface temperature < 29°C), low salinity (31.5 – 33.5) shelf waters formed in the MAB flow southward (Churchwell and Berger 1998). This mass meets with warm (surface temperature > 29°C) and high salinity (>34.5) northward-flowing waters

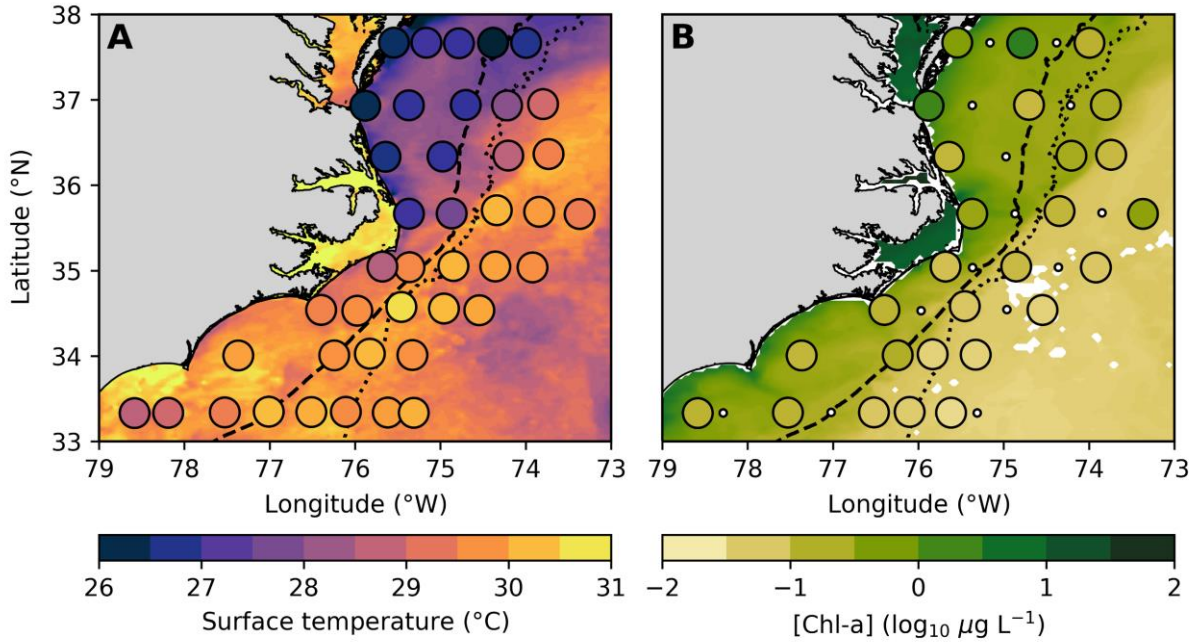

Figure 10. Mean MODIS (NASA Goddard Space Flight Center 2018 Reprocessing) sea surface temperature (A) and chl-a concentration (B) from August 12th to 19th, 2016, overlain by surface (< 3 m) temperature and extracted chl-a values at each station. White dots represent stations where chl-a concentration was not measured directly. The dashed and dotted lines indicate the 200 and 2000 m isobaths, representing the edges of the shelf and slope, respectively.

from the SAB continental shelf and GS (Fig. 10A). The GS separates from the continental boundary at Cape Hatteras—thus ceasing to be a western boundary current—and flows to the northeast. The exact point at which these water masses meet and mix is variable, as is the separation point of the GS. At their convergence point, shelf waters are entrained by the GS, transporting shelf material seaward (Churchwell and Berger 1998). This flow pattern results in the formation of a gyre along the continental slope between the MAB shelfbreak and the GS (Csanady and Hamilton 1988). At the time of this study, surface chl-a was elevated within MAB slope waters relative to the GS—on par with concentrations observed across the shelf (Fig. 10B).

Both MAB and SAB shelf waters are subject to inputs from the GS and freshwater sources. GS waters intrude directly on the SAB, or may be transported to the SAB and MAB shelves via eddies and meanders (Atkinson 1977). At the time of this study, low surface salinities (28.6 and 30.6, respectively) were observed at stations 14 and 15 on the inner shelf north of Cape Hatteras. These anomalies were likely due to outflow from Albemarle and Pamlico Sounds via Oregon Inlet (Fig. 9B), which can deliver terrestrial carbon and nutrients to the shelf (Churchwell and Berger 1998).

MAB shelf waters are characterized by a sharp, shallow thermocline, which occurred around 25 m at the time of this study (Fig. 11A). Below the mixed layer on the MAB shelf, the water temperature was typically ~10°C. SAB shelf waters and MAB slope waters were warmer by comparison, reaching ~15°C in deeper (>100 m) waters (Fig. 11A), though significant variability was observed in mean hydrographic characteristics of MAB slope water (Fig. 11). This variability was likely the result of significant water mass mixing in the portion of the MAB slope captured during our cruise. GS waters were warm (Fig. 11A) and oligotrophic (Fig. 11C, D), typically exhibiting deeper chl-a maxima than in shelf or MAB slope waters (Fig. 11B).

N+N was drawn down in surface waters across the region (Fig. 11C). However, significant concentrations (< 5µM) were typically observed in bottom waters at MAB shelf stations, below ~25 m in MAB slope waters, and below ~75 m in SAB shelf waters (Fig. 11C). SRP, in contrast, was detectable in surface waters along the MAB shelf, and elevated (< 0.25 µM) throughout the water column at MAB shelf and slope stations (Fig. 11D). In GS waters, SRP—like N+N—remained low throughout the upper water column at slope stations and until ~100 m at shelf stations (Fig. 11C).

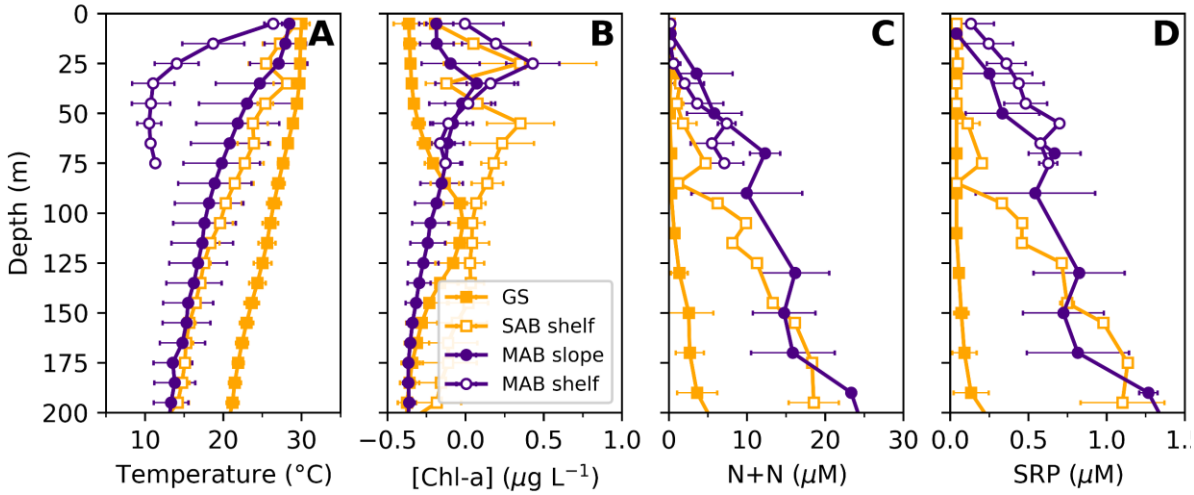

Figure 11. Mean temperature (A), chl-a (B), N+N (C) and SRP (D) for Gulf Stream (GS) stations (sea surface temperature > 29°C, seafloor depth > 200 m; closed orange squares), SAB shelf stations (latitude < 35.5°N, seafloor depth < 200 m; open orange squares), and Mid-Atlantic Bight (MAB) shelf (latitude > 35.5°N, seafloor depth < 200 m; open indigo circles) and slope (latitude > 35.5°N, sea surface temperature < 29°C, seafloor depth < 200 m; closed indigo circles) stations. All values were binned at 10 m intervals except for SRP and N+N in slope waters, which were binned at 20 m intervals. Horizontal bars represent the standard deviation of values within a given bin i.e., the variability of each parameter within a given bin.

Figure 12. Representative NFR profiles arranged left-to-right by latitude and top-to-bottom by distance from shore. Black dots = measured NFRs. Error bars = ± 1 standard deviation. White dots = the LOD where N_2 fixation was measured but not detected. Model 1 (purple) predicts NFR from depth, seafloor depth, temperature, salinity and chl-a concentration. Model 2 (orange) predicts NFR from N+N and SRP concentrations in addition to the parameters included in Model 1. The dotted line indicates temperature. The green bar indicates the depth of the primary chl-a maximum.

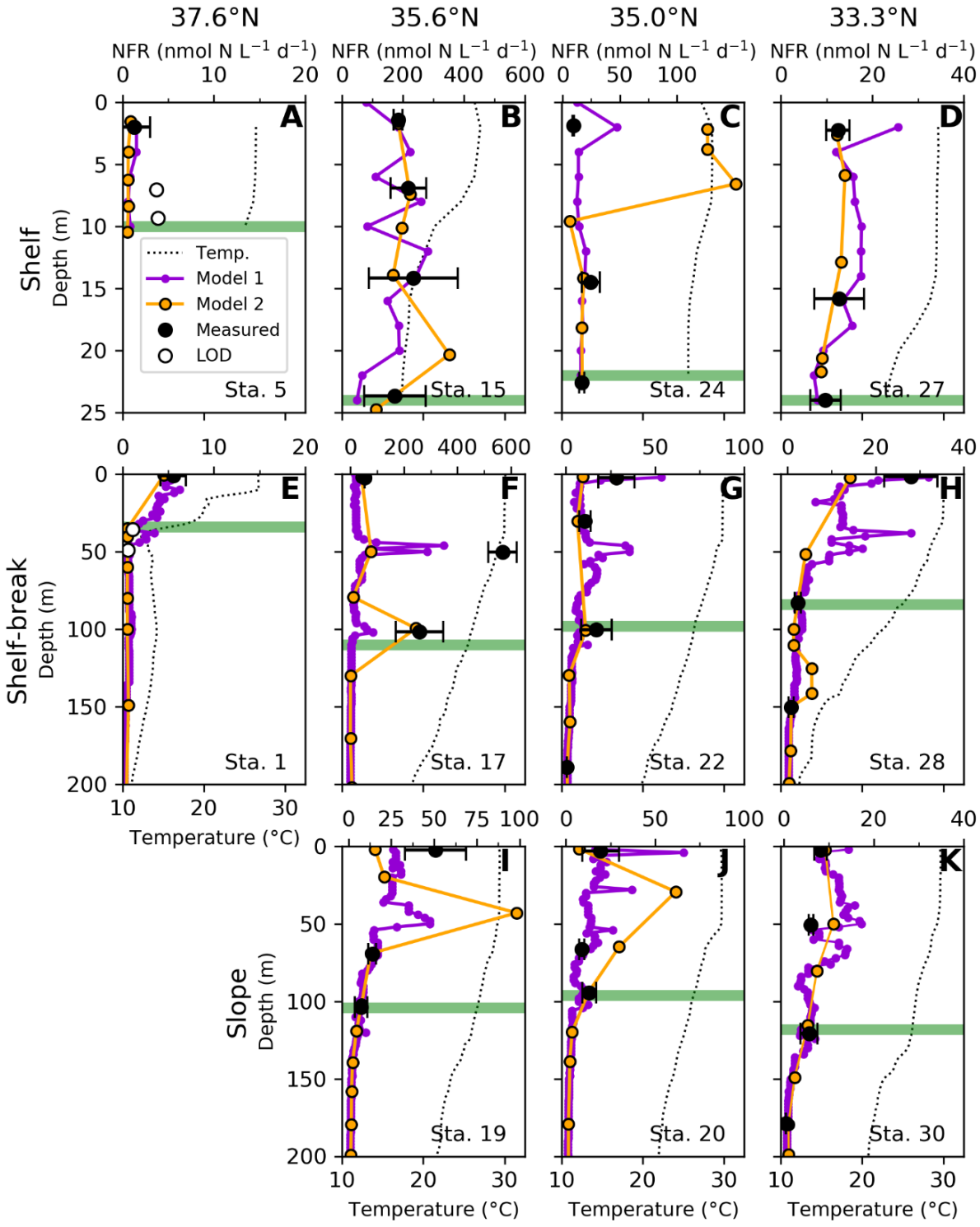

See figure legend on preceding page.

Direct NFR measurements

Undoubtedly the most striking finding of this study was an N_2 fixation hotspot near Cape Hatteras, NC, that appeared to extend across the shelf to the slope (Fig. 11B, F, I). Stations nearest the coast along the 36.3 and 35.6°N transects (stations 14 and 15), where low sea surface salinity anomalies were observed (see above), exhibited NFRs exceeding 100 nmol N L^{-1} d^{-1} (mean = 300 ±160 nmol N L^{-1} d^{-1}, n = 7 surveyed depths) throughout the water column (see Suppl. Table 7). Here, N+N was undetectable and SRP was low but typically measurable (>0.5 µM; Suppl. Table 7). NFRs remained elevated at the outer shelf and shelfbreak (stations 12, 13, 17; mean = 220 ±180 nmol N L^{-1} d^{-1}, n = 9 depths). NFRs were lower in slope waters along hotspot transects, reaching 7.1 ±2.0 and 51 ±18 nmol N L^{-1} d^{-1} (n = 3) in surface waters at stations 11 and 19, respectively. Both N+N and SRP were undetectable in the upper water column at these stations.

In comparison, the two transect to the north of the hotspot (37.7 and 36.9°N) were characterized by undetectable to low NFRs (Fig. 12A, E; Suppl. Table 7). Elevated NFRs were, however, observed in surface waters near the shelfbreak (5.6 and 18.3 nmol N L^{-1} d^{-1} at stations 1 and 10, respectively). In SAB shelf waters south of the hotspot, NFRs in the upper 150 m averaged 13.9 ±6.2 (n = 16 surveyed depths). NFRs in GS waters off the SAB shelfbreak averaged 10.3 ±8.8 (n = 25) nmol N L^{-1} d^{-1} (<150 m).

NFRs (Eqn. 1) are the product of PN concentration and the rate of specific N_2 uptake (Eqn. 2) i.e., the rate at which N atoms are transferred from the N_2 pool to the PN pool. Consequently, NFRs may increase if either biomass or diazotroph activity increases. Examining the rate of specific N_2 uptake thus offers a means of assessing diazotroph activity that is independent of biomass, which is advantageous when analyzing N_2 fixation across steep gradients in PN concentration. In this study, PN was higher across the continental shelf and in MAB slope waters

(Suppl. Fig. 4; Suppl. Table 7), contributing to higher rates inshore throughout the region (Fig. 12). However, the relative contribution of diazotroph communities to PN turnover was an order of magnitude greater in N-deplete offshore waters than in shelf waters to the north and south of the hotspot (Table 4). This finding suggests that the relative importance of diazotrophy to community N supply is greater in more oligotrophic waters, and thus supports the historical paradigm (Carpenter and Capone 2008).

Along the hotspot transects, however, there was no significant difference between SURs on and off the shelf (Table 4). SURs at these stations (12-15, 17) ranged from 0.026 ±0.016 d^{-1} (station 13 at 25 m, n = 3) to 0.57 ±0.05 d^{-1} (station 17 at 50 m, n = 3). These values are more than an order of magnitude greater than anywhere else (Table 4; Suppl. Table 7). This suggests that high NFRs at hotspot stations were not driven by high PN concentrations (Suppl. Table 7), but rather by an increase in the relative importance of N_2 fixation to PN turnover. The noted decrease in NFRs across the hotspot transects resulted from both reduced PN concentration and reduced specific N_2 uptake (Suppl. Table 7).

Table 4. Comparison of shelf (< 200 m) and offshore (>200 m) replicated specific N_2 uptake rates in the upper 150 m (one-way ANOVA).

Region	Mean SUR on shelf (d^{-1})[a]	Mean SUR offshore (d^{-1})[a]	Degrees of freedom	Test statistic (F)	p value[b]
North of hotspot (36.5 – 38 °N)	$3.55 \pm 5.94 \times 10^{-4}$	$5.87 \pm 7.51 \times 10^{-3}$	16	6.14	0.047
NFR hotspot (36.5 – 35.5 °N)	$1.14 \pm 0.79 \times 10^{-1}$	$1.59 \pm 0.19 \times 10^{-1}$	20	0.47	0.498
South of hotspot (33.0 – 35 °N)	$9.85 \pm 4.57 \times 10^{-3}$	$2.19 \pm 1.86 \times 10^{-2}$	36	5.70	0.017

[a]A value of zero was used where N_2 fixation was not detected. Mean error given as ±1 standard deviation.
[b]Based on 10,000 random permutations.

Throughout the region, NFR vertical profiles displayed relatively little variability within shelf waters (Fig. 12A-D). At the shelfbreak and slope, where the water column exhibited greater structure, rates were typically highest in surface waters and decreased with depth (Fig. 12E-K), although NFR maxima were frequently observed near chlorophyll-a maxima. These trends were driven by both changes in PN concentration and specific N_2 uptake rates (Suppl. Table 7).

NFRs were measured in deep waters (200 – 500 m depth) at select stations (10, 20, 34, 39). N_2 fixation was detectable in all deep waters surveyed (Suppl. Table 7). The mean NFR measured below 200 m was 0.90 ±0.57 nmol N L^{-1} d^{-1} (n = 6 surveyed depths). N+N concentrations for these deep samples exceeded 5 µM; particulate C concentrations ranged from 1.9 to 7.1 µM (Suppl. Table 7). These values are consistent with the observation of low NFRs (~1 nmol N L^{-1} d^{-1}) elsewhere in the interior ocean, particularly under organic-carbon replete conditions (Moisander et al. 2017 and references therein). Supplementing organic carbon in incubations has been observed to increase NFRs in mesopelagic (Moisander et al. 2017) and coastal (Rahav et al. 2016) waters. Organic carbon additions may provide a substrate for heterotrophic respiration, support the formation of high-metabolic microenvironments, or both. Recently, Pedersen et al. (2018) demonstrated that estuarine non-cyanobacterial diazotrophs can colonize natural particles, although pre-colonization by other bacterioplankton appears to be requisite. Similarly, Farnelid et al. (2019) found that suspended particles are loci for diazotrophs in the North Pacific Subtropical Gyre. I hypothesize that the low NFRs observed in deep waters during this study were supported by organic carbon inputs from the North Atlantic continental shelf.

Figure 13. Abundance of *Trichodesmium* spp. (A-B), UCYN-A1 (C-D) and UCYN-A2 (E-F) *nifH* genes and transcripts (normalized to gene abundance) in surface (< 3 m) waters. Large open circles indicate stations where sequences were not detected. Where transcripts but not their corresponding genes were detectable, transcript abundance was normalized to the ELOD. The dashed and dotted lines represent the 200 and 2000 m isobaths, respectively.

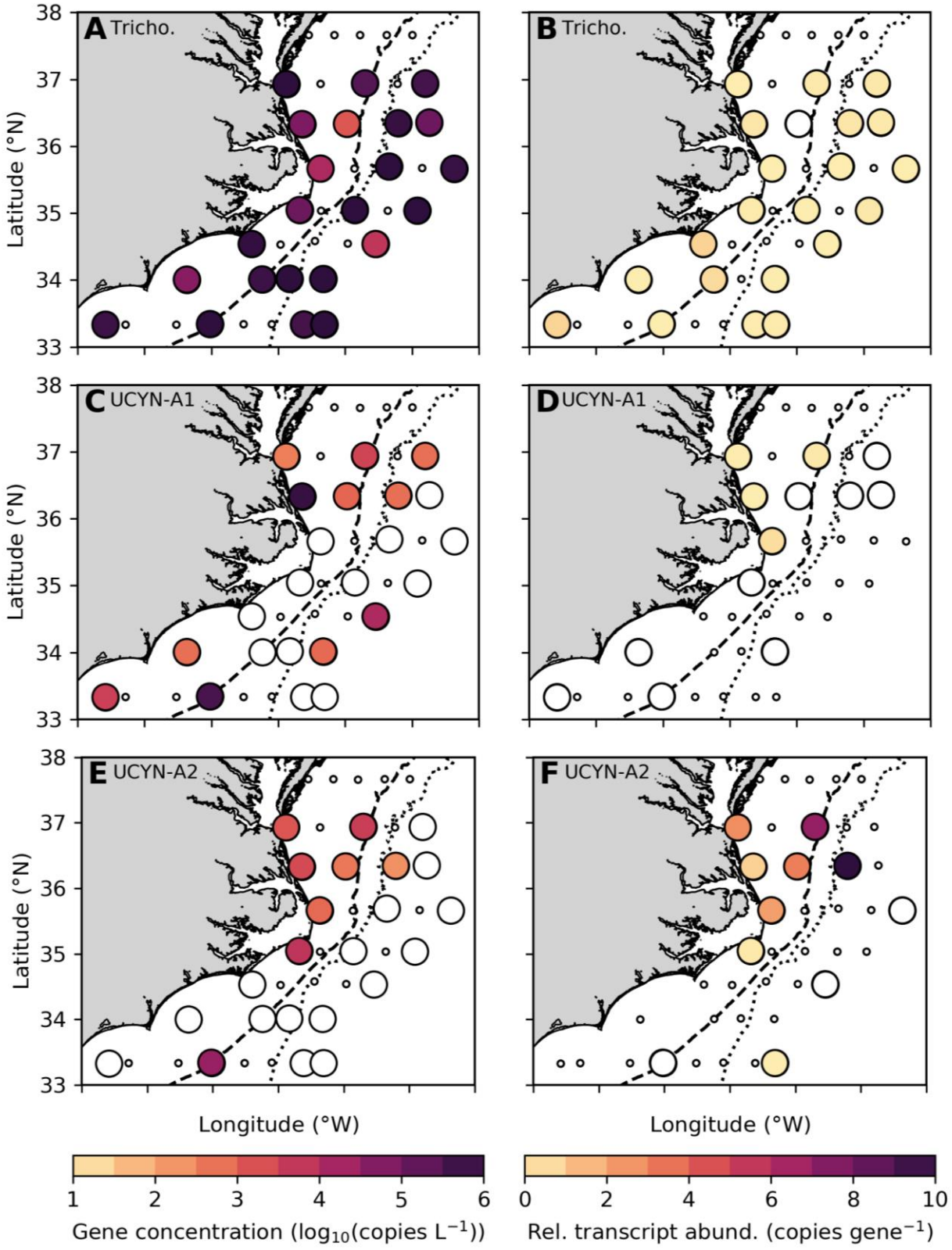

See figure legend on preceding page.

Diazotroph diversity and abundance

Different diazotrophic clades display disparate ecophysiologies. To determine the diazotroph taxa present in the study region, I sequenced *nifH* in a subset of surface samples (Suppl. Fig. 5). I found that *Trichodesmium* spp. dominated the *nifH* DNA pool (>70% of reads) in GS (stations 19 and 22) and MAB slope (stations 10 and 12) surface waters (Suppl. Fig. 5A). Most of these reads were identified as *T. thiebautii*; however, *T. erythraeum* dominated the DNA pool at a SAB shelfbreak station (22). In the NFR hotspot on the shelf (station 15), freshwater cyanobacterial *nifH* sequences abounded (Suppl. Fig. 5A) in the low salinity (28.6) surface waters. These organisms were likely transported from the nearby Albemarle and Pamlico Sounds on to the shelf (Mulholland et al. 2012).

As diazotroph presence is not diagnostic of activity, I also sequenced the *nifH* transcript pool (Suppl. Fig. 5B). UCYN-A dominated *nifH* transcript reads at both shelf and shelfbreak hotspot stations (stations 15 and 12; Suppl. Fig. 5B). At station 15, the relative abundance of UCYN-A transcripts was greater at the chl-a maximum (97%) than at the surface (64%). At the surface, *nifH* transcripts associated with the freshwater diazotroph *Anabaenopsis* sp. (22%), gammaproteobacteria (7%), and *T. thiebautii* (6%) were also present. *Anabaenopsis* sp. is known to continue fixing N_2 at relatively high salinity (~20; Moisander et al. 2002), and consequently may have contributed to the high NFRs observed at stations 14 and 15, which were slightly brackish (28.6 – 30.6). However, no sequences from this preferentially freshwater organism were recovered in the more marine waters offshore. Consequently, it is unlikely that it contributed substantially to the observed hotspot.

In MAB slope waters to the north (station 10), *Cyanothece* sp. sequences dominated the transcript pool (67%), although gammaproteobacterial *nifH* transcripts were present as well (11%).

However, it should be noted that this sample was collected at night when *Cyanothece* sp. are known to be active (Colón-López et al. 1997) and UCYN-A and *Trichodesmium* spp. are not (Church et al. 2005b). In SAB shelfbreak waters (station 22) collected in the evening, UCYN-A (27%), gammaproteobacteria (36%), *T. erythraeum* (21%) and *T. thiebautii* (16%) were all active.

Given the prevalence of *Trichodesmium* spp. throughout the region and apparent activity of UCYN-A at the hotspot, the absolute abundance of *Trichodesmium* spp. and UCYN-A sublineages 1 and 2 *nifH* genes and transcripts were quantified in surface waters across the study area via qPCR. *Trichodesmium* spp. were highly abundant throughout the region (mean *nifH* gene abundance = 10^5 copies L^{-1}, n = 23 triplicated samples; Fig. 13A). *Trichodesmium* spp. *nifH* expression tended to be low relative to its abundance except in SAB shelf waters (Fig. 13B). UCYN-A1 and 2 were both abundant at hotspot stations (Fig. 13C, E). While the relative expression of UCYN-A1 *nifH* was low at these stations (Fig. 13D), the relative expression of UCYN-A2 *nifH* was high, ~650 transcripts $gene^{-1}$ on average (n = 6 replicated samples).

There is concern within the community that the broadly applied *nifH* sequencing approach employed here may be discriminatory towards some diatom symbionts. Diatom community analysis of surface waters detected a high relative abundance of *Rhizosolenia* sp., a potential diazotroph host (Villareal 1992), concentrated near the N_2 fixation hotspot on the shelf (Chappell, unpublished). Consequently, the abundance of *nifH* sequences diagnostic of the *Rhizosolenia* sp. symbiont (Het-1) was also quantified. However, Het-1 was not detected at hotspot shelf stations and was at low abundance or undetectable throughout the entire study region (Suppl. Fig. 6).

Additionally, UCYN-A can become dislodged from its host during filtration (Thompson et al. 2014). As free UCYN-A cells are small (<1 μm; Thompson et al. 2014), they may not have been caught on the filters that I used for qPCR (1.2 μm). For this reason, I also assessed the

abundance of the only identified UCYN-A host, *Braarudosphaera bigelowii* (7 - 10 µm; Thompson et al. 2014). *B. bigelowii* was abundant in MAB shelf waters and at the shelfbreak along hotspot transects (Suppl. Fig. 7). Additionally, *B. bigelowii* was detected at low abundance at some SAB shelf stations and in GS waters.

Machine learning-based estimates of N_2 fixation

NFR model performance

Three random forest regressor models were built to predict NFRs in the region during the study period from (1) depth profiles of physical (sample depth, seafloor depth, temperature and salinity) and biological (chl-a concentration) parameters, (2) depth profiles of physical, biological and biogeochemical (N+N and SRP concentrations) parameters, and (3) sea surface parameters (temperature and chl-a concentration) and seafloor depth. All three models performed well (R^2 > 0.80) when tested against validation data withheld from model training (Fig. 14; Suppl. Table 6), but tended to overpredict low values and underpredict high values, as has been previously observed in machine learning-based NFR estimates (Tang et al. 2019a). Greater fidelity at NFR extremes was achieved when nutrient concentrations (N+N and SRP) were included (Fig. 14). However, the coverage of nutrient data was low relative to the other parameters. Consequently, NFR predictions by Model 2 were at lower depth resolution than those from Model 1 (Fig. 12).

Modeled N_2 fixation profiles. Models 1 and 2 offer greater depth coverage of NFR rates and suggest complexities in NFR profiles that could not have been resolved from direct measurements alone (Fig. 12). As observed from in situ measurements, NFRs at shallow shelf stations were typically uniform through the water column. At deeper stations, however, NFRs displayed

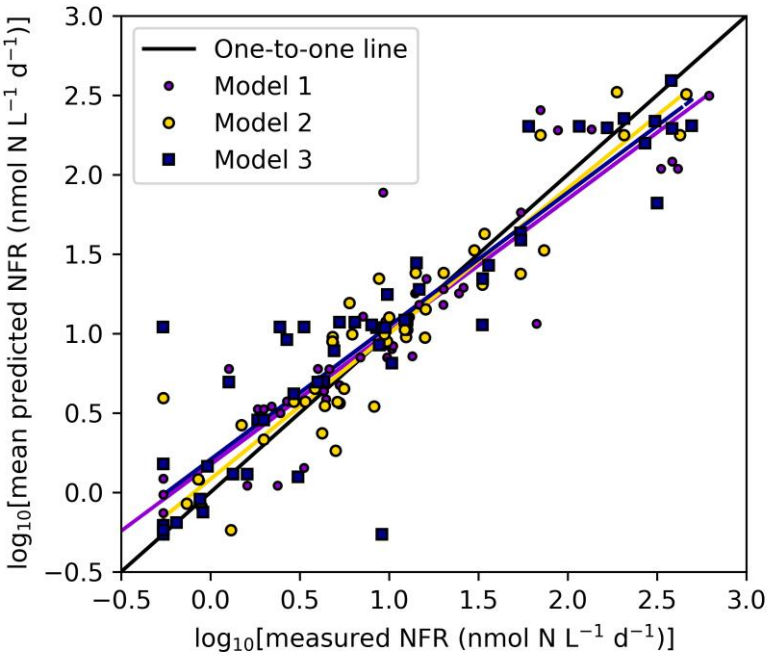

Figure 14. Performance of models on discrete validation datasets. Model 1 (physical and biological predictors): y = 0.84x + 0.18, df = 50, R^2 = 0.86, $p < 10^{-6}$. Model 2 (physical, biological and biogeochemical predictors): y = 0.92x + 0.08, df = 45, R^2 = 0.89, $p < 10^{-6}$. Model 3 (sea surface variables and seafloor depth): y = 0.84x + 0.21, df = 50, R^2 = 0.83, $p < 10^{-6}$.

significant variability. Narrow maxima were often observed at the bottom of the mixed layer and near the primary chl-a maximum (Fig. 12E-K). Below this point, both predicted and measured rates were typically low (< 1 nmol N L^{-1} d^{-1}).

The highest rates predicted by Model 1 occurred in (1) warm, low salinity (<31.5) waters associated with freshwater outflow from Oregon Inlet (stations 14 and 15; Suppl. Table 7), and (2) under cool (<29°C), moderate salinity (31.5 – 33.5) conditions characteristic of the MAB shelf waters (Fig. 11; 6A). High rates (>30 nmol N L^{-1} d^{-1}; Fig. 15A) were also observed in the cooler (27 – 29°C) surface waters of the MAB slope (salinity <34.5; Fig. 15A). Rates were moderate in

GS surface waters (~10 nmol N L^{-1} d^{-1}) and decreased with depth until they were at the detection limit (Fig. 15A), typically just below the chl-a maximum (Fig. 12I-K). In mid-salinity mixing waters, rates were low to moderate (~1-10 nmol N L^{-1} d^{-1}). These findings are highly consistent with direct observations (described above).

Model 2, which included N+N and SRP as NFR predictors, generally agreed well with Model 1 (Fig. 15B). Both models were able to predict NFR to the order of magnitude at shelf stations within the NFR hotspot (stations 14, 15; Fig. 12B). However, the inclusion of nutrients in Model 2 generally resulted in lower predicted NFRs in mid-salinity mixing waters (Fig. 15B), though SRP was in slight excess of N+N here. Interestingly, Model 2 also predicted higher NFRs

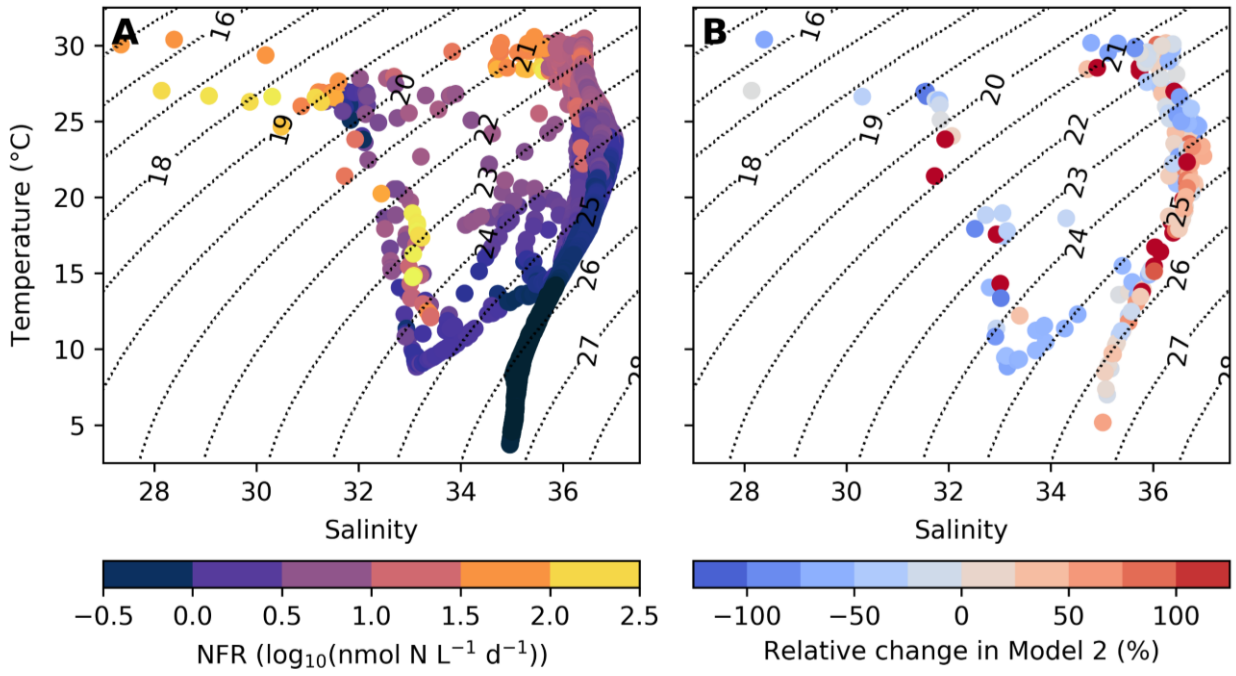

Figure 15. Temperature-salinity diagrams. Colored dots depict (A) Model 1 results and (B) results of ((Model 2 – Model 1) / Model 1) × 100 i.e., the relative change associated with the inclusion of nutrients in the model. Dotted lines indicate isopycnals (σ_t, kg m^{-3}).

than Model 1 in GS waters below the nutricline. These waters bore N+N:SRP ratios exceeding 20, suggesting that dissolved inorganic N was not limiting. This finding contrasts with the longstanding paradigm that N_2 fixation occurs predominantly in waters where N+N is limiting, and suggests that this paradigm was not reflected in the larger training dataset (i.e., the measured NFRs).

I hypothesize that the inclusion of waters where UCYN-A was highly active in the training set skewed the relationship of between NFRs and nutrients. Unlike *Trichodesmium* spp. and other cyanobacterial diazotrophs, UCYN-A continues to fix N_2 under both N-limited and N-replete conditions (Mills et al. 2020). Though ostensibly paradoxical given the high energetic cost of N_2 versus N+N assimilation, both UCYN-A1 and UCYN-A2 hosts appear unable to utilize ambient NO_3^- and, consequently, require their symbionts to fix N constitutively (Mills et al. 2020). Furthermore, recent work by Mills et al. (2020) suggests that UCYN-A NFRs can be enhanced by N+N additions, potentially due to secondary ecological effects (e.g., enhanced production of siderophores and thus iron availability by bacterioplankton). Future machine learning-based models of N_2 fixation may be able to better tease apart the complex relationships among different diazotrophic clades and ambient N+N concentrations using larger training datasets, or by parameterizing the abundance of distinct groups.

Areal NFR estimation. Measured NFRs and those predicted from Model 1 (depth, seafloor depth, temperature, salinity, chl-a concentration) were trapezoidally depth-integrated from 0 to 100 m. At stations exhibiting more complex water column structure, the fine-scale resolution of the model often served to reduce or increase depth-integrated NFRs, depending on the locality of the

Table 5. Predicted (Model 1) and measured NFRs depth-integrated over the upper 100 m[a].

Sta.	Lat. (°N)	Long. (°W)	Mean temp. at 2 m (°C)	Mean salinity at 2 m	Seafloor depth (m)	Areal NFR calculated from predicted rates (μmol N m^{-2} d^{-1})	Areal NFR calculated from measured rates (μmol N m^{-2} d^{-1})
1	37.67	73.99	26.7	33.3	1261	292	101
3	37.66	74.78	26.9	31.5	42	169	BDL
5	37.67	75.54	26.4	31.7	14	BDL	5.64
6	36.93	75.88	26.3	31.3	14	10.4	11.9
8	36.94	74.70	26.9	32.1	88	143	74
10	36.93	73.81	28.9	35.6	2651	1030	375
11	36.35	73.75	29.4	35.8	2947	1130	465
12	36.34	74.21	28.4	34.7	2327	2950	25500
13	36.33	74.97	26.9	31.3	41	891	5220
14	36.33	75.64	26.6	30.3	21	3890	9090
15	35.67	75.37	27.0	28.1	22	3730	4580
17	35.69	74.35	30.2	36.3	2312	4150	42600
19	35.66	73.37	29.4	35.9	3682	3030	2820
20	35.04	73.92	29.6	36.1	3488	1510	1840
22	35.04	74.86	30.2	34.8	2715	2240	2200
24	35.05	75.68	28.5	34.9	30	493	521
25	33.33	78.58	28.7	35.9	21	372	483
27	33.34	77.53	29.4	30.2	34	389	387
28	33.34	77.03	30.4	28.4	217	913	1380
29	33.34	76.52	30.0	36.1	615	1370	1930
30	33.34	76.10	29.6	35.7	1650	1070	895
31	33.34	75.62	~	~	3298	1010	296
35	34.01	75.84	30.1	35.3	1106	2910	1460
36	34.01	76.24	29.7	34.7	256	1170	408
37	34.01	77.37	29.9	35.7	26	548	278
41	34.54	76.40	29.5	35.7	18	262	258

[a]Or to the seafloor when seafloor depth was less than 100 m.

measured depths (Table 5). Thin but significant NFR peaks were often predicted by Model 1 at the surface, thermocline, and at or above the chl-a maximum (Fig. 12). Areal rates calculated from direct measurements may thus over- or underestimate NFRs if sampling was biased toward or failed to resolve these peaks. For example, model-based areal rates were more than double measurement-based estimates at stations 10 and 11 on the MAB slope. Model 1 results suggest that there were NFR peaks (20 – 30 nmol N L^{-1} d^{-1}) at the base of the mixed layer that were not resolved by direct measurements. Conversely, depth-integrated measured rates at shelfbreak stations along the hotspot transects (12 and 17) exceeded those calculated from Model 1 output by about an order of magnitude. Though exacerbated by the tendency of our models to underestimate very high NFRs (Fig. 14), direct measurements at these stations were made at water column features where Model 1 predicted relatively thin NFR peaks. Consequently, the areal rates calculated from these direct measurements likely overestimate water column NFR.

Our work highlights the significant impact of sampling strategy on areal rate calculations when coverage of direct measurements is low. Discrepancies among studies in sampling strategy and depth coverage must be accounted for when comparing rates across regions and when using areal rates to build predictive or descriptive models.

Sea surface N_2 fixation. Surface NFRs were predicted from regional bathymetry and mean sea surface conditions (temperature, chl-a concentration) at the time of the study (Fig. 16). The model suggests that NFRs are undetectable to low (< 4 nmol N L^{-1} d^{-1}) in the high chl-a waters that are immediately adjacent to the coastline (mean MODIS chl-a concentratio*n* = 3.9 µg L^{-1} where seafloor depth < 15 m; Figs. 10B, 16, 17). These conditions were present at the coastal

stations on the two northernmost transects (stations 5 and 6; seafloor depth = 11 m, chl-a concentration > 1 μg L^{-1}) where measured NFRs were low or undetectable (Suppl. Table 7).

Predicted NFRs peaked away from the coast, near the 20 m isobath where chl-a was moderate (mean MODIS chl-a concentrati*on* = 0.87 μg L^{-1} where seafloor depth was 15 – 25 m; Fig. 17A), then declined. The magnitude of this peak was greater in MAB waters (>35.5°N; maximum 5 m running mean: 44.6 nmol N L^{-1} d^{-1}), which included the hotspot, than in the SAB (<35.5°N; maximum 5 m running mean: 24.6 nmol N L^{-1} d^{-1}). From the 40 m isobath to the shelfbreak (200 m), mean surface NFRs predicted by Model 3 were 5.3 ±2.9 (*n* = 387) and 9.4 ±5.8 (*n* = 455) nmol N L^{-1} d^{-1} in the MAB and SAB, respectively. These middle to outer shelf waters were warmer in the SAB and bore lower chl-a concentrations than in the MAB (Fig. 10). The abundance of *Trichodesmium* spp. *nifH* transcripts relative to genes was elevated in these SAB waters, as well (Fig. 13B).

Model 3 also predicted high NFRs along the offshore frontal zone (~29°C) between the MAB shelf waters and the GS, which occurs just beyond the 2000 m isobath (Figs. 16, 17B). This finding is consistent with NFR measurements in surface waters (stations 10, 12, 17; Fig. 16; Suppl. Table 7) and results from Models 1 and 2. Our sequencing (Suppl. Fig. 5) and qPCR results (Fig. 13; Suppl. Figs. 3, 4) suggest that a myriad of diazotrophs may have been present and/or active here, including *Trichodesmium* spp., UCYN-A, *Cyanothece* sp., gammaproteobacteria, and Het-1. Het-1 sequences were recovered from surface waters via transcript sequencing at station 10 (<1% relative abundance), and they were observed at low abundance at stations 10 (120 ±64 gene copies L^{-1}) and 12 (147 ±108 gene copies L^{-1}), which were within the offshore band of high predicted NFRs.

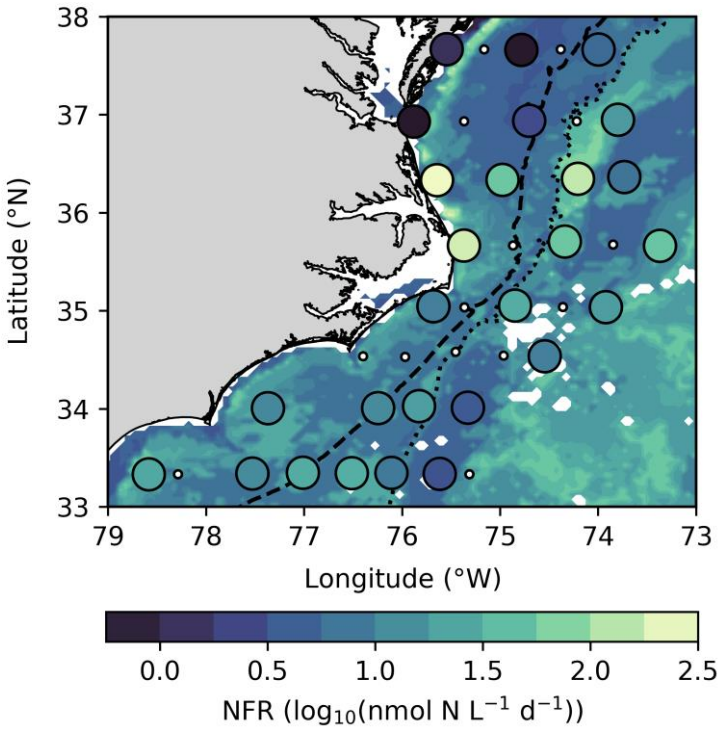

Figure 16. NFRs predicted by model 3 from mean MODIS sea surface temperature and chl-a concentrations from Aug. 12-19, 2016 (NASA Goddard Space Flight Center 2018 Reprocessing) and model-derived bathymetry (Amante and Eakins 2009) overlain by in situ NFR measured within the surface mixed layer. The dashed line indicates the 200 m isobath i.e., the shelfbreak. The dotted line indicates the 2000 m isobath.

High rates (~30 nmol N L^{-1} d^{-1}) were also predicted in oligotrophic open-ocean waters to the southeast. This finding fits within the existing conceptual model of the factors governing *Trichodesmium* activity (Carpenter and Capone 2008). However, these waters were poorly represented in the training dataset (i.e., among direct measurements) and should be interpreted with caution.

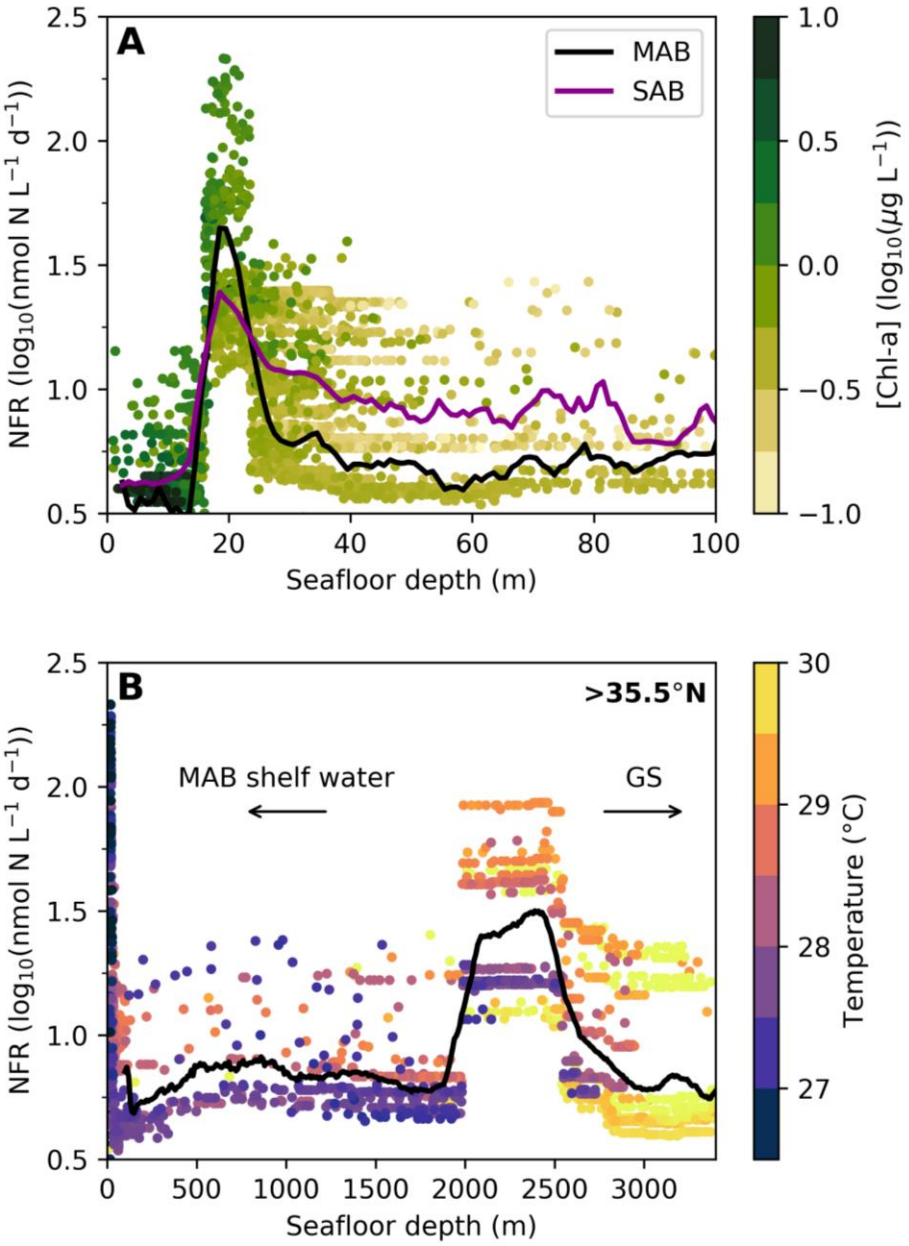

Figure 17. Panel A: NFRs predicted by Model in surface shelf waters as a function of seafloor depth. Colors correspond to MODIS chl-a concentrations. The lines represent the 5 m running mean for predicted NFRs in the MAB (black) and SAB (purple), respectively. Panel B: NFRs predicted by Model 3 in surface waters across the MAB shelf and slope (>35.5°N). Colors correspond to MODIS temperature. The black line represents the 200 m predicted NFR running mean.

I note that measured rates as well as Models 1 and 2 suggest the presence of high NFRs deeper in the water column along hotspot transects in the MAB (36.3 and 35.6°N; e.g., Fig. 12F; Suppl. Table 7). Indeed, there was no significant difference between N_2 SURs at shelf and slope stations along these transects, indicating that diazotroph activity was elevated througout these waters relative to others in the region. These high subsurface rates would not have been captured by Model 3 as the satellite-based measurements it used to predict NFRs lack the necessary depth-resolution. The extension of high NFRs across the shelf, following the net flow, suggest that inner shelf waters may have provided seed communities or resources for N_2 fixation offshore.

The findings presented here suggest that the consumption of continental inputs by phytoplankton creates a coastal niche for diazotrophs. These likely include UCYN-A in the colder MAB waters, *Trichodesmium* spp., particularly in the warmer SAB waters, and potentially some recently flushed freshwater cyanobacteria (see 'Diazotroph diversity and abundance' section). Additionally, our results imply that conditions in the frontal regions between MAB shelf waters and SAB shelf and GS waters create conditions that are favorable for diazotrophs—predominantly UCYN-A2 based on our diazotroph community analysis (Fig. 13; Suppl. Fig. 5).

CONCLUSIONS

N_2 fixation has long been hypothesized to occur in warm, oligotrophic surface waters and decline where fixed N is no longer limiting and phototrophic diazotrophs are outcompeted by other phytoplankton (Carpenter and Capone 2008). Consequently, NFRs are generally expected to decline when chl-a concentrations are high. Research from the Western North American continental shelf, including the findings presented here, paint a very different picture. NFRs on the shelf (Mulholland et al. 2012; Mulholland et al. 2019; Tang et al. 2019b; this study) frequently

exceed those measured in the tropical North Atlantic basin (e.g., Martinez-Perez et al. 2016). Indeed, high-resolution underway surface NFRs crossing the Western North Atlantic continental shelf displayed a significant positive correlation to chl-a concentration in August 2015 and 2016 (Tang et al. 2019b). There are two explanations for these observations: (1) Diazotroph abundance and activity scale with biomass, which could occur if a subset of the total community is constitutively fixing N_2 as has been demonstrated for UCYN-A (Mills et al. 2020), or (2) conditions in coastal waters favor N_2 fixation and diazotrophs are consequently more active, which should be reflected by higher rates of diazotroph-driven PN turnover (i.e., specific N_2 uptake rates).

I found that specific N_2 uptake rates were significantly greater in N-deplete offshore waters than on the continental shelf, except along transects aligned with and just north of Cape Hatteras (Table 4). NFRs on the shelf that are high relative to measurements from tropical, oligotrophic waters (e.g., Martinez-Perez et al. 2016) thus likely arise because conditions near the ocean-continent transition are favorable for phytoplankton growth in general, rather than for diazotrophs specifically. This finding supports both the traditional paradigm that oligotrophic ocean waters offer a more significant niche for diazotrophs than coastal environments, and the idea that some (presumably symbiotic) diazotrophs may be constitutively fixing N_2. However, empirical model results hint at greater nuance. Model 3 predicts enhanced NFRs along coastline, just seaward of the coastal chl-a maximum (Figs. 16, 17A). It is unlikely that this peak was driven by high PN concentrations because PN tends to scale with chl-a (Fig. 10; Suppl. Fig. 4). Rather, it indicates that the conditions present here favor diazotrophic metabolism.

Both direct measurements and model results indicate that the frontal mixing zone between cool MAB shelf waters and warm SAB shelf and GS waters created conditions conducive to exceptionally high levels of diazotrophy (>100 nmol N L^{-1} d^{-1}) both on and off the shelf during the

study period (e.g., Figs. 12, 16). Based on the distribution of high NFRs, I hypothesize that high NFRs offshore were supported by shelf water properties (e.g., communities, nutrients) advected there. This N_2 fixation hotspot likely resulted from the proliferation and activity of the haptophyte-symbiont UCYN-A (Fig. 13; Suppl. Fig. 5), though other diazotrophs were present and active as well. Mills et al. (2020) have hypothesized that N_2 fixation by UCYN-A may be linked to the activity of their larger community. I proffer that either altered ecological dynamics or nutrient availability may have played a role in the formation of the N_2 fixation hotspot documented here. As the GS transports a significant fraction of shelf organic matter offshore (Churchwell and Berger 1998), primary productivity fueled here by high NFRs may act as a carbon sink by removing drawn-down carbon to the deep ocean.

By applying a supervised machine learning approach, this study offers a nuanced view of N_2 fixation and hints at unresolved complexities in its spatial distribution. Our work highlights the possibly confounding role of sampling strategy on calculating areal rates, which are frequently used to resolve global patterns and build models (e.g., Tang et al. 2019a), and the potential for dynamic frontal systems to augment fixed N inputs. Understanding the spatial heterogeneity of key biogeochemical processes in the ocean will facilitate the ongoing efforts to constrain N budgets on regional to global scales.

CHAPTER V

MAJOR FINDINGS AND FUTURE WORK

Diazotroph niches

Until recently, our understanding of the niche occupied by marine diazotrophs has largely been based on our knowledge of the environmental factors regulating the distribution of *Trichodesmium*, which has long been viewed as the quantitatively most important N_2 fixer in the ocean (Carpenter and Capone 2008). As these environmental factors (e.g., warm temperatures, high light, low DIN concentrations) are often used to parameterize N_2 fixation in ocean models, our conceptual understanding of marine diazotrophs' niche is pertinent to efforts to close the global N budget (Zehr and Capone 2020) and accurately predict biogeochemical and ecosystem dynamics on local scales. Moreover, our understanding of the factors regulating marine N_2 fixation affect the development of conceptual models of N cycle feedbacks and climatic shifts. The research presented here supports the view that diazotrophs do not represent a single functional group. Rather, my findings along with other recent work suggest that different diazotrophic groups occupy distinct niches within the ocean.

Deep waters and ODZs. My observation that N_2 fixation below the mixed layer in the ETNP and ETSP was mostly restricted to the upper oxycline/ODZ support that idea that reduced O_2 concentrations may make N_2 fixation a more favorable N acquisition mechanism (e.g., Großkopf and LaRoche 2012) for the non-cyanobacterial diazotrophs that inhabit these waters (e.g., Loscher et al. 2014; Jayakumar et al. 2017). In the ETSP, sub-euphotic rates were low and mostly restricted to relatively nearshore or high-productivity stations. In the ETNP ODZ, N_2

fixation was stimulated by organic C additions. These finding suggest that diazotrophy here is largely C limited, as is often observed for NO_3^- respiration and other metabolic functions in ODZs (e.g., Chang et al. 2014). Moreover, I observed exceedingly high NFRs in the upper ODZ near the Revillagigedo Islands. Concurrent measurements from J. Moffett's lab (unpublished) showed a subsurface plume of dFe that corresponded to these high rates. This observation echoes that of Loscher et al. (2014) who reported similarly high NFRs in ETSP shelf waters following the onset of sulfidic conditions. *Together, these findings paint a picture of generally C-limited sub-euphotic microbial populations that up-regulate N_2 fixation when Fe-limitation is relieved and O_2 concentrations are low.*

Early work in the ETSP and other anoxic systems inspired a flurry of subsequent studies focused on the potential for low but persistent NFRs throughout the mesopelagos. This topic has already been the subject of relatively extensive review (e.g., Bombar et al. 2016; Moisander et al. 2017; Benavides et al. 2018). However, no consensus has yet been reached as to whether these waters can contribute significantly to new N_r inputs either locally or globally (Zehr and Capone 2020). As discussed in Chapter III, I believe that a substantial proportion of the NFRs reported from deep waters may have resulted from propagating analytical noise through Eqn. 1. Indeed, deep N_2 fixation has frequently been observed to scale with indicators of particle mass, including particulate C and transparent exopolymer concentrations (e.g., Rahav et al. 2013; Benavides et al. 2016), which could reflect the misinterpretation of noise as low SURs and its subsequent scaling to [PN] to calculate a NFR (Eqn. 1). More work will be needed within the community to disentangle low but real NFRs at depth from false data, and thus investigate the niche and potential importance of non-cyanobacterial diazotrophs at depth. *The work presented here does*

not support the view that N_2 fixation is widespread in sub-euphotic ocean waters (e.g., Benavides et al. 2018), but rather suggest that it is temporally and spatially patchy.

Continental shelves. The work presented in Chapter IV, along with other work that I took part in as a graduate student (Mulholland et al. 2019), demonstrate that broad continental shelf environments can support significant N_r inputs via N_2 fixation. UCYN-A likely represents the major N_2 fixer along the Western North Atlantic continental shelf (this work; Mulholland et al. 2019). UCYN-A is also present in the waters overlying the ETNP ODZ, particularly to the north near where I observed high surface rates (White et al. 2013). In these waters, NFRs are typically highest near the coast where biomass peaks. This finding indicates that UCYN-A and potentially other diazotrophs residing here constitutively fix N. For UCYN-A, this behavior is likely due to its relationship to its host (see Mills et al. 2020).

I observed an increase in relative expression of UCYN-A *nifH* genes and host abundance at Cape Hatteras front. Consequently, it is reasonable to assume that *water mass interactions facilitated the proliferation of the UCYN-A symbiosis*. More work is necessary to unravel why this occurred. However, I have recently made similar observations at the New England shelf-break front (Selden et al. in prep.), indicating that frontal interactions play a persistent role in UCYN-A ecology and activity throughout the region.

My modeling efforts in Chapter IV also revealed an enhancement in NFRs away from the coastline as phytoplankton populations begin to decline. This trend would not have been observed without the augmentation of my dataset by machine learning and highlights the need for enhanced spatial and temporal resolution in biogeochemical sampling. Moreover, it may represent a broad trend. Continental shelf sediments can supply Fe and SRP, which frequently

limits N_2 fixation throughout marine waters (Zehr and Capone 2020). *Consequently, a "coastal" niche for diazotrophs may be present where terrestrial N+N inputs have been exhausted but SRP and Fe are available from either terrestrial inputs or shelf sediments.* This fits within the prevailing view of N_2 fixation but has important implications for local N budgets in productive continental shelf environments.

Finally, the work presented here and throughout this dissertation highlights the importance of fine-scale spatial and temporal variability in physico-chemical dynamics in regulating marine N_2 fixation at ocean margins. Investigating the role of ephemeral features on modulating N_2 fixation rates will require technical advances to enable increased temporal and spatial resolution (see Benavides and Robidart 2020 for in-depth discussion). As stable isotope rate measurements are labor-intensive and costly, future work will likely need to leverage less accurate measures that can assess trends at high resolution, e.g., H_2 supersaturation or the acetylene method (Tang et al. 2019b), in conjunction with advanced computational approaches such as the one applied here.

Conceptual model of N_2 fixation at ocean margins

How to parameterize N_2 fixation in conceptual and quantitative ocean models has been the subject of intense discussion in the past decade. Much of this debate has focused on the role of DIN concentrations (assumed to preclude N_2 fixation when high) and Fe concentrations, which are typically considered to be a function of dust deposition (e.g., Weber & Deutsch 2014). However, freshwater inputs supply significant quantities of dFe to the coastal ocean (Hunter & Boyd 2007). As salinity increases, this dFe either flocculates or binds to weak ligands (e.g., humics) that are unlikely to be easily accessible to marine microbes (e.g., Bundy et al. 2015; Laglera and van den

Berg 2009). Similarly, Fe supplied via shelf sediment resuspension in oxic systems (e.g., Johnson et al. 1999) is likely to be weakly bound mostly by organic degradation products (Bundy et al. 2014).

This dynamic may explain why NFRs are typically low in estuaries despite N_r limitation (Marino et al. 2002). Moreover, it may play an important role in driving the high NFRs reported here at coastal margins where this weakly-ligated Fe mixes with oceanic waters where plankton communities produce stronger and more widely bioavailable Fe-binding ligands in excess (Gledhill & Buck 2012). While we did not investigate the abundance of Fe-binding ligands in Chapter IV, I hypothesize that the GS may be particularly rich in these compounds given that (1) *Trichodesmium* are at high abundance in these waters (e.g., Martinez-Perez et al. 2016), (2) *Trichodesmium*-associated bacteria are known to produce strong, highly bioavailable Fe-binding ligands (Basu et al. 2019), (3) *in situ* and model-based evidence suggest high biological uptake rates of Fe in surface waters of the western North Atlantic, resulting in low dFe concentrations in the upper water column (Pham & Ito 2019), and (4) strong Fe-binding ligands are typically in excess in surface waters (Gledhill & Buck 2012).

In addition to the abundance of Fe and bioavailable complexes to bind it, energy acquisition undoubtedly represents another potentially limiting factor for N_2 fixation rates. This is particularly important to consider in sub-euphotic waters where N_2 fixation may be carbon-limited (e.g., Chapter III). Understanding the metabolic proclivities of deep sea diazotrophs is necessary to piece apart the factors controlling aphotic N_2 fixation.

There are two factors in calculating NFRs—PN concentration i.e., biomass and the specific N_2 uptake rate (see Eqn. 1). Organic C concentrations (in sub-euphotic waters) and Fe bioavailability likely affect predominantly the former and the latter, respectively. These limiting

agents aside, the question remains: What controls the magnitude of N_2 fixation in marine systems? In Chapter IV, I report that high NFRs on the continental shelf are driven by the high PN concentrations there and that specific N_2 uptake rates were actually higher offshore (Table 4). This observation echoes results from Knapp et al. (2012) that demonstrate that cell-specific N_2 uptake rates increase in diazotroph cultures under low DIN:SRP while diazotroph biomass increases when concentrations of DIN and SRP increase (without a significant change in cell-specific N_2 uptake). Thus, the abundance of macronutrients (DIN and SRP) and their stoichiometry are likely important in regulating the observed magnitude of N_2 fixation in marine systems.

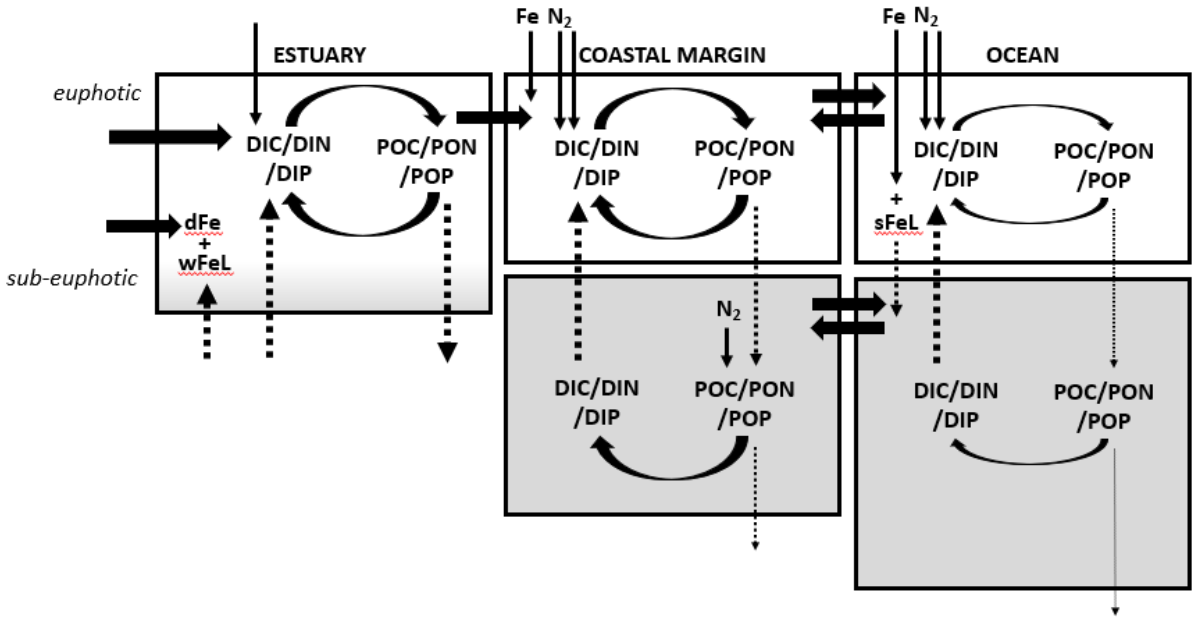

Figure 18. Box model depicting the inputs and processes affecting N_2 fixation rate magnitude along the estuarine to ocean continuum.

These factors—Fe concentrations, concentration of strong bioavailable Fe-binding ligands, organic C availability (in sub-euphotic waters), and macronutrient concentrations and stoichiometry—in combination may explain the observed distribution and magnitude of NFRs in both open ocean and coastal systems (Fig. 18). For example, I observed high rates along the coastal margin in surface waters of the ETNP but not the ETSP. This discrepancy could be explained by the lower DIN:SRP ratio of residual nutrients in the upper waters of the ETNP compared to the ETSP (Suppl. Figs. 1, 3) as well as potential differences between these systems in Fe concentrations and bioavailability. Additionally, low bioavailability of the presumably sizable dFe pool in MAB shelf waters could explain why NFRs there were low until this water mass mixed with the GS. Higher availability of organic C in sub-euphotic waters along the productive North Atlantic continental shelf and at coastal stations in the ETSP could also explain why NFRs were detected here and not in other deep waters. Moving forward, significantly more work is needed to elucidate the net effect of these factors in combination as drivers of marine N_2 fixation.

REFERENCES

Albani, S. and others 2014. Improved dust representation in the Community Atmosphere Model. J. Adv. Mod. Earth Sys. 6: 541-570.

Altschul, S. F., W. Gish, W. Miller, E. W. Myers, and D. J. Lipman. 1990. Basic local alignment search tool. J. Mol. Biol. 215: 403-410.

Amante, C., and B. W. Eakins. 2009. ETOPO1 1 Arc-Minute Global Relief Model: Procedures, Data Sources and Analysis. NOAA Technical Memorandum NESDIS NGDC-24.

Atkinson, L. P. 1977. Modes of Gulf Stream intrusion into the South Atlantic Bight shelf waters. Geophys. Res. Lett. 4: 583-586.

Andersson, B., K. Sundbäck, M. Hellman, S. Hallin, and C. Alsterberg. 2014. Nitrogen fixation in shallow-water sediments: Spatial distribution and controlling factors. Limnol. Oceanogr. 59: 1932-1944.

Basu, S., M. Gledhill, D. de Beer, S. P. Matondkar, and Y. Shaked. 2019. Colonies of marine cyanobacteria Trichodesmium interact with associated bacteria to acquire iron from dust. Comm. Biol. 2: 1-8.

Benavides, M. and J. Robidart. 2020. Bridging the spatiotemporal gap in diazotroph activity and diversity with high-resolution measurements. Front. Mar. Sci. 7: 810.

Benavides, M., S. Bonnet, I. Berman-Frank, and L. Riemann. 2018. Deep into oceanic N_2 fixation. Front. Mar. Sci. 5: 108. doi: 10.3389/fmars.2018.00108

Benavides, M. and others. 2016. Basin-wide N_2 fixation in the deep waters of the Mediterranean Sea. Global Biogeochem. Cycles 30(6): 952-961. doi: 10.1002/2015GB005326

Benavides, M., P. Moisander, H. Berthelot, T. Dittmar, O. Grosso, and S. Bonnet. 2015. Mesopelagic N_2 fixation related to organic matter composition in the Solomon and Bismarck Seas (Southwest Pacific). PloS One 10(12): e0143775.

Bentzon-Tilia, M., S. Traving, M. Mantikci, H. Knudsen-Leerbeck, J. Hansen, S. Markager, and L. Riemann. 2015. Significant N_2 fixation by heterotrophs, photoheterotrophs and heterocystous cyanobacteria in two temperate estuaries. ISME J. 9(2): 273-285.

Berges, J. A. and M. Mulholland. 2008. Enzymes and nitrogen cycling, p. 1385-1444. In D. G. Capone, D. A. Bronk, M. R. Mulholland, and E. J. Carpenter [eds.], Nitrogen in the marine environment. Academic Press.

Blais, M., J. Tremblay, A. Jungblut, J. Gagnon, J. Martin, M. Thaler, and C. Lovejoy. 2012. Nitrogen fixation and identification of potential diazotrophs in the Canadian Arctic. Global Biogeochem. Cycles 26(3): GB3022. doi: 10.1029/2011GB004096

Bombar, D., R. W. Paerl, R. Anderson, and L. Riemann. 2018. Filtration via conventional glass fiber filters in $^{15}N_2$ tracer assays fails to capture all nitrogen-fixing prokaryotes. Front. Mar. Sci. 5: 6. doi: 10.3389/fmars.2018.00006

Bombar, D., R. W. Paerl, and L. Riemann. 2016. Marine non-cyanobacterial diazotrophs: moving beyond molecular detection. Trends Microbiol. 24: 916-927. doi: 10.1016/j.tim.2016.07.002

Bonnet, S., M. Caffin, H. Berthelot, and T. Moutin. 2017. Hot spot of N_2 fixation in the Western tropical South Pacific pleads for a spatial decoupling between N_2 fixation and denitrification. PNAS 114: E2800-E2801.

Bonnet, S. and others 2013. Aphotic N_2 fixation in the eastern tropical South Pacific Ocean. PloS One 8: e81265. doi:10.1371/journal.pone.0081265

Böttjer, D. and others 2017. Temporal variability of nitrogen fixation and particulate nitrogen export at Station ALOHA. Limnol. Oceanogr. 62(1): 200-216.

Breiman, L. 2001. Random forests. Machine Learning 45: 5-32.

Bustin, S. A., R. Mueller, and T. Nolan. 2020. Parameters for successful PCR primer design, p. 5-22. In R. Biassoni and A. Raso [eds.], Quantitative Real-Time PCR: Methods and protocols. Methods in Molecular Biology. Springer Science and Business Media, LLC, part of Springer Nature.

Bundy, R. M., D. V. Biller, K. N. Buck, K. W. Bruland, and K. A. Barbeau. 2014. Distinct pools of dissolved iron-binding ligands in the surface and benthic boundary layer of the California Current. Limnol. Oceanogr. 59: 769-787.

Bundy, R. M., H. A. Abdulla, P. G. Hatcher, D. V. Biller, K. N. Buck, and K. A. Barbeau. 2015. Iron-binding ligands and humic substances in the San Francisco Bay estuary and estuarine-influenced shelf regions of coastal California. Mar. Chem. 173: 183-194.

Capone, D. G. and others. 2005. Nitrogen fixation by Trichodesmium spp.: An important source of new nitrogen to the tropical and subtropical North Atlantic Ocean. Global Biogeochem. Cycles 19: GB2024, doi:10.1029/2004GB002331

Capone, D. G., J. P. Zehr, H. W. Paerl, B. Bergman, and E. J. Carpenter. 1997. Trichodesmium, a globally significant marine cyanobacterium. Science 276: 1221-1229.

Caputo, A., M. Stenegren, M. Pernice, and R. Foster. 2018. A short comparison of two marine planktonic diazotrophic symbioses highlights an un-quantified disparity. Front. Mar. Sci. 5: 2. doi: 10.3389/fmars.2018.00002

Carpenter, E. J. and D. Capone. 2008. Nitrogen fixation in the marine environment, p. 141-198. In D. G. Capone, D. A. Bronk, M. R. Mulholland, and E. J. Carpenter [eds.], Nitrogen in the marine environment. Academic Press.

Carpenter, E. J., J. Montoya, J. Burns, M. Mulholland, A. Subramaniam, and D. Capone 1999. Extensive bloom of a N_2-fixing diatom/cyanobacterial association in the tropical Atlantic Ocean. Mar. Ecol. Prog. Ser.: 273-283.

Chang, B. X. and others 2019. Low rates of dinitrogen fixation in the eastern tropical South Pacific. Limnol. Oceanogr. doi: 10.1002/lno.11159

Chang, B., J. Rich, A. Jayakumar, H. Naik, A. Pratihary, R. Keil, B. Ward, A. Devol. 2014. The effect of organic carbon on fixed nitrogen loss in the eastern tropical South Pacific and Arabian Sea oxygen deficient zones. *Limnol. Oceanogr.* 59(4): 1267-1274. doi: 10.4319/lo.2014.59.4.1267

Church, M. J., B. D. Jenkins, D. M. Karl, and J. P. Zehr. 2005a. Vertical distributions of nitrogen-fixing phylotypes at Stn ALOHA in the oligotrophic North Pacific Ocean. Aquat. Microb. Ecol. 38: 3-14, doi:10.3354/ame038003

Church, M. J., C. M. Short, B. D. Jenkins, D. M. Karl, and J. P. Zehr. 2005b. Temporal patterns of nitrogenase gene (nifH) expression in the oligotrophic North Pacific Ocean. Appl. and Environ. Microbiol. 71: 5362-5370, doi: 10.1128/aem.71.9.5362-5370.2005

Climate Prediction Center. Historical El Niño/La Niña episodes (1950-present). http://origin.cpc.ncep.noaa.gov/products/analysis_monitoring/ensostuff/ONI_v5.php (21 January 2019, date last accessed).

Churchwell, J. H., and T. J. Berger. 1998. Transport of middle Atlantic Bight shelf water to the Gulf Stream near Cape Hatteras. J. Geophys. Res.: Oceans 103: 30605-30621.

Codispoti, L. 2007. An oceanic fixed nitrogen sink exceeding 400 Tg N a^{-1} vs. the concept of homeostasis in the fixed-nitrogen inventory. Biogeosci. 4(2): 233-253.

Colón-López, M. S., D. M. Sherman, and L. A. Sherman. 1997. Transcriptional and translational regulation of nitrogenase in light-dark-and continuous-light-grown cultures of the unicellular cyanobacterium Cyanothece sp. strain ATCC 51142. J. Bacteriol. 179: 4319-4327.

Csanady, G., and P. Hamilton. 1988. Circulation of slopewater. Cont. Shelf Res. 8: 565-624.

Cutter, G. A., J. W. Moffett, M. C. Nielsdóttir, and V. Sanial. 2018. Multiple oxidation state trace elements in suboxic waters off Peru: In situ redox processes and advective/diffusive horizontal transport. Mar. Chemi. 201: 77-89. doi: 10.1016/j.marchem.2018.01.003

Dabundo, R. and others 2014. The contamination of commercial $^{15}N_2$ gas stocks with ^{15}N–labeled nitrate and ammonium and consequences for nitrogen fixation measurements. PloS One 9: e110335. doi: 10.6084/m9.figshare.1170194

Dekaezemacker, J., S. Bonnet, O. Grosso, T. Moutin, M. Bressac, and D. Capone. 2013. Evidence of active dinitrogen fixation in surface waters of the eastern tropical South Pacific during El Niño and La Niña events and evaluation of its potential nutrient controls. Global Biogeochem. Cycles 27: 768-779. doi: 10.1002/gbc.20063

Deutsch, C., N. Gruber, R. Key, J. Sarmiento, and A. Ganachaud. 2001. Denitrification and N_2 fixation in the Pacific Ocean. Global Biogeochem. Cycles 15(2): 483-506. doi: 10.1029/2000GB001291

Deutsch, C., J. L. Sarmiento, D. M. Sigman, N. Gruber, and J. P. Dunne. 2007. Spatial coupling of nitrogen inputs and losses in the ocean. Nature 445: 163-167.

Deutsch, C., D. M. Sigman, R. C. Thunell, A. N. Meckler, and G. H. Haug. 2004. Isotopic constraints on glacial/interglacial changes in the oceanic nitrogen budget. Global Biogeochem. Cycles 18: GB4012. doi: 10.1029/2003GB002189

Devol, A. 2008. Denitrification including anammox, p. 263-301. In D. G. Capone, D. A. Bronk, M. R. Mulholland, and E. J. Carpenter [eds.], Nitrogen in the marine environment. Academic Press.

DeVries, T., C. Deutsch, F. Primeau, B. Chang, and A. Devol. 2012. Global rates of water-column denitrification derived from nitrogen gas measurements. Nature Geoscience 5(4): 547-550. doi: 10.1038/ngeo1515.

Dixon, R., and D. Kahn, 2004. Genetic regulation of biological nitrogen fixation. Nat. Rev. Microbiol. 2(8): 621-631.

Druffel, E., P. Williams, J. Bauer, and J. Ertel, 1992. Cycling of dissolved and particulate organic matter in the open ocean. J. Geophys. Res.: Oceans 97(C10): 15639-15659.

Dugdale, R. C., J. J. Goering, and J. H. Ryther. 1964. High nitrogen fixation rates in the Sargasso Sea and the Arabian Sea. Limnol. Oceanogr. 9: 507-510.

Eren, A. M., H. G. Morrison, P. J. Lescault, J. Revewellaud, J. H. Vineis, and M. L. Sogin. 2015. Minimum entropy decomposition: unsupervised oligotyping for sensitive partitioning of high-throughput marker gene sequences. ISME J. 9: 968, doi:10.1038/ismej.2014.195

Farnelid, H. and others 2019. Diverse diazotrophs are present on sinking particles in the North Pacific Subtropical Gyre. ISME J. 13: 170, doi:10.1038/s41396-018-0259-x

Farnelid, H. and others. 2013. Active nitrogen-fixing heterotrophic bacteria at and below the chemocline of the central Baltic Sea. ISME J. 7(7): 1413-1423.

Falkowski, P. G. 1983. Enzymology of nitrogen assimilation, p. 839-868. In D. G. Capone, E. J. Carpenter [eds.], Nitrogen in the marine environment. Elsevier.

Falkowski. 1997. Evolution of the nitrogen cycle and its influence on the biological sequestration of CO_2 in the ocean. Nature 387: 272-275.

Farnelid, H., K. Turk-Kubo, H. Ploug, J. Ossolinski, J. Collins, B. Van Mooy, and J. Zehr. 2019. Diverse diazotrophs are present on sinking particles in the North Pacific Subtropical Gyre. ISME J. 13(1): 170-182.

Fernandez, C., L. Farías, and O. Ulloa. 2011. Nitrogen fixation in denitrified marine waters. PloS One 6: e20539. doi: :10.1371/journal.pone.0020539

Fiedler, P. C., and L. D. Talley. 2006. Hydrography of the eastern tropical Pacific: a review. Prog. Oceanogr. 69: 143-180. doi: 10.1016/j.pocean.2006.03.008

Flores, E., and A. Herrero. 2005. Nitrogen assimilation and nitrogen control in cyanobacteria. Biochem. Soc. Transact. 33, 164-167.

Fonseca-Batista, D. and others 2019. Evidence of high N_2 fixation rates in the temperate northeast Atlantic. Biogeosci. 16: 999-1017, doi:10.3929/ethz-b-000332762

Garcia, H. and others 2018. World Ocean Atlas 2018 Vol. 3: Dissolved Oxygen. Apparent Oxygen Utilization, and Dissolved Oxygen Saturation, NOAA Atlas NESDIS 83.

Gledhill, M., and K. N. Buck. 2012. The organic complexation of iron in the marine environment: a review. Front. Microbiol. 3: 69.

Glibert, P., and D. Capone. 1993. Mineralization and assimilation in aquatic, sediment, and Itland systems, p. 243–272. In R. Knowles and T. H. Blackburn [eds.], Nitrogen Isotope Techniques. Academic Press: San Diego, CA.

Goering, J. J., R. C. Dugdale, and D. W. Menzel. 1966. Estimates of in situ rates of nitrogen uptake by Trichodesmium sp. in the tropical Atlantic Ocean. Limnol. Oceanogr. 11: 614-620.

Gradoville, M. R., D. Bombar, B. Crump, R. Letelier, J. Zehr, and A. White. 2017. Diversity and activity of nitrogen-fixing communities across ocean basins. Limnol. Oceanogr. http:doi.org/10.1002/lno.10542

Großkopf, T., and J. LaRoche. 2012. Direct and indirect costs of dinitrogen fixation in Crocosphaera watsonii WH8501 and possible implications for the nitrogen cycle. Front. Microbiol. 3: 236. doi: 10.3389/fmicb.2012.0023

Grosse, J., D. Bombar, H. Doan, L. Nguyen, and M. Voss, 2010. The Mekong River plume fuels nitrogen fixation and determines phytoplankton species distribution in the South China Sea during low and high discharge season. Limnol. Oceanogr. 55(4): 1668-1680.

Gruber, N., and J. Galloway. 2008. An Earth-system perspective of the global nitrogen cycle. Nature 451(7176): 293.

Gruber, N. 2004. The dynamics of the marine nitrogen cycle and its influence on atmospheric CO2 variations, p. 97-148. The ocean carbon cycle and climate. Springer.

Halm, H., P. Lam, T. Ferdelman, G. Lavik, T. Dittmar, J. LaRoche, S. D'hondt, and M. Kuypers. 2012. Heterotrophic organisms dominate nitrogen fixation in the South Pacific Gyre. ISME J. 6: 1238-1249. doi: 10.1038/ismej.2011.182

Hamersley, M. R., K. Turk, A. Leinweber, N. Gruber, N., J. Zehr, T. Gunderson, and D. Capone. 2011. Nitrogen fixation within the water column associated with two hypoxic basins in the Southern California Bight. Aquat. Microbial Ecol. 63(2): 193-205.

Hansell, D. A., and C. Carlson. 1998. Deep-ocean gradients in the concentration of dissolved organic carbon. Nature 395: 263-266.

Harding, K., K. Turk-Kubo, R. Sipler, M. Mills, D. Bronk, and J. Zehr. 2018. Symbiotic unicellular cyanobacteria fix nitrogen in the Arctic Ocean. PNAS 115(52): 13371-13375.

Holmes, R. M., A. Aminot, R. Kérouel, B. Hooker, and B. Peterson. 1999. A simple and precise method for measuring ammonium in marine and freshwater ecosystems. Can. J. Fisher. Aquat. Sci. 56(10): 1801-1808.

Hunt, B. P., S. Bonnet, H. Berthelot, B. J. Conroy, R. A. Foster, and M. Pagano. 2016. Contribution and pathways of diazotroph-derived nitrogen to zooplankton during the VAHINE mesocosm experiment in the oligotrophic New Caledonia lagoon. Biogeosci. 13: 3131-3145, doi:10.5194/bg-13-3131-2016

Hutchins, D. A., G. R. DiTullio, and K. W. Burland. 1993. Iron and regenerated production: Evidence for biological iron recycling in two marine environments. Limnol. Oceanogr. 38: 1242-1255.

Jayakumar, A., B. X. Chang, B. Widner, P. Bernhardt, M. R. Mulholland, and B. B. Ward. 2017. Biological nitrogen fixation in the oxygen-minimum region of the eastern tropical North Pacific ocean. ISME J. doi: 10.1038/ismej.2017.97

Jayakumar, A., M. Al-Rshaidat, B. Ward, and M. Mulholland. 2012. Diversity, distribution, and expression of diazotroph nifH genes in oxygen-deficient waters of the Arabian Sea. FEMS Microbiol. Ecol. 82(3): 597-606.

Johnson, K. S., F. P. Chavez, and G. E. Friederich. 1999. Continental-shelf sediment as a primary source of iron for coastal phytoplankton. Nature 398: 697.

Karl, D., M. Church, J. Dore, R. Letelier, C. Mahaffey. 2012. Predictable and efficient carbon sequestration in the North Pacific Ocean supported by symbiotic nitrogen fixation. PNAS 109(6): 1842-1849. doi: 10.1073/pnas.1120312109

Jickells, T. and others. 2005. Global iron connections between desert dust, ocean biogeochemistry, and climate. Science 308(5718): 67-71.

Karl, D. and others. 2002. Dinitrogen fixation in the world's oceans, p. 47-98. In Biogeochemistry Vol. 57/58. The Nitrogen Cycle at Regional to Global Scales. Springer.

Knapp, A., K. Mccabe, O. Grosso, N. Leblond, T. Moutin, and S. Bonnet. 2018. Distribution and rates of nitrogen fixation in the Western tropical South Pacific Ocean constrained by nitrogen isotope budgets. Biogeosci. 15: 2619-2628. doi: 10.5194/bg-15-2619-2018

Knapp, A. N., K. L. Casciotti, W. M. Berelson, M. G. Prokopenko, and D. G. Capone. 2016. Low rates of nitrogen fixation in eastern tropical South Pacific surface waters. PNAS 113: 4398-4403. doi: 10.1073/pnas.1515641113

Knapp, A. N. 2012. The sensitivity of marine N_2 fixation to dissolved inorganic nitrogen. Front. Microbiol. 3.

Knapp, A. N., J. Dekaezemacker, S. Bonnet, J. A. Sohm, and D. G. Capone. 2012. Sensitivity of Trichodesmium erythraeum and Crocosphaera watsonii abundance and N2 fixation rates to varying NO3− and PO43− concentrations in batch cultures. Aquat. Microb. Ecol. 66: 223-236.

Kondo, Y., and J. W. Moffett. 2015. Iron redox cycling and subsurface offshore transport in the eastern tropical South Pacific oxygen minimum zone. Mar. Chem. **168:** 95-103. doi: 10.1016/j.marchem.2014.11.007

Laughlin, R. J., and R. J. Stevens. 2003. Changes in composition of nitrogen-15-labeled gases during storage in septum-capped vials. Soil Sci. Soc. Am. J. 67: 540-543, doi:10.2136/sssaj2003.5400

Löescher, C. R. and others 2014. Facets of diazotrophy in the oxygen minimum zone waters off Peru. ISME J. **8:** 2180-2192. doi: 10.1038/ismej.2014.71

Loh, A. N. and J. Bauer. 2000. Distribution, partitioning and fluxes of dissolved and particulate organic C, N and P in the eastern North Pacific and Southern Oceans. Deep Sea Res. Part I: Oceanogr. Res. Papers 47(12): 2287-2316.

Luo, Y. and others. 2012. Database of diazotrophs in global ocean: abundance, biomass, and nitrogen fixation rates. Earth Syst. Sci. Data 4(1).

Manly, B. F. 2006. Randomization, bootstrap and Monte Carlo methods in biology. CRC Press.

Marino, R., F. Chan, R. W. Howarth, M. Pace, and G. E. Likens. 2002. Ecological and biogeochemical interactions constrain planktonic nitrogen fixation in estuaries. Ecosystems 5: 0719-0725.

Martin, J. H., G. Knauer, D. Karl, and W. Broenkow. 1987. VERTEX: carbon cycling in the northeast Pacific. Deep Sea Res. 34(2): 267-285.

Martinez-Perez, C. and others. 2016. The small unicellular diazotrophic symbiont, UCYN-A, is a key player in the marine nitrogen cycle. Nat. Microbiol. 1(11): 16163. doi: 10.1038/NMICROBIOL.2016.163

McGlathery, K.J., N. Risgaard-Petersen, and P. Christensen. 1998. Temporal and spatial variation in nitrogen fixation activity in the eelgrass Zostera marina rhizosphere. Mar. Ecol. Prog. Ser. 168: 245-258.

Meissner, T., F. Intz, A. Manaster, and L. R. 2019. Remote Sensing Systems SMAP Ocean Surface Salinities [Level 2C, Level 3 Running 8-day, Level 3 Monthly], Version 4.0 validated release.

Miller, J.C. and J.N. Miller. 1988. Basic statistical methods for analytical chemistry, p. 1351-1356. In Part I: Statistics of repeated measurements, 113(9).

Mills, M. M. and others 2020. Unusual marine cyanobacteria/haptophyte symbiosis relies on N_2 fixation even in N-rich environments. ISME J, doi:10.1038/s41396-020-0691-6

Mohr, W., T. Grosskopf, D. W. Wallace, and J. LaRoche. 2010. Methodological underestimation of oceanic nitrogen fixation rates. PLOS One **5:** e12583. doi: 10.1371/journal.pone.0012583

Moisander, P. H., M. Benavides, S. Bonnet, I. Berman-Frank, A. E. White, and L. Riemann. 2017. Chasing after non-cyanobacterial nitrogen fixation in marine pelagic environments. Front. Microbiol. **8:** 1736. doi: 10.3389/fmicb.2017.01736

Moisander, P., E. McClinton, and H. Paerl. 2002. Salinity effects on growth, photosynthetic parameters, and nitrogenase activity in estuarine planktonic cyanobacteria. Microb. Ecol. 43: 432-442, doi:10.1007/s00248-001-1044-2

Moisander, P. H. and others. 2010. Unicellular cyanobacterial distributions broaden the oceanic N_2 fixation domain. Science 327(5972): 1512-1514.

Montoya, J. P., M. Voss, P. Kahler, and D. G. Capone. 1996. A Simple, High-Precision, High-Sensitivity Tracer Assay for N_2 Fixation. Appl. Environ. Microbiol. **62:** 986-993.

Moore, C. and others 2013. Processes and patterns of oceanic nutrient limitation. Nature Geosci. **6:** 701. doi: 10.1038/NGEO3006

Monteiro, F., S. Dutkiewicz, M. Follows. 2011. Biogeographical controls on the marine nitrogen fixers. Global Biogeochem. Cycles 25: GB2003. doi: 10.1029/2010GB003902

Mulholland, M. R. and others. 2012. Rates of dinitrogen fixation and the abundance of diazotrophs in North American coastal waters between Cape Hatteras and Georges Bank. Limnol. Oceanogr. 57(4): 1067-1083.

Mulholland, M., P. Bernhardt, B. Widner, C. Selden, P.D.Chappell, S. Clayton, A. Mannino, and K. Hyde. 2019. High rates of N_2 fixation in temperate, Western North Atlantic coastal waters expands the realm of marine diazotrophy. Global Biogeochem. Cycles 33. doi: 10.1029/2018GB006130

Mulholland, M. R., D. Bronk, and D. Capone. 2004. Dinitrogen fixation and release of ammonium and dissolved organic nitrogen by Trichodesmium IMS101. Aquat. Microb. Ecol. 37(1): 85-94.

Mulholland, M. R., K. Ohki, and D. Capone. 2001. Nutrient controls on nitrogen uptake and metabolism by natural populations and cultures of Trichodesmium (Cyanobacteria). J. Phycol. 37(6): 1001-1009.

Mulholland, M. R., and D. G. Capone. 1999. Nitrogen fixation, uptake and metabolism in natural and cultured populations of Trichodesmium spp. Marine Ecology Progress Series 188: 33-49.

NASA Goddard Space Flight Center, O. B. P. G. Reprocessing. 2018. Moderate-resolution Imaging Spectroradiometer (MODIS) Aqua Chlorophyll Data. NASA Ocean Biology Distibuted Active Archive Center (OB.DAAC), Goddard Space Flight Center, Greenbelt MD.

Nedwell, D. B. 1999. Effect of low temperature on microbial growth: lowered affinity for substrates limits growth at low temperature. FEMS Microbiol. Ecol. 30(2): 101-111.

Nixon, S. and others 1996. The fate of nitrogen and phosphorus at the land-sea margin of the North Atlantic Ocean. Biogeochem. 35: 141-180.

Pai, S. C., C. C. Yang, and J. P. Riley. 1990. Formation kinetics of the pink azo dye in the determination of nitrite in natural waters. Anal. Chim, Acta 232: 345-349.

Parsons, T. R., Y. Maita, and C. M. Lalli. 1984. A manual of biological and chemical methods for seawater analysis. Publ. Pergamon Press, Oxford.

Paulmier, A. and D. Ruiz-Pino 2009. Oxygen minimum zones (OMZs) in the modern ocean. Prog. Oceanogr. 80(3): 113-128.

Pedersen, J. N., D. Bombar, R. W. Paerl, and L. Riemann. 2018. Diazotrophs and N_2 fixation associated with particles in coastal estuarine waters. Front. Microbiol. 9: 2759, doi:10.3389/fmicb.2018.02759

Pedregosa, F. and others 2011. Scikit-learn: Machine learning in Python. J. Mach. Learn. Res. 12: 2825-2830.

Pennington, J. T., K. L. Mahoney, V. S. Kuwahara, D. D. Kolber, R. Calienes, and F. P. Chavez. 2006. Primary production in the eastern tropical Pacific: A review. Prog. Oceaongraph. 69: 285-317. doi: 10.1016/j.pocean.2006.03.012

Pham, A. L., and T. Ito. 2019. Ligand binding strength explains the distribution of iron in the north atlantic ocean. Geophys. Res. Lett. 46: 7500-7508.

Price, P. B. and T. Sowers. 2004. Temperature dependence of metabolic rates for microbial growth, maintenance, and survival. PNAS 101(13): 4631-4636.

Prufert-Bebout, L., H. W. Paerl, and C. Lassen. 1993. Growth, nitrogen fixation, and spectral attenuation in cultivated Trichodesmium species. Appl Environ. Microbiol. 59: 1367-1375.

Ripp, J. 1996. Analytical detection limit guidance and laboratory guide for determining method detection limits. Wisconsin Department of Natural Resources, Laboratory Certification Program.

Rahav, E. and others. 2013. Dinitrogen fixation in aphotic oxygenated marine environments. Front. Microbiol. 4: 227. doi: 10.3389/fmicb.2013.00227

Rahav, E., B. Herut, M. Mulholland, N. Belkin, H. Elifantz, and I. Berman-Frank. 2015. Heterotrophic and autotrophic contribution to dinitrogen fixation in the Gulf of Aqaba. Mar. Ecol. Prog. Ser. 522: 67-77.

Rahav, E., M. Giannetto, and E. Bar-Zeev. 2016. Contribution of mono and polysaccharides to heterotrophic N_2 fixation at the eastern Mediterranean coastline. Sci. Rep. 6: 27858, doi:10.1038/srep27858

Rees, A. P., Gilbert, J. A., and Kelly-Gerreyn, B. A. (2009). Nitrogen fixation in the Western English Channel (NE Atlantic ocean). Marine Ecology Progress Series, 374, 7-12.

Sakamoto, C. M., Friederich, G. E., and Codispoti, L. A. (1990). MBARI procedures for automated nutrient analyses using a modified Alpkem Series 300 Rapid Flow Analyzer. Technical Report No. 90-2. Monterey Bay, CA: Monterey Bay Aquarium Research Institute.

Sammartino, M., S. Marullo, R. Santoleri, and M. Scardi. 2018. Modelling the vertical distribution of phytoplankton biomass in the Mediterranean Sea from satellite data: A neural network approach. Remote Sens. 10: 1666, doi:10.3390/rs10101666

Scholz, F. and others 2016. Nitrate-dependent iron oxidation limits iron transport in anoxic ocean regions. Earth Planet. Sci. Lett. 454: 272-281.

Selden, C. Mulholland, M., Bernhardt, P., Widner, B., Macías-Tapia, A., Qi, J., and A. Jayakumar. 2019. Dinitrogen fixation across physico-chemical gradients of the Eastern Tropical North Pacific oxygen deficient zone. Global Biogeochem. Cycles 33. doi: 10.1029/2019GB006242

Severin, I., M. Bentzon-Tilia, P. Moisander, and L. Riemann. 2015. Nitrogenase expression in estuarine bacterioplankton influenced by organic carbon and availability of oxygen. FEMS Microbiol. Lett. 362(14). doi: 10.1093/femsle/fnv105

Sharp, Z. 2017. Principles of stable isotope geochemistry (2nd ed.). https://digitalrepository.unm.edu/unm_oer/1/ (2 February 2019, date last accessed).

Shiozaki, T., T. Nagata, M. Ijichi, and K. Furuya. 2015. Nitrogen fixation and the diazotroph community in the temperate coastal region of the northwestern North Pacific. Biogeosci. 12(15): 4751-4764. doi: 10.5194/bg-12-4751-2015

Sipler, R. E., D. Gong, S. Baer, M. Sanderson, Q. Roberts, M. Mulholland, and D. Bronk. 2017. Preliminary estimates of the contribution of Arctic nitrogen fixation to the global nitrogen budget. Limnol. Oceanogr. Lett. 2(5): 159-166.

Sohm, J. A., J. A. Hilton, A. E. Noble, J. P. Zehr, M. A. Saito, and E. A. Webb. 2011. Nitrogen fixation in the South Atlantic Gyre and the Benguela upwelling system. Geophys. Res. Lett. 38. doi: 10.1016/j.epsl.2016.09.025

Stewart, F. J. and others 2012. Experimental incubations elicit profound changes in community transcription in OMZ bacterioplankton. PLoS One 7: e37118. doi:10.1038/ismej.2010.18

Subramaniam, A. and others. 2008. Amazon River enhances diazotrophy and carbon sequestration in the tropical North Atlantic Ocean. PNAS 105(30): 10460-10465.

Tang, W., Z. Li, and N. Cassar. 2019a. Machine Learning Estimates of Global Marine Nitrogen Fixation. Journal of Geophysical Research: Biogeosci. 124: 717-730, doi:10.1029/2018JG004828

Tang, W. and others 2019b. Revisiting the distribution of oceanic N_2 fixation and estimating diazotrophic contribution to marine production. Nat. Comm. 10: 831, doi:10.1038/s41467-019-08640-0

Thamdrup, B., T. Dalsgaard, and N. P. Revsbech. 2012. Widespread functional anoxia in the oxygen minimum zone of the Eastern South Pacific. Deep Sea Res., Part I 65: 36-45. doi: 10.1016/j.dsr.2012.03.001

Thompson, A., B. J. Carter, K. Turk-Kubo, F. Malfatti, F. Azam, and J. P. Zehr. 2014. Genetic diversity of the unicellular nitrogen-fixing cyanobacteria UCYN-A and its prymnesiophyte host. Environ. Microbiol. 16: 3238-3249, doi:10.1111/1462-2920.12490

Voss, M., J. W. Dippner, and J. P. Montoya. 2001. Nitrogen isotope patterns in the oxygen-deficient waters of the Eastern Tropical North Pacific Ocean. Deep Sea Res., Part I 48: 1905-1921.

Tyrrell, T. and C. Law. 1997. Low nitrate:phosphate ratios in the global ocean. Nature 387(6635): 793-796.

Villareal, T. A. 1992. Marine nitrogen-fixing diatom-cyanobacteria symbioses, p. 163-175. In: E. J. Carpenter, D. G. Capone, J. G. Rueter [eds.], Marine pelagic cyanobacteria: Trichodesmium and other diazotrophs. Springer.

Vitousek, P. M. and others. 2002. Towards an ecological understanding of biological nitrogen fixation, p. 1-45. In E. W. Boyer and R. W. Howarth [eds.], The nitrogen cycle at regional to global scales. Springer.

Weber, T., and C. Deutsch. 2014. Local versus basin-scale limitation of marine nitrogen fixation. PNAS 111: 8741-8746.

Welschmeyer, N. A. 1994. Fluorometric analysis of chlorophyll a in the presence of chlorophyll b and pheopigments. Limnol. Oceanogr. 39(8): 1985-1992.

Wen, Z., W. Lin, R. Shen, H. Hong, S. Kao and D. Shi. 2017. Nitrogen fixation in two coastal upwelling regions of the Taiwan Strait. Sci. Rep. 7(1): 17601. doi: 10.1038/s41598-017-18006-5

White, A. E. and others. 2013. Nitrogen fixation in the Gulf of California and the Eastern Tropical North Pacific. Prog. Oceanogr. 109: 1-17.

Wilson, S. T., D. Böttjer, M. Church, and D. Karl. 2012. Comparative assessment of nitrogen fixation methodologies, conducted in the oligotrophic North Pacific Ocean. Appl. Environ. Microbiol. 78(18): 6516-6523.

White, A. E. and others 2020. A critical review of the $^{15}N_2$ tracer method to measure diazotrophic production in pelagic ecosystems. Limnol. Oceanogr.: Methods. doi: 10.1002/lom3.10353

Zehr, J. P., and D. G. Capone. 2020. Changing perspectives in marine nitrogen fixation. Science 368: eaay9514. doi: 10.1126/science.aay9514

Zehr, J. P., and H. W. Paerl. 2008. Molecular ecological aspects of nitrogen fixation in the marine environment. Microb. Ecol. Oceans**:** 481-525.

Zehr, J., and P. Turner. 2001. Nitrogen Fixation: Nitrogenase Genes and Gene Expression, p. 271-286. In J. H. Paul [ed.], Methods in Microbiology. Academic Press Ltd.

APPENDIX A

SUPPLEMENTAL INFORMATION FOR CHAPTER II

Suppl. Text 1: Materials and methods

Hydrographic and nutrient measurements. Samples for chlorophyll *a* analysis via the non-acidification method (Welschmeyer, 1994) were filtered onto Whatman GF-75 filters (0.3 μm nominal pore size) and extracted in 90% acetone for 24 hours at -20°C. Filtrate for dissolved nutrient analysis was collected in sterile acid-washed (10% HCl) and sample-rinsed Falcon tubes directly from Niskin bottles through a 0.2 μm Supor cartridge filter. Detection limits for shipboard NO_3^-+NO_2^-, SRP, NO_2^- and NH_4^+ concentrations were 0.14, 0.03, 0.20 and 0.011 μM, respectively (3σ, n=7). The detection limit for chlorophyll *a* was 0.025 μg L^{-1} (3σ, n=7). The uncertainty reported for NO_3^- concentrations was calculated from the standard deviation of the NO_3^-+NO_2^- and NO_2^- concentrations using standard propagation of errors, and that of DIN, defined as the sum of NO_3^-+NO_2^- and NH_4^+ concentration, was calculated similarly from the standard deviation of these measurements. The detection limit for pump profiling system NO_3^- +NO_2^- , NO_2^-, and NH_4^+ concentrations were 0.30, 0.02, and 0.05 μM, respectively.

N_2 fixation incubation experiments – sample collection and handling. Site water from above and below the OMZ (and DEEP samples) was collected from Niskin bottles affixed to the CTD rosette. Incubation bottles were rinsed three times with sample water and then filled completely. Bottles were capped, and any remaining air was displaced by injecting site water. After the removal of any remaining air bubbles, highly enriched $^{15}N_2$ gas (~99%, Cambridge Isotopes, Tewksbury, MA) was added to initiate uptake experiments. While contamination of $^{15}N_2$ gas

with isotopically-heavy NH_4^+ and NO_3^- has been noted as a concern in measuring NFRs, contaminants have only been reported from Cambridge Isotopes stocks at trace levels (Dabundo et al. 2014). Furthermore, I routinely observed undetectable rates of N_2 fixation throughout our study area, in both DIN-deplete and replete waters, which would have been unlikely had there been contamination of our $^{15}N_2$ stock in the present study. To increase the rate of $^{15}N_2$ gas dissolution, sample bottles were gently inverted for 15 minutes on a large see-saw. The remaining gas bubble was then removed with a syringe so that the atom-% enrichment of the source pool was constant in bottles over the remainder of the incubation period.

Samples from within the OMZ were collected at and below the secondary NO_2^- maximum at every station, the depths of which were determined using the high resolution NO_2^- profiles generated from the autoanalyzer interfaced with the PPS. Water was pumped directly from depth into 4 L amber glass bottles. Each bottle was rinsed three times with sample water, filled from the bottom using the PPS hose, and submerged in a 50 L tub of ODZ water while continuing the flow of site water into the bottle. This arrangement allowed for a layer of low-oxygen water to be maintained above the bottle as it displaced the water already in the bottle thereby preventing contamination of the incubation water with air. As the bottles were continuously refilled, water at the surface of the tub was replaced with fresh, low oxygen water being displaced from the incubation bottles. The positive pressure achieved in the bottle further precluded the back-flow of oxygen-contaminated water from the tub into the sample. Sufficient water was pumped from depth to displace the bottle volume at least three times before the bottle was capped underwater. This sampling process also served to maintain subsurface water temperatures as incubation bottles were being filled. The exposed portion of the PPS sampling tube was wrapped in black electrical tape to prevent light-shock of microbes, and tarps were

hung above the tub to shade samples and reduce further warming. Once capped, sample bottles were treated as described above for those collected from above and below the OMZ.

NFR calculations and error analysis – estimation of uncertainty. Following Montoya et al. (1996) and Gradoville et al. (2017), a sensitivity analysis attributing error among these components, averaged by sample type, is presented in Suppl. Table 1. When A_{N_2} data was not available, the arithmetic mean and standard deviation of all samples collected either from euphotic (3.78 ±1.05 atom-%) or subeuphotic (3.02 ±0.97 atom-%) waters were used instead. I also used initial PN concentration ([PN]) rather than the average of initial and final [PN] (Montoya et al. 1996) due to the better accuracy of the volume measurement associated with initial PN samples. The uncertainty of the initial PN concentration was calculated by propagating the standard deviation of three replicate PN mass samples and the error associated with volume measurement.

The incubation time is denoted as Δt. Uncertainty in Δt is affected by the length of filtration, which can be time-consuming for large-volume incubations, and biological processes may continue in the sample throughout this duration. For oligotrophic 1 and 4 L samples, I estimated maximum filtration times of 15 min and 1 h, respectively, representing uncertainties of approximately 1, 4, and 2% in the Δt of surface (24 h, 1 L), ODZ (24 h, 4 L), and deep (48 h, 4 L) incubations, respectively. This error was always greater than any variation in the Δt of triplicate incubations. The propagated error of each NFR was calculated as described by Montoya et al. (1996).

Suppl. Table 1. Sensitivity analysis for NFR (NFR) calculation, performed as in Montoya et al. (1996) and Gradoville et al. (2017) on values averaged by depth horizon.[a]

Depth horizon	Parameter (X)[b]	Average value	Error[c]	δNFR/δX[d]	Error contribution (Error × [δNFR/δX])^{2}[e]	% Total error[f]	Summary
EUPH	Δt	1.00	1.04×10^{-2}	-3.01×10^{0}	9.81×10^{-4}	0.03	Count..…... ….68 Mean……..….3.05 LOQ……...….2.60 LOD…….....0.78
	A_{N_2}	3.83	7.06×10^{-1}	-7.32×10^{-1}	2.67×10^{-1}	6.68	
	A_{PN_0}	0.370	9.26×10-^{4}	-1.86×10^{2}	2.98×10^{-2}	29.3	
	A_{PN_f}	0.386	1.09×10^{-2}	1.87×10^{2}	4.20×10^{0}	58.6	
	PN mass	6.48×10^{2}	7.17×10^{1}	4.71×10^{-3}	1.14×10^{-1}	5.36	
	Volume	0.99	8.87×10^{-3}	0.00×10^{0}	7.27×10^{-4}	0.03	
	$[PN]_i$	6.51×10^{2}					
OMZ	Δt	1.25	4.17×10^{-2}	-9.73×10^{-1}	1.65×10^{-3}	0.29	Count…….39 Mean……..….1.26 LOQ...…….1.53 LOD……...0.46
	A_{N_2}	3.06	5.45×10^{-1}	-3.89×10^{-1}	4.50×10^{-2}	7.27	
	A_{PN_0}	0.370	7.65×10^{-4}	-5.34×10^{1}	1.67×10^{-3}	27.9	
	A_{PN_f}	0.393	6.77×10^{-3}	5.39×10^{1}	1.33×10^{-1}	60.8	
	PN mass	5.61×10^{2}	5.31×10^{1}	2.24×10^{-3}	1.42×10^{-2}	3.65	
	Volume	3.09	2.41×10^{-2}	1.21×10^{1}	9.48×10^{-5}	0.01	
	$[PN]_i$	1.81×10^{2}					
DEEP	Δt	1.92	4.17×10^{-2}	-2.12×10^{-1}	7.78×10^{-5}	0.10	Count……...12 Mean…….0.41 LOQ……..0.27 LOD…….0.08
	A_{N_2}	3.01	9.03×10^{-1}	-1.17×10^{-1}	1.12×10^{-2}	16.0	
	A_{PN_0}	0.370	1.32×10^{-3}	-2.15×10^{1}	8.02×10^{-4}	34.8	
	A_{PN_f}	0.389	7.01×10^{-3}	2.16×10^{1}	2.30×10^{-2}	40.4	
	PN mass	3.59×10^{2}	4.92×10^{1}	1.16×10^{-3}	3.23×10^{-3}	8.75	
	Volume	3.28	1.62×10^{-2}	8.08×10^{0}	4.14×10^{-6}	0.01	
	$[PN]_i$	1.09×10^{2}					

[a]Organic matter additions, bioassays and other measurements subject to extra manipulation are not included here.
[b]The parameters Δt, $\boldsymbol{A_{PN_0}}$, $\boldsymbol{A_{PN_f}}$ and $\boldsymbol{A_{N_2}}$ represent incubation length (days), initial and final particulate N (PN) isotopic composition (atom-%), $^{15}N_2$ enrichment (atom-%) and PN concentration ($[PN]_i$, nmol N L^{-1}).
[c]Determined as described in the text and in Text S1.
[d]The partial derivative of NFR with respect to each parameter, calculated using the values in the third and fourth columns.
[e]The absolute contribution of each parameter to the total uncertainty in the final NFR.
[f]The relative contribution of each parameter to the total uncertainty.

Suppl. Table 2. Summary of NFRs from above (EUPH), within (OMZ), and below (DEEP) the ETNP ODZ.

Sta.	Depth (m)	Depth horizon	Lat. (°N)	Long. (°W)	Temp. (°C)	Sal.	[O_2] (µmol kg^{-1})	[Chl-a] (µg L^{-1})	[DIN] (µM)	[SRP] (µM)	NFR (nmol N m^{-2} d^{-1})	NFR prop. error	LOD (nmol N m^{-2} d^{-1})	LOQ (nmol N m^{-2} d^{-1})	Flag
1	9	EUPH	25.791	-115.261	19.5	34.4	222	0.15	0.16	0.3	9.55	6.51	0.57	1.9	
1	63	EUPH	25.791	-115.262	18.8	34.2	217	0.55	0.88	0.41	11.06	9.39	0.67	2.23	
1	77	EUPH	25.791	-115.262	17	34	187	0.23	5.54	0.81	4.45	2.65	0.49	1.63	
1	96	EUPH	25.791	-115.262	13.4	33.7	148	0.06	13.25	1.27	2.49	1.19	0.33	1.1	
1	199	OMZ	25.475	-115.156	11.5	34.3	52	nan	25.98	2.32			0.24	0.8	BDL
2	10	EUPH	24.041	-112.891	21	34.6	215	0.16	0.38	0.3	89.32	83.54	0.51	1.7	
2	69	EUPH	24.041	-112.891	20.2	34.5	204	0.41	0.49	0.38	37.82	14.37	0.7	2.33	
2	79	EUPH	24.04	-112.891	19	34.3	188	0.35	3.49	0.63			0.53	1.77	BDL
2	90	EUPH	24.041	-112.891	17.8	34.3	128	0.16	12.76	1.53			0.35	1.17	BDL
2	150	OMZ	24.024	-112.534	12.8	34.4	51	nan	24.54	2.49			2.48	8.27	BDL
2	300	OMZ	24.024	-112.534	10.2	34.6	8	nan	28.63	2.85			0.61	2.03	BDL
3	10	EUPH	22.608	-110.202	21.9	34.6	211	0.14	0.27	0.34	2	0.57	0.32	1.07	
3	55	EUPH	22.608	-110.203	20.9	34.4	196	0.23	0.25	0.37			0.4	1.33	BDL
3	66	EUPH	22.608	-110.203	19.2	34.3	175	0.45	5.21	0.83			0.35	1.17	BDL
3	88	EUPH	22.608	-110.203	15.9	34.3	76	0.12	18.12	2.08			0.28	0.93	BDL
3	180	OMZ	22.366	-110.121	12.3	34.6	17	nan	26.2	2.77			2.13	7.1	BDL
3	300	OMZ	22.366	-110.121	10.6	34.6	5	nan	28.17	2.95			1.18	3.93	BDL
4	10	EUPH	21.292	-108.242	24.3	34.5	203	0.13	0.15	0.3			0.27	0.9	DNQ
4	47	EUPH	21.292	-108.242	23.2	34.5	206	0.14	0.18	0.32			0.3	1	DNQ
4	57	EUPH	21.292	-108.242	22.4	34.5	188	0.35	1.03	0.44			0.31	1.03	BDL
4	73	EUPH	21.292	-108.242	20.2	34.5	92	0.19	14.9	1.6			0.35	1.17	BDL
4	300	OMZ	21.176	-108.146	10.7	34.7	<3	nan	27.5	2.97			0.65	2.17	BDL
5	10	EUPH	19.985	-106.313	25.2	34.6	204	0.15	0.57	0.37	14.97	2.82	0.6	2	
5	49	EUPH	19.985	-106.313	23.7	34.6	205	0.41	0.59	0.45			1.18	3.93	DNQ

Suppl. Table 2. *Continued.*

Sta.	Depth (m)	Depth horizon	Lat. (°N)	Long. (°W)	Temp. (°C)	Sal.	[O_2] (µmol kg^{-1})	[Chl-a] (µg L^{-1})	[DIN] (µM)	[SRP] (µM)	NFR (nmol N m^{-2} d^{-1})	NFR prop. error	LOD (nmol N m^{-2} d^{-1})	LOQ (nmol N m^{-2} d^{-1})	Flag
5	63	EUPH	19.985	-106.313	22.3	34.6	168	0.61	2.67	0.79			0.88	2.93	BDL
5	76	EUPH	19.985	-106.313	18.6	34.6	73	0.24	18.74	2			0.51	1.7	BDL
6	10	EUPH	18.688	-104.416	25.3	34.4	199	0.41	0.64	0.44	9.15	2.4	1.82	6.07	
6	30	EUPH	18.689	-104.416	22.3	34.5	110	0.98	10.71	1.34			2	6.67	BDL
6	46	EUPH	18.689	-104.416	20.4	34.5	53	0.61	19.2	1.98			1.03	3.43	BDL
6	79	EUPH	18.689	-104.416	15.1	34.8	4	0.18	26.06	2.57			1.18	3.93	BDL
6	120	OMZ	18.414	-104.25	13.5	34.8	<3	nan	26.3	2.61			0.29	0.97	BDL
6	158	OMZ	18.413	-104.25	12.5	34.8	<3	nan	26.96	2.67			0.27	0.9	BDL
6	310	OMZ	18.413	-104.25	10.4	34.7	<3	nan	25.69	2.8			0.15	0.5	BDL
6	500	DEEP	18.689	-104.416	7.5	27	<3	nan	36.33	3.19			0.17	0.57	BDL
6	998	DEEP	18.689	-104.416	4.3	27.4	11	nan	46.33	3.37			0.13	0.43	BDL
6	2002	DEEP	18.688	-104.416	2.2	27.7	82	nan	42.44	2.95			0.12	0.4	BDL
7	10	EUPH	17.5	-102.7	26.6	34.3	196	0.16	0.37	0.32	3.99	1.07	0.87	2.9	
7	37	EUPH	17.5	-102.7	22.5	34.4	104	0.86	8.37	1.21			1.21	4.03	BDL
7	48	EUPH	17.5	-102.7	19.6	34.5	37	0.36	23.64	2.28			0.51	1.7	BDL
7	86	EUPH	17.5	-102.7	14.8	34.8	4	0.23	26.92	2.63			0.53	1.77	BDL
7	144	OMZ	17.3	-102.42	13	34.8	<3	nan	26.91	2.73			0.29	0.97	BDL
7	168	OMZ	17.3	-102.42	12.6	34.8	<3	nan	27.97	nan			0.14	0.47	BDL
7	334	OMZ	17.3	-102.42	10.1	34.7	<3	nan	28.35	nan			0.18	0.6	BDL
8	10	EUPH	16.25	-100.845	27	34.2	197	0.21	0.15	0.36	10.11	4.27	1	3.33	
8	33	EUPH	16.25	-100.845	24.2	34.3	175	1.29	0.24	0.54			3.24	10.8	DNQ
8	37	EUPH	16.25	-100.845	21.8	34.4	59	0.74	19.93	1.95			1.54	5.13	BDL
8	82	EUPH	16.25	-100.845	14.8	34.8	3	0.19	28.28	2.64			0.82	2.73	BDL
8	120	OMZ	16.15	-100.506	13.8	34.9	<3	nan	28.51	2.66			0.26	0.87	BDL
8	165	OMZ	16.15	-100.506	12.8	34.8	<3	nan	30.09	2.67			0.31	1.03	BDL
8	336	OMZ	16.15	-100.506	9.9	34.7	<3	nan	27.45	3.01			0.1	0.33	BDL
9	10	EUPH	15	-98.999	28.7	33.7	192	0.18	0.24	0.27			0.39	1.3	BDL

Suppl. Table 2. *Continued.*

Sta.	Depth (m)	Depth horizon	Lat. (°N)	Long. (°W)	Temp. (°C)	Sal.	[O_2] (µmol kg^{-1})	[Chl-a] (µg L^{-1})	[DIN] (µM)	[SRP] (µM)	NFR (nmol N m^{-2} d^{-1})	NFR prop. error	LOD (nmol N m^{-2} d^{-1})	LOQ (nmol N m^{-2} d^{-1})	Flag
9	47	EUPH	15	-98.999	22.6	34.3	114	0.96	13.13	1.31			1.04	3.47	BDL
9	56	EUPH	15	-98.999	20.6	34.5	45	0.53	24.18	2.22			0.51	1.7	BDL
9	100	EUPH	15.001	-99	14.2	34.8	4	0.18	28.21	2.66			0.35	1.17	BDL
9	110	OMZ	15	-98.999	14.2	34.8	3	nan	28.48	2.65			0.38	1.27	BDL
9	120	OMZ	15.001	-99	13.3	34.8	3	nan	29.52	2.66			0.13	0.43	BDL
9	135	OMZ	15	-99	13.1	34.8	<3	nan	29.64	2.67	1.55	0.41	0.35	1.17	
9	333	OMZ	15	-99	10	34.7	<3	nan	27.12	2.99			0.12	0.4	BDL
9	1000	DEEP	15	-99	4.4	34.6	11	nan	47.71	3.62	0.87	0.99	0.13	0.43	
9	2002	DEEP	15	-99	2.1	34.6	85	nan	42.26	3.04			0.04	0.13	DNQ
9	3001	DEEP	15.001	-99	1.9	34.7	100	nan	40.86	3.01			0.04	0.13	BDL
10	10	EUPH	15.469	-101.502	29.2	33.6	191	0.11	0.14	0.19			0.74	2.47	BDL
10	64	EUPH	15.469	-101.502	24.6	34.3	158	0.79	2.95	0.76			1.41	4.7	BDL
10	80	EUPH	15.469	-101.502	20.7	34.5	52	0.47	19.84	1.99	4.47	1.86	1	3.33	
10	153	OMZ	15.281	-101.301	13.6	34.8	<3	nan	27.33	2.84			0.78	2.6	BDL
10	190	OMZ	15.281	-101.301	12.8	34.8	<3	nan	28.45	2.63			0.45	1.5	BDL
10	330	OMZ	15.281	-101.301	10.7	34.7	<3	nan	26.03	2.63			0.3	1	BDL
11	10	EUPH	15.901	-103.799	29.1	33.6	185	0.11	0.14	0.2			0.33	1.1	DNQ
11	69	EUPH	15.901	-103.799	23.4	34.4	167	0.44	7.25	1.05			0.6	2	BDL
11	77	EUPH	15.901	-103.799	20.8	34.5	57	0.41	21.19	1.99			0.37	1.23	BDL
11	123	EUPH	15.901	-103.799	14.4	34.8	4	0.18	26.28	2.61			0.25	0.83	BDL
11	160	OMZ	15.541	-103.482	13.1	34.8	<3	nan	26.62	2.73			0.32	1.07	BDL
11	175	OMZ	15.541	-103.482	12.6	34.8	<3	nan	28.33	2.68			0.47	1.57	BDL
11	338	OMZ	15.541	-103.482	10.4	34.7	<3	nan	27.07	2.86			0.33	1.1	BDL
12	10	EUPH	16.315	-106.091	28	33.5	190	0.12	0.14	0.15			1.5	5	BDL
12	92	EUPH	16.315	-106.091	24.5	34.2	168	0.49	0.83	0.48			1.3	4.33	BDL
12	103	EUPH	16.315	-106.091	22	34.4	107	0.28	10.64	1.23			0.87	2.9	BDL
12	147	EUPH	16.315	-106.091	14.3	34.7	4	0.1	24.68	2.8			0.77	2.57	BDL

Suppl. Table 2. *Continued.*

Sta.	Depth (m)	Depth horizon	Lat. (°N)	Long. (°W)	Temp. (°C)	Sal.	[O_2] (µmol kg^{-1})	[Chl-a] (µg L^{-1})	[DIN] (µM)	[SRP] (µM)	NFR (nmol N m^{-2} d^{-1})	NFR prop. error	LOD (nmol N m^{-2} d^{-1})	LOQ (nmol N m^{-2} d^{-1})	Flag
12	150	OMZ	16.19	-106.055	14.4	34.7	4	nan	26.47	nan			0.73	2.43	BDL
12	170	OMZ	16.19	-106.055	13.5	34.8	3	nan	26.45	2.80 (0.01)			0.47	1.57	BDL
12	195	OMZ	16.189	-106.055	12.6	34.8	<3	nan	23.76	2.88			0.33	1.1	BDL
12	330	OMZ	16.189	-106.055	10.5	34.7	<3	nan	25.8	3.03			0.16	0.53	BDL
12	501	DEEP	16.317	-106.092	8	34.6	<3	nan	46.96	3.57			0.06	0.2	BDL
12	1500	DEEP	16.316	-106.092	3	34.6	47	nan	46.12	3.38			0.08	0.27	BDL
12	3001	DEEP	16.317	-106.091	1.7	34.7	112	nan	41.08	2.86			0.05	0.17	BDL
13	10	EUPH	16.778	-108.398	27.7	33.9	191	0.09	0.14	0.17			0.55	1.83	BDL
13	70	EUPH	16.778	-108.398	24.3	34.3	180	0.45	0.44	0.58			1.01	3.37	BDL
13	80	EUPH	16.778	-108.398	20.9	34.4	131	0.32	12.86	1.39			0.42	1.4	BDL
13	145	EUPH	16.778	-108.398	13.5	34.7	4	0.05	23.33	2.71			0.31	1.03	BDL
13	155	OMZ	16.466	-108.238	13.3	34.7	<3	nan	22.83	2.8			0.3	1	BDL
13	187	OMZ	16.466	-108.238	12.1	34.8	<3	nan	23.57	2.74			1.11	3.7	BDL
13	330	OMZ	16.466	-108.238	10	34.6	<3	nan	27.59	2.93			0.2	0.67	BDL
14	10	EUPH	17.204	-110.712	25.9	34.1	196	0.06	0.14	0.22			0.49	1.63	BDL
14	65	EUPH	17.204	-110.712	24	34.3	185	0.28	0.15	0.34			0.9	3	BDL
14	83	EUPH	17.204	-110.712	21.9	34.4	172	0.47	3.16	0.65			0.69	2.3	BDL
14	98	EUPH	17.204	-110.712	18.7	34.3	93	0.35	13.52	1.52			0.98	3.27	BDL
14	185	OMZ	17.124	110.427	12.9	34.8	<3	nan	23.96	2.91			0.37	1.23	BDL
14	215	OMZ	17.124	110.427	12.1	34.8	<3	nan	24.27	2.86			0.45	1.5	BDL
14	330	OMZ	17.124	110.427	10.2	34.6	<3	nan	26.27	3.06			0.3	1	BDL
15	11	EUPH	17.625	-113.001	27	33.7	192	0.07	0.15	0.17			0.67	2.23	BDL
15	68	EUPH	17.625	-113.001	24.5	34.2	198	0.26	0.19	0.28			0.73	2.43	BDL
15	76	EUPH	17.625	-113	23.4	34.3	154	0.48	4.46	0.78			0.72	2.4	BDL
15	101	EUPH	17.625	-113	18.6	34.4	60	0.24	18.1	1.99			0.81	2.7	BDL
15	174	OMZ	17.375	-112.598	13.1	34.7	3	nan	24.8	2.9	1.01	1.34	0.3	1	

Suppl. Table 2. *Continued.*

Sta.	Depth (m)	Depth horizon	Lat. (°N)	Long. (°W)	Temp. (°C)	Sal.	[O_2] (µmol kg^{-1})	[Chl-a] (µg L^{-1})	[DIN] (µM)	[SRP] (µM)	NFR (nmol N m^{-2} d^{-1})	NFR prop. error	LOD (nmol N m^{-2} d^{-1})	LOQ (nmol N m^{-2} d^{-1})	Flag
15	205	OMZ	17.375	-112.598	12.4	34.7	<3	nan	24.63	2.85			0.18	0.6	DNQ
16	10	EUPH	19.508	-111.895	24	34.6	201	0.10	0.25	0.38			0.82	2.73	BDL
16	62	EUPH	19.508	-111.895	21.3	34.4	201	0.21	0.39	0.35			1.56	5.2	BDL
16	73	EUPH	19.508	-111.895	20.4	34.3	180	0.2	3.08	0.63			1.26	4.2	BDL
16	87	EUPH	19.508	-111.895	18.4	34.2	142	0.36	6.84	0.96			0.27	0.9	BDL
16	184	OMZ	19.304	-111.538	13.1	34.8	6	nan	24.49	2.8	9.88	3.85	0.09	0.3	
16	200	OMZ	19.304	-111.538	12.6	34.8	<3	nan	24.44	2.75	35.9	12	0.14	0.47	
16	1000	DEEP	19.506	-111.897	4.3	34.5	12	nan	47.17	3.51	2.37	1.09	0.06	0.2	
16	2000	DEEP	19.506	-111.896	2.2	34.6	81	nan	43.31	3.06	0.35	0.15	0.01	0.03	
16	3001	DEEP	19.507	-111.895	1.7	34.7	110	nan	41.12	2.85	0.36	0.15	0.01	0.03	

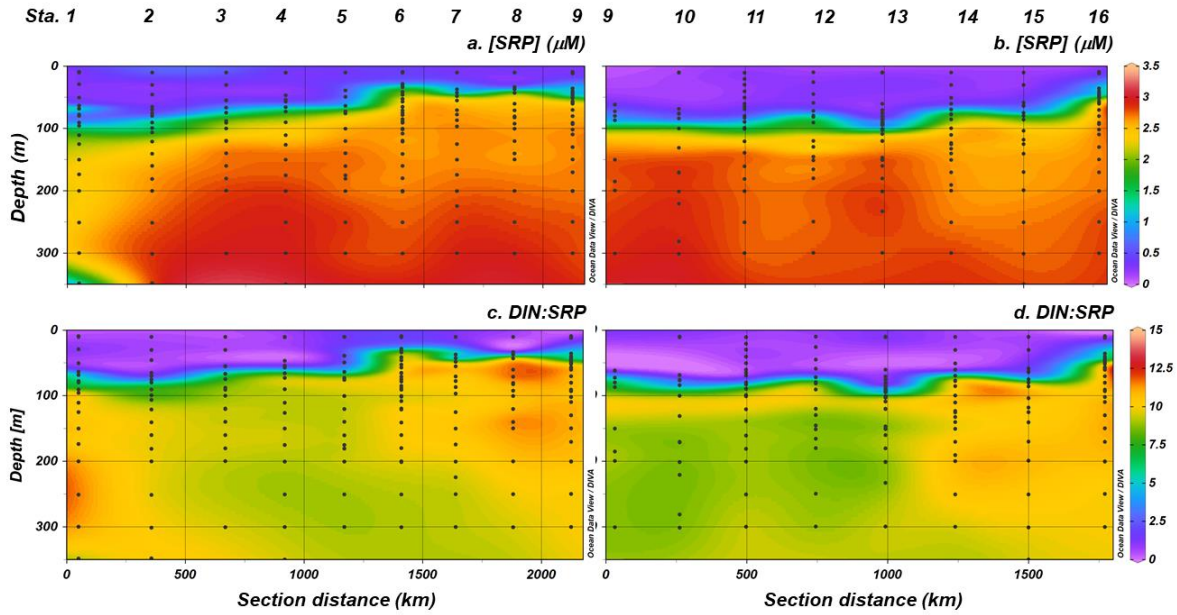

Suppl. Figure 1. Soluble reactive phosphate concentrations ([SRP], a-b) and the ratio of dissolved inorganic nitrogen (defined as the sum of nitrate, nitrite and ammonium) to SRP in upper 350 m of nearshore (left) and offshore (right) transects. Black dots represent discrete sampling points.

APPENDIX B

SUPPLEMENTAL INFORMATION FOR CHAPTER III

Suppl. Text 2. There remains little consensus on how to quantify NFR uncertainty, which is important for any study aiming to assess differences among low rates (e.g., analyze low NFRs with respect to hydrographic characteristics). Simply taking the standard deviation of rates from replicate incubations does not constrain variability in the initial (and independent) ^{15}N-PN enrichment measurement, which may significantly influence whether rates are deemed detectable and the magnitude of rates when ^{15}N enrichment at the final time point is low. An alternative approach for calculating NFR error is to propagate the analytical error associated with the five component measurements in Eqn. 1—source pool (N_2) ^{15}N enrichment, initial and final target pool (PN) ^{15}N enrichment, PN concentration, and time—following traditional statistical approaches in analytical chemistry (Miller and Miller 1988). This value is sometimes applied as a "minimum quantifiable rate" (e.g., Gradoville et al. 2017) or alternate LOD (White et al. 2020). If using the bubble removal technique, analytical error must be propagated first for each incubation individually because source pool (N_2) enrichment can vary among replicate incubations, affecting final target pool (PN). In this study, N_2 enrichment was measured only once for each incubation due to the prohibitive cost of the analysis. Additionally, difficulties with achieving sufficient filter N mass often precluded replication of $A_{PN_{t=0}}$ measurements. In some cases, a mean value was applied (see above). Consequently, I could not accurately assess the analytical error of each measurement individually.

Suppl. Text 3. Non-diazotrophic N cycling processes may theoretically affect $A_{PN_{t=f}}$ (White et al. 2020). I conducted control incubations (no $^{15}N_2$ addition) at three depths at station 1 and several locations around the ETNP ODZ on a cruise in 2017 (Suppl. Table 3). $A_{PN_{t=f}}$ was greater than $A_{PN_{t=0}}$ at five of seven locations with a mean change in enrichment of 0.0009 atom-%. The difference between control incubation $A_{PN_{t=f}}$ and $A_{PN_{t=0}}$ never exceeded the minimum detectable difference in enrichment (3σ, n = 7 12.5 μg standards), meaning that it did not represent a detectable change. However, given the potential significance of small changes in enrichment to the detection/calculation of low NFRs, I advise that future studies attempting to detect low NFRs consider conducting incubation controls more extensively.

Suppl. Table 3. Mean NFRs from ETSP (January 2015). A NFR was only calculated if the minimum detectable A_{PN} difference exceeded 3σ (n = 7 12.5 µg N standards).

Collect. method	Date	Sta.	Lat.	Lon.	Depth (m)	Seafloor depth (m)	Euphotic depth (m)	[O_2] (µmol kg^{-1})	NFR (nmol N L^{-1} d^{-1})	NFR SD	LOD (nmol N L^{-1} d^{-1})	LOQ (nmol N L^{-1} d^{-1})	Rep. bottles (#)	Detectable replicates (#)
CTD	1/1/2015	1	-19.999	-74.001	5.4	4760	90	217	0.00	0.00	1.22	4.05	2	0
CTD	1/1/2015	1	-19.999	-74.001	40	4760	90	201	0.00	0.00	1.83	6.11	3	0
CTD	1/1/2015	1	-19.999	-74.001	50	4760	90	125	0.00	0.00	1.07	3.57	3	0
PPS	1/1/2015	1	-19.999	-74.001	113.4	4760	90	0	0.77	0.00	0.28	0.92	2	2
PPS	1/1/2015	1	-19.999	-74.001	79.7	4760	90	125	0.52	0.08	0.21	0.69	2	2
PPS	1/1/2015	1	-19.999	-74.001	200	4760	90	0	0.00	0.00	0.15	0.50	3	0
PPS	1/1/2015	1	-19.999	-74.001	108	4760	90	0	0.21	0.30	0.32	1.07	3	1
CTD	1/2/2015	2	-19.400	-75.085	5	4941	78	213	0.00	0.00	1.21	4.03	3	0
CTD	1/2/2015	2	-19.400	-75.085	30	4941	78	215	0.00	0.00	3.23	10.77	3	0
CTD	1/2/2015	2	-19.400	-75.085	45	4941	78	60.8	0.00	0.00	0.85	2.82	2	0
CTD	1/2/2015	2	-19.400	-75.085	60	4941	78	8	0.00	0.00	1.43	4.76	3	0
PPS	1/2/2015	2	-19.400	-75.085	300	4941	78	0	0.00	0.00	0.08	0.27	3	0
PPS	1/2/2015	2	-19.400	-75.085	200	4941	78	0	0.06	0.09	0.08	0.26	3	1
PPS	1/2/2015	2	-19.400	-75.085	100	4941	78	0	0.00	0.00	0.16	0.53	3	0
CTD	1/3/2015	3	-18.798	-76.200	10	4911	103	218	0.00	0.00	1.35	4.52	3	0
CTD	1/3/2015	3	-18.798	-76.200	38	4911	103	214	0.00	0.00	2.11	7.02	3	0
CTD	1/3/2015	3	-18.798	-76.200	43	4911	103	208	0.00	0.00	2.36	7.88	3	0
CTD	1/3/2015	3	-18.798	-76.200	80	4911	103	32	0.00	0.00	1.25	4.18	3	0
PPS	1/3/2015	3	-18.798	-76.200	255	4911	103	0	0.00	0.00	0.12	0.41	3	0
PPS	1/3/2015	3	-18.798	-76.200	173	4911	103	0	0.00	0.00	0.34	1.14	3	0
PPS	1/3/2015	3	-18.798	-76.200	110	4911	103	0	0.00	0.00	1.18	3.95	3	0
CTD	1/4/2015	4	-18.500	-77.501	10	4311	120	224	0.00	0.00	1.47	4.90	3	0
CTD	1/4/2015	4	-18.500	-77.501	30	4311	120	225	0.00	0.00	1.45	4.83	3	0

Suppl. Table 3. *Continued.*

Collect. method	Date	Sta.	Lat.	Lon.	Depth (m)	Seafloor depth (m)	Euphotic depth (m)	[O_2] (µmol kg^{-1})	NFR (nmol N L^{-1} d^{-1})	NFR SD	LOD (nmol N L^{-1} d^{-1})	LOQ (nmol N L^{-1} d^{-1})	Rep. bottles (#)	Detectable replicates (#)
CTD	1/4/2015	4	-18.500	-77.501	60	4311	120	220	0.00	0.00	0.87	2.89	2	0
CTD	1/4/2015	4	-18.500	-77.501	75	4311	120	214	0.00	0.00	0.56	1.87	3	0
CTD	1/4/2015	4	-18.500	-77.501	41	4311	120	226	0.00	0.00	2.17	7.24	3	0
CTD	1/4/2015	4	-18.500	-77.501	58	4311	120	216	0.00	0.00	1.50	5.01	3	0
PPS	1/4/2015	4	-18.500	-77.501	275	4311	120	0	0.00	0.00	0.13	0.44	3	0
PPS	1/4/2015	4	-18.500	-77.501	150	4311	120	145	0.00	0.00	0.18	0.61	2	0
PPS	1/4/2015	4	-18.500	-77.501	95	4311	120	214	0.00	0.00	0.18	0.59	3	0
CTD	1/5/2015	5	-17.000	-78.504	10	3333	109	221	0.00	0.00	5.68	18.94	3	0
CTD	1/5/2015	5	-17.000	-78.504	40	3333	109	223	0.00	0.00	4.74	15.79	3	0
CTD	1/5/2015	5	-17.000	-78.504	110	3333	109	190	0.00	0.00	1.24	4.13	1	0
CTD	1/6/2015	6	-15.000	-79.751	6	4593	127	221	0.00	0.00	9.78	32.61	3	0
CTD	1/6/2015	6	-15.000	-79.751	25	4593	127	222	0.00	0.00	10.25	34.17	3	0
CTD	1/6/2015	6	-15.000	-79.751	50	4593	127	199	0.00	0.00	2.84	9.46	3	0
PPS	1/6/2015	6	-15.000	-79.751	300	4593	127	0	0.00	0.00	0.19	0.64	3	0
PPS	1/6/2015	6	-15.000	-79.751	145	4593	127	0	0.00	0.00	0.26	0.88	3	0
CTD	1/7/2015	7	-13.000	-80.801	10	4646	100	214	0.00	0.00	2.48	8.27	3	0
CTD	1/7/2015	7	-13.000	-80.801	28	4646	100	214	0.00	0.00	4.82	16.08	3	0
CTD	1/7/2015	7	-13.000	-80.801	50	4646	100	202	0.00	0.00	3.79	12.62	2	0
PPS	1/7/2015	7	-13.000	-80.801	275	4646	100	0	0.00	0.00	0.17	0.57	3	0
PPS	1/7/2015	7	-13.000	-80.801	160	4646	100	0	0.00	0.00	0.25	0.82	3	0
CTD	1/9/2015	8	-11.500	-81.401	10	4563	99	212	0.00	0.00	1.85	6.17	3	0
CTD	1/9/2015	8	-11.500	-81.401	40	4563	99	205	0.00	0.00	1.59	5.30	3	0
CTD	1/9/2015	8	-11.500	-81.401	75	4563	99	103	0.00	0.00	0.66	2.21	3	0
CTD	1/9/2015	8	-11.500	-81.401	130	4563	99	0	0.00	0.00	0.63	2.11	1	0
PPS	1/9/2015	8	-11.500	-81.401	210	4563	99	0	0.00	0.00	0.15	0.52	3	0
PPS	1/9/2015	8	-11.500	-81.401	120	4563	99	0	0.00	0.00	0.46	1.52	3	0
CTD	1/11/2015	9	-12.000	-84.000	10	4518	102	209	0.00	0.00	2.74	9.13	3	0

Suppl. Table 3. *Continued.*

Collect. method	Date	Sta.	Lat.	Lon.	Depth (m)	Seafloor depth (m)	Euphotic depth (m)	$[O_2]$ (µmol kg^{-1})	NFR (nmol N L^{-1} d^{-1})	NFR SD	LOD (nmol N L^{-1} d^{-1})	LOQ (nmol N L^{-1} d^{-1})	Rep. bottles (#)	Detectable replicates (#)
CTD	1/11/2015	9	-12.000	-84.000	34	4518	102	208	0.00	0.00	4.40	14.66	3	0
CTD	1/11/2015	9	-12.000	-84.000	60	4518	102	208	0.00	0.00	0.95	3.18	3	0
PPS	1/11/2015	9	-12.000	-84.000	193	4518	102	0	0.00	0.00	0.36	1.21	3	0
CTD	1/12/2015	10	-12.000	-81.202	10	4491	98	212	0.97	1.37	2.65	8.84	3	1
CTD	1/12/2015	10	-12.000	-81.202	25	4491	98	211	0.00	0.00	2.08	6.95	3	0
CTD	1/12/2015	10	-12.000	-81.202	50	4491	98	200	0.00	0.00	1.84	6.13	3	0
PPS	1/12/2015	10	-12.000	-81.202	263	4491	98	0	0.00	0.00	0.25	0.82	3	0
PPS	1/12/2015	10	-12.000	-81.202	107	4491	98	0	0.00	0.00	0.27	0.90	3	0
CTD	1/13/2015	11	-13.857	-80.178	10	4606	74	213	0.00	0.00	1.19	3.97	3	0
CTD	1/13/2015	11	-13.857	-80.178	35	4606	74	174	0.00	0.00	3.66	12.21	3	0
CTD	1/13/2015	11	-13.857	-80.178	40	4606	74	166	0.00	0.00	3.71	12.38	3	0
CTD	1/13/2015	11	-13.857	-80.178	80	4606	74	0	0.00	0.00	0.85	2.85	2	0
CTD	1/13/2015	11	-13.866	-80.195	100	4606	74	0	0.00	0.00	0.34	1.13	3	0
CTD	1/13/2015	11	-13.866	-80.195	350	4606	74	0	0.00	0.00	0.12	0.39	1	0
PPS	1/13/2015	11	-13.857	-80.178	220	4606	74	0	0.00	0.00	0.29	0.96	3	0
PPS	1/13/2015	11	-13.857	-80.178	90	4606	74	0	0.00	0.00	1.45	4.83	3	0
CTD	1/14/2015	12	-12.549	-77.601	10	890	104	224	0.00	0.00	4.37	14.57	3	0
CTD	1/14/2015	12	-12.549	-77.601	26	890	104	213	0.00	0.00	4.79	15.96	3	0
CTD	1/14/2015	12	-12.549	-77.601	60	890	104	94	0.00	0.00	1.01	3.38	3	0
CTD	1/14/2015	12	-12.549	-77.601	110	890	104	0	0.00	0.00	0.80	2.66	3	0
CTD	1/14/2015	12	-12.545	-77.600	800	890	104	35	0.00	0.00	0.12	0.40	2	0
PPS	1/14/2015	12	-12.549	-77.601	400	890	104	0	0.00	0.00	0.37	1.25	2	0
PPS	1/14/2015	12	-12.549	-77.601	250	890	104	0	0.00	0.00	0.36	1.19	3	0
PPS	1/14/2015	12	-12.549	-77.601	115	890	104	0	0.00	0.00	1.03	3.43	3	0
CTD	1/15/2015	13	-13.499	-76.600	5	146	65	186	0.00	0.00	34.64	115.45	3	0
CTD	1/15/2015	13	-13.499	-76.600	8	146	65	186	0.00	0.00	27.31	91.02	3	0

Suppl. Table 3. *Continued.*

Collect. method	Date	Sta.	Lat.	Lon.	Depth (m)	Seafloor depth (m)	Euphotic depth (m)	[O_2] (µmol kg^{-1})	NFR (nmol N L^{-1} d^{-1})	NFR SD	LOD (nmol N L^{-1} d^{-1})	LOQ (nmol N L^{-1} d^{-1})	Rep. bottles (#)	Detectable replicates (#)
CTD	1/15/2015	13	-13.499	-76.600	40	146	65	2.5	0.00	0.00	1.30	4.33	2	0
CTD	1/15/2015	13	-13.499	-76.600	80	146	65	1.3	0.00	0.00	1.25	4.18	3	0
CTD	1/15/2015	13	-13.499	-76.600	135	146	65	0	0.00	0.00	2.37	7.89	3	0
PPS	1/15/2015	13	-13.499	-76.600	110	146	65	0	0.00	0.00	0.34	1.12	3	0
PPS	1/15/2015	13	-13.499	-76.600	50	146	65	2.6	0.00	0.00	0.21	0.71	3	0
CTD	1/16/2015	14	-14.200	-77.500	5	4964	28	270	0.00	0.00	33.11	110.37	3	0
CTD	1/16/2015	14	-14.200	-77.500	15	4964	28	270	0.00	0.00	33.60	112.00	3	0
CTD	1/16/2015	14	-14.200	-77.500	20	4964	28	175	0.00	0.00	11.83	39.43	2	0
CTD	1/16/2015	14	-14.200	-77.500	80	4964	28	0	0.00	0.00	1.55	5.15	3	0
CTD	1/16/2015	14	-14.205	-77.509	1500	4964	28	77	0.00	0.00	0.08	0.25	1	0
CTD	1/16/2015	14	-14.205	-77.509	2500	4964	28	122	0.00	0.00	0.06	0.19	1	0
PPS	1/16/2015	14	-14.200	-77.500	300	4964	28	0	0.28	0.07	0.19	0.63	3	3
PPS	1/16/2015	14	-14.200	-77.500	170	4964	28	0	0.11	0.16	0.27	0.88	3	1
PPS	1/16/2015	14	-14.200	-77.500	90	4964	28	0	0.00	0.00	0.41	1.36	3	0
CTD	1/17/2015	15	-15.000	-76.601	5	4580	108	217	0.00	0.00	2.84	9.48	3	0
CTD	1/17/2015	15	-15.000	-76.601	30	4580	108	224	0.00	0.00	2.38	7.93	3	0
CTD	1/17/2015	15	-15.000	-76.601	75	4580	108	185	0.00	0.00	0.73	2.43	1	0
PPS	1/17/2015	15	-15.000	-76.601	190	4580	108	0	0.00	0.00	0.15	0.51	3	0
CTD	1/17/2015	16	-14.509	-76.203	5	146	56	134	0.00	0.00	15.97	53.23	3	0
CTD	1/17/2015	16	-14.509	-76.203	15	146	56	43.9	0.00	0.00	7.72	25.73	3	0
CTD	1/17/2015	16	-14.509	-76.203	40	146	56	1	0.00	0.00	2.50	8.32	3	0
CTD	1/18/2015	16	-14.509	-76.202	2	146	56	74	0.00	0.00	12.21	40.71	3	0
CTD	1/18/2015	16	-14.509	-76.202	8	146	56	110	0.00	0.00	8.38	27.92	3	0
CTD	1/18/2015	16	-14.509	-76.202	20	146	56	24	0.00	0.00	2.91	9.68	3	0
CTD	1/18/2015	16	-14.509	-76.202	45	146	56	0.8	0.00	0.00	4.18	13.95	3	0
PPS	1/18/2015	16	-14.509	-76.202	100	146	56	0	0.00	0.00	1.42	4.73	3	0
PPS	1/18/2015	16	-14.509	-76.202	82	146	56	0	0.00	0.00	1.08	3.60	3	0

Suppl. Table 3. *Continued.*

Collect. method	Date	Sta.	Lat.	Lon.	Depth (m)	Seafloor depth (m)	Euphotic depth (m)	$[O_2]$ (µmol kg^{-1})	NFR (nmol N L^{-1} d^{-1})	NFR SD	LOD (nmol N L^{-1} d^{-1})	LOQ (nmol N L^{-1} d^{-1})	Rep. bottles (#)	Detectable replicates (#)
PPS	1/18/2015	16	-14.509	-76.202	52	146	56	0	0.00	0.00	0.73	2.45	3	0
CTD	1/19/2015	17	-16.201	-76.600	5	3003	70	212	0.00	0.00	1.28	4.25	3	0
CTD	1/19/2015	17	-16.201	-76.600	20	3003	70	151	0.00	0.00	2.05	6.83	3	0
CTD	1/19/2015	17	-16.201	-76.600	35	3003	70	0	0.00	0.00	1.36	4.55	3	0
CTD	1/19/2015	17	-16.201	-76.600	65	3003	70	0	0.00	0.00	0.48	1.60	3	0
PPS	1/19/2015	17	-16.201	-76.600	350	3003	70	0	0.05	0.07	0.12	0.41	3	1
PPS	1/19/2015	17	-16.201	-76.600	250	3003	70	0	0.06	0.08	0.14	0.48	3	1
PPS	1/19/2015	17	-16.201	-76.600	102	3003	70	0	0.00	0.00	0.26	0.87	3	0
CTD	1/20/2015	18	-15.600	-75.335	10	1361	62	240	1.13	1.60	2.64	8.81	3	1
CTD	1/20/2015	18	-15.600	-75.335	25	1361	62	100	0.00	0.00	4.54	15.13	3	0
CTD	1/20/2015	18	-15.600	-75.335	43	1361	62	48	0.00	0.00	0.61	2.04	3	0
CTD	1/20/2015	18	-15.600	-75.335	80	1361	62	0	0.00	0.00	0.49	1.63	3	0
CTD	1/20/2015	18	-15.592	-75.371	500	1361	62	13	0.00	0.00	0.15	0.49	3	0
CTD	1/20/2015	18	-15.592	-75.371	900	1361	62	48	0.08	0.11	0.13	0.44	3	1
CTD	1/20/2015	18	-15.592	-75.371	1300	1361	62	80	0.00	0.00	0.08	0.26	3	0
PPS	1/20/2015	18	-15.600	-75.335	350	1361	62	0	0.23	0.08	0.09	0.30	3	3
PPS	1/20/2015	18	-15.600	-75.335	250	1361	62	0	0.52	0.12	0.16	0.53	3	3
PPS	1/20/2015	18	-15.600	-75.335	100	1361	62	0	0.28	0.04	0.14	0.46	3	3
CTD	1/21/2015	19	-16.299	-73.901	95	680	39	1.7	0.00	0.00	0.30	0.98	3	0
PPS	1/21/2015	19	-16.299	-73.901	240	680	39	0	0.18	0.13	0.17	0.56	3	2
PPS	1/21/2015	19	-16.299	-73.901	125	680	39	0	0.74	0.11	0.40	1.35	3	3

Suppl. Table 4. Results from control incubations conducted within and around the ETSP and ETNP ODZs.

Region	Date	Lat	Lon	Depth (m)	$[O_2]$ (µmol kg^{-1})	$PN_{t=f}$ filter mass (µg N)	$A_{PNt=f.}$ (atom-%)	$PN_{t=0}$ filter mass (µg N)	$A_{PNt=0.}$ (atom-%)	Min. det. ΔA_{PN} (atom-%)	Measured ΔA_{PN} (atom-%)
ETSP	1/1/2015	-19.999	-74.001	5.4	217	20.8	0.374	12.2	0.372	0.007	0.002
ETSP	1/1/2015	-19.999	-74.001	40	201	63.4	0.374	16.9	0.372	0.007	0.002
ETSP	1/1/2015	-19.999	-74.001	50	125	12.0	0.370	10.4	0.369	0.007	0.001
ETNP	4/15/2017	15.902	103.799	338	0	11.0	0.372	11.0	0.370	0.002	0.002
ETNP	4/15/2017	15.902	103.799	175	0	10.6	0.371	10.6	0.370	0.002	0.001
ETNP	4/15/2017	15.902	103.799	160	0	8.6	0.369	8.6	0.370	0.004	-0.001
ETNP	4/26/2017	21.292	108.242	57	188	10.4	0.370	10.4	0.371	0.005	-0.001

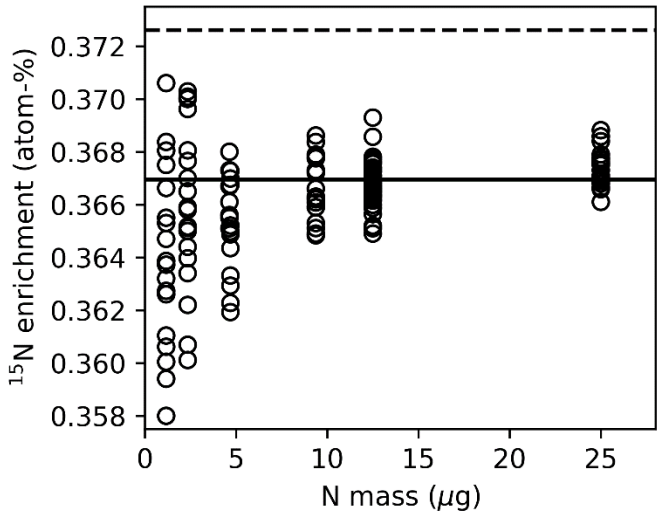

Suppl. Figure 2. Isotope ratio mass spectrometer linearity at low mass. Open dots represent low mass (≤ 25 µg N) ammonium sulfate standards from all standard curves (run daily) measured during sample analysis. Solid and dashed lines represent, respectively, the standard enrichment (0.367 atom-%) and the standard enrichment plus the mean detectable difference ($A_{PNt=f} - A_{PNt=0}$) i.e., the mean LOD (the standard deviation of all 12.5 µg standards analyzed alongside samples multiplied by 3).

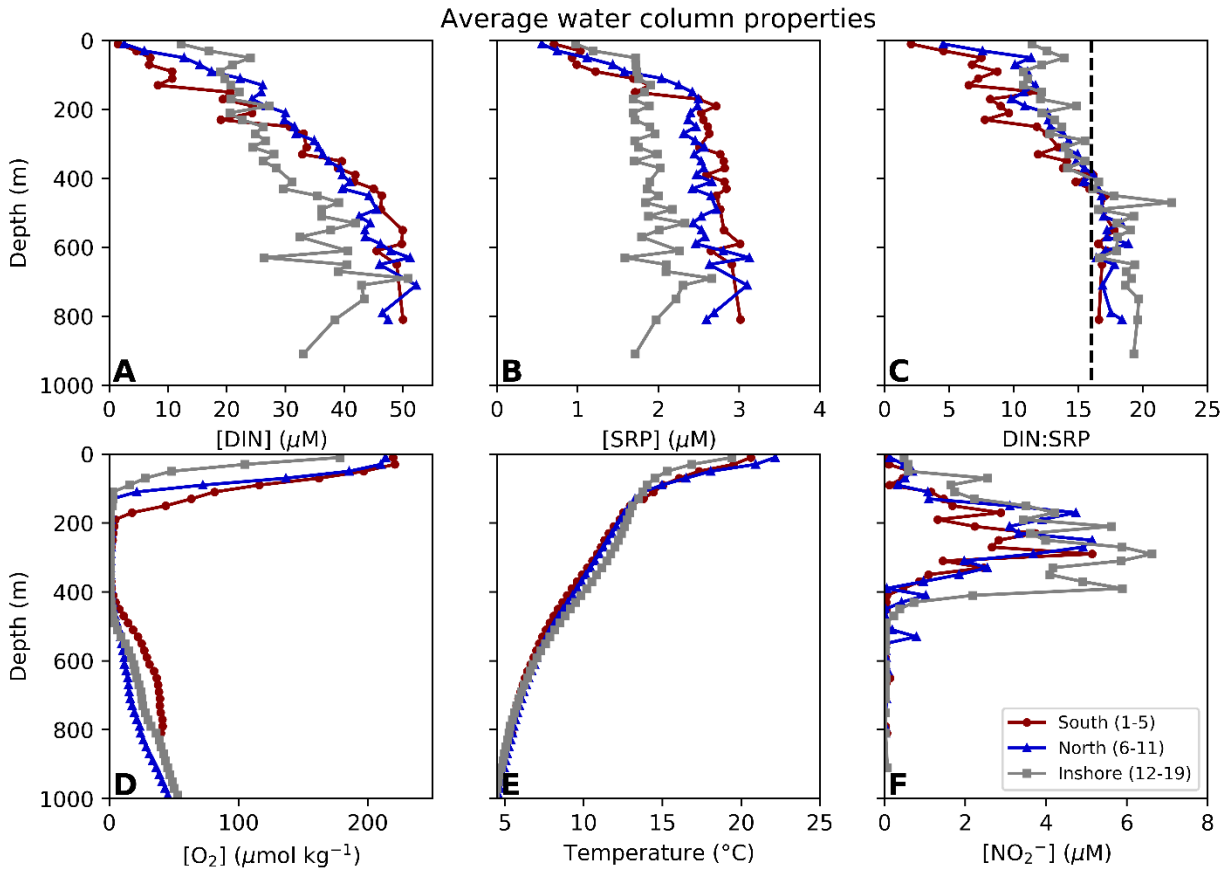

Suppl. Figure 3. Profiles of DIN concentration (A), SRP concentration (B), DIN:SRP (C), O_2 concentration (D), temperature (E), and NO_2^- concentration (F) averaged at 20 m intervals for southern (1-5), northern (6-11) and inshore (12-19) stations. The black dashed line in panel C marks the canonical Redfield ratio (16:1).

APPENDIX C

SUPPLEMENTAL INFORMATION FOR CHAPTER IV

Suppl. Table 5. Quantitative PCR primer and probe sequences used in this study.

Target organism	Target gene	GenBank accession number	Forward primer (5' to 3')	Reverse primer (5' to 3')	Probe (5' to 3')	Probe 5' dye	Probe 3' quencher	Refs.
Tricho. spp.	nifH	AO5202A44	CAGGTTTCGGTGGCATTAAG	CAACGTCACCTAGTACGTCA	TGGTGTAGGTTGCGCTGGCC	FAM	TAMRA	This study
Richelia intracellularis associated with Rhizosolenia	nifH	AY706888	AGAGGTGCAGTTGAAGACTT	TACCACGACCCGCACAACC	TCCGGTGGTCCTGAGCCTGGTGT	FAM	TAMRA	This study; Church et al. 2005b
UCYN-A1	nifH	AF059642	AGCTATAACAACGTTTTATGCGTTGA	ACCACGACCAGCACATCCA	TCTGGTGGTCCTGAGCCTGGA	FAM	TAMRA	Church et al. 2005a
UCYN-A2/A3/A4	nifH	KF806604	GGTTACAACAACGTTTTATGTGTTGA	ACCACGACCAGCACATCCA	TCTGGTGGTCCTGAGCCCGGA	FAM	TAMRA	Thompson et al. 2014
B. bigelowii	18S rRNA	KF771248	GGTTTTGCCGGTCTGCCGTT	ATCCGTCTCCGACACCCACTC	CTGGTGCGAGCGTCCTTCCT	FAM	TAMRA	Thompson et al. 2014

Suppl. Table 6. Mean performance and optimized hyperparameters for each model based on K-fold (n = 9) cross-validation.

Model	Mean R^{2d}	Maximum depth	Total estimators
1[a]	0.854 ±0.083	17	41
2[b]	0.853 ±0.152	11	29
3[c]	0.848 ±0.046	19	19

[a]Model 1 predictors: depth, seafloor depth, temperature, salinity, chl-a concentration
[b]Model 2 predictors: depth, seafloor depth, temperature, salinity, chl-a concentration, N+N concentration, SRP concentration
[c]Model 3 predictors: seafloor depth, temperature, chl-a concentration
[d] Error = ±1 standard deviation

Suppl. Table 7. Summary of N_2 fixation rates and corresponding hydrographic parameters on R/V Hugh R. Sharp cruise (northwestern Atlantic continental shelf).

Sta.	Lat.	Lon.	Depth (m)	Seafloor Depth (m)	Temp. (°C)	Sal.	[Chl-a] (µg L^{-1})	[N+N] (µM)	[SRP] (µM)	SUR (d^{-1})	SUR SD	NFR (nmol N L^{-1} d^{-1})	NFR SD	LOD	Flag
1	37.665	-73.995	1	1210	26.8	33.83	0.59	0.38	0.04	0.0102	0.0025	5.55	1.39	0.44	
1	37.665	-73.996	35	1210	15.0	35.07	2.36	1.90	0.21					1.09	BDL
1	37.667	-73.998	49	1210	13.7	35.22	1.12	nan	nan					0.60	BDL
3	37.660	-74.782	2	47	26.9	31.79	0.57	0.43	0.65					12.63	BDL
3	37.663	-74.783	9	47	26.9	31.79	0.64	nan	nan					6.81	BDL
3	37.661	-74.782	20	47	14.0	32.74	2.78	0.21	0.42					6.79	BDL
3	37.661	-74.782	24	47	11.3	32.89	6.75	0.27	0.26					2.79	BDL
5	37.668	-75.544	2	11	26.4	31.80	2.21	0.23	0.16	0.0005	0.0007	1.25	1.76	2.91	
5	37.668	-75.544	7	11	26.2	31.83	2.75	0.31	0.18					3.71	BDL
5	37.668	-75.545	9	11	25.1	31.84	5.93	0.21	0.34					3.86	BDL
6	36.929	-75.880	2	11	26.3	31.52	1.27	0.09	0.04					3.98	BDL
6	36.929	-75.880	7	11	24.1	32.04	2.88	0.18	0.07	0.0010	0.0014	3.03	4.29	5.85	
6	36.929	-75.881	10	11	23.8	32.08	3.32	0.21	0.10					6.63	BDL
8	36.938	-74.702	1	84	26.9	32.14	0.69	0.16	0.04	0.0018	0.0014	2.73	2.10	1.76	
8	36.938	-74.702	15	84	17.6	32.85	1.55	0.19	0.04	0.0014	0.0001	4.22	0.24	3.02	
8	36.938	-74.702	26	84	11.7	33.29	3.87	0.68	0.12					4.85	BDL
10	36.948	-73.797	2	298	29.0	35.97	0.89	0.22	0.04	0.0187	0.0047	18.28	4.54	0.62	
10	36.947	-73.797	33	298	26.8	36.40	1.97	0.50	0.04	0.0005	0.0003	0.54	0.40	0.65	
10	36.929	-73.808	215	298	11.9	35.47	0.55	25.04	1.40	0.0008	0.0002	0.13	0.03	0.08	
11	36.364	-73.732	2	1015	29.5	36.36	0.48	0.22	0.04	0.0111	0.0031	7.14	2.01	0.43	
11	36.358	-73.737	84	1015	26.0	36.65	1.19	0.36	0.04	0.0029	0.0016	2.11	1.17	0.47	
11	36.362	-73.733	179	1015	17.6	36.37	0.49	10.65	0.51	nan	nan	nan	nan	0.87	

Suppl. Table 7. *Continued.*

Sta.	Lat.	Lon.	Depth (m)	Seafloor Depth (m)	Temp. (°C)	Sal.	[Chl-a] (µg L^{-1})	[N+N] (µM)	[SRP] (µM)	SUR (d^{-1})	SUR SD	NFR (nmol N L^{-1} d^{-1})	NFR SD	LOD	Flag
12	36.346	-74.205	2	2400	28.7	35.38	0.57	0.07	0.04	0.1010	0.0645	157.56	100.80	0.82	
12	36.343	-74.206	16	2400	28.3	35.68	0.77	0.07	0.04	0.2180	0.0174	423.38	33.72	1.01	
12	36.344	-74.206	38	2400	25.9	36.32	2.29	11.06	0.71	0.1470	0.0000	245.75	0.00	0.87	
13	36.335	-74.975	2	40	26.9	31.45	0.71	0.07	0.04	0.0446	0.0086	54.02	10.44	1.66	
13	36.335	-74.974	10	40	26.5	31.55	0.73	nan	nan	0.2900	0.0593	318.69	65.15	1.51	
13	36.335	-74.974	26	40	12.2	33.37	2.56	0.07	0.36	0.0269	0.0160	56.32	33.43	2.83	
13	36.335	-74.973	31	40	12.2	33.40	2.03	0.07	0.39	0.0271	0.0044	38.99	6.28	1.93	
14	36.332	-75.643	2	23	26.7	30.61	1.38	0.07	0.09	0.1410	0.0300	269.28	57.26	2.86	
14	36.332	-75.643	8	23	19.2	32.73	1.45	0.07	0.37	0.1750	0.0226	400.37	51.57	3.42	
14	36.332	-75.643	19	23	14.8	33.04	2.35	0.07	0.46	0.1880	0.0024	619.29	7.89	4.89	
15	35.665	-75.368	1	25	27.0	28.60	1.52	0.07	0.12	0.0809	0.0063	183.93	14.26	2.91	
15	35.665	-75.368	7	25	25.6	30.27	1.29	0.07	0.21	0.1090	0.0296	217.50	58.77	2.55	
15	35.665	-75.368	14	25	18.8	33.08	1.59	0.07	0.40	0.1380	0.0861	233.42	145.59	2.15	
15	35.665	-75.368	24	25	17.4	33.20	4.25	0.07	0.54	0.0326	0.0190	173.57	101.14	6.75	
17	35.706	-74.339	2	2368	30.2	36.37	0.38	0.07	0.04	0.0528	0.0000	54.42	0.00	1.52	
17	35.705	-74.340	50	2368	29.1	36.36	0.53	0.07	0.04	0.5650	0.0523	568.15	52.54	1.64	
17	35.702	-74.341	102	2368	25.9	36.70	1.21	0.07	0.04	0.5170	0.1780	258.19	88.75	0.46	
19	35.662	-73.368	2	297	29.4	36.31	0.41	0.07	0.04	0.0888	0.0313	50.78	17.86	0.52	
19	35.662	-73.369	69	297	28.4	36.35	0.65	0.07	0.04	0.0274	0.0045	13.93	2.27	0.49	
19	35.663	-73.368	104	297	26.6	36.55	1.06	0.07	0.04	0.0156	0.0075	7.38	3.55	0.45	
20	35.037	-73.920	3	3450	29.7	36.31	0.42	0.07	0.04	0.0282	0.0148	19.43	10.21	0.20	
20	35.035	-73.919	66	3450	27.6	36.36	0.59	0.07	0.04	0.0137	0.0022	8.98	1.44	0.16	
20	35.034	-73.919	94	3450	26.3	36.57	1.12	0.07	0.04	0.0212	0.0064	13.07	3.96	0.20	
20	35.042	-73.921	209	3450	21.5	36.85	0.44	5.16	0.22	0.0059	0.0014	1.77	0.44	0.38	
20	35.041	-73.921	332	3450	19.2	36.62	0.44	7.64	0.35	0.0043	0.0004	0.81	0.07	0.47	

Suppl. Table 7. *Continued.*

Sta.	Lat.	Lon.	Depth (m)	Seafloor Depth (m)	Temp. (°C)	Sal.	[Chl-a] (µg L^{-1})	[N+N] (µM)	[SRP] (µM)	SUR (d^{-1})	SUR SD	NFR (nmol N L^{-1} d^{-1})	NFR SD	LOD	Flag
22	35.053	-74.847	2	219	30.2	36.38	0.39	0.07	0.04	0.0665	0.0237	28.37	10.12	0.17	
22	35.054	-74.845	30	219	29.8	36.38	0.44	0.07	0.04	0.0242	0.0073	10.56	3.17	0.22	
22	35.047	-74.853	100	219	26.3	36.63	1.31	0.45	0.04	0.0360	0.0181	17.08	8.59	0.19	
22	35.055	-74.844	189	219	20.6	36.79	0.48	6.99	0.32	0.0031	0.0001	0.62	0.03	0.10	
24	35.046	-75.679	2	26	28.6	35.69	0.66	0.07	0.04	0.0084	0.0006	9.34	0.62	1.31	
24	35.046	-75.680	15	26	26.2	36.36	0.76	0.07	0.04	0.0171	0.0055	24.47	7.90	0.29	
24	35.046	-75.681	23	26	25.6	36.37	1.10	0.07	0.04	0.0090	0.0013	16.75	2.39	0.26	
25	33.331	-78.583	2	22	28.7	35.92	0.74	nan	nan	0.0156	0.0032	24.89	5.06	0.28	
25	33.332	-78.584	18	22	25.2	36.36	6.73	nan	nan	0.0066	0.0030	22.03	9.98	0.55	
27	33.340	-77.526	2	25	29.4	35.92	0.49	0.09	0.04	0.0133	0.0027	12.47	2.53	0.14	
27	33.336	-77.529	16	25	28.2	36.08	0.74	nan	0.07	0.0093	0.0040	12.73	5.44	0.20	
27	33.336	-77.529	24	25	23.0	36.42	11.46	0.07	0.04	0.0028	0.0009	9.73	3.32	0.50	
28	33.348	-77.011	2	202	30.3	36.39	0.47	0.25	0.04	0.0419	0.0090	27.99	6.02	0.63	
28	33.345	-77.015	83	202	25.6	36.64	1.86	1.05	0.04	0.0033	0.0011	2.34	0.75	0.56	
28	33.343	-77.020	150	202	14.8	35.94	0.53	16.14	0.98	0.0022	0.0017	0.77	0.59	0.29	
29	33.344	-76.512	1	450	30.1	36.35	0.41	0.07	0.04	0.0652	0.0570	29.90	26.16	0.33	
29	33.341	-76.516	98	450	26.7	36.48	1.33	0.45	0.04	0.0099	0.0030	4.80	1.46	0.40	
29	33.341	-76.515	149	450	23.7	36.93	0.58	3.78	0.13	0.0065	0.0026	3.61	1.42	0.45	
30	33.346	-76.108	2	1340	29.7	36.38	0.42	0.07	0.04	0.0205	0.0035	8.13	1.39	0.50	
30	33.346	-76.105	51	1340	28.9	36.38	0.49	0.07	0.04	0.0149	0.0013	6.02	0.52	0.32	
30	33.344	-76.109	121	1340	26.1	36.65	1.08	0.87	0.04	0.0130	0.0044	5.61	1.88	0.34	
30	33.350	-76.093	179	1340	21.2	36.70	0.46	1.61	0.04	0.0019	0.0000	0.44	0.00	0.20	
30	33.351	-76.083	398	1340	17.3	36.39	0.52	nan	nan	nan	nan	nan	nan	0.20	
30	33.348	-76.086	717	1340	8.6	35.05	0.60	27.63	2.01	nan	nan	nan	nan	0.24	
31	33.336	-75.615	3	3150	29.9	36.38	0.39	0.07	0.04	0.0112	0.0048	3.16	1.34	0.20	
31	33.337	-75.616	92	3150	25.4	36.68	1.30	0.30	0.04	0.0049	0.0003	1.99	0.13	0.33	

Suppl. Table 7. *Continued.*

Sta.	Lat.	Lon.	Depth (m)	Seafloor Depth (m)	Temp. (°C)	Sal.	[Chl-a] (µg L^{-1})	[N+N] (µM)	[SRP] (µM)	SUR (d^{-1})	SUR SD	NFR (nmol N L^{-1} d^{-1})	NFR SD	LOD	Flag
33	34.011	-75.327	2	3135	29.7	36.30	0.40	0.07	0.04	0.0140	0.0052	3.84	1.42	0.36	
33	34.004	-75.329	103	3135	26.6	36.51	1.42	nan	nan	nan	nan	nan	nan	0.35	
34	34.027	-75.826	3	733	30.2	36.39	0.41	0.07	0.04	0.0566	0.0133	19.91	4.68	0.31	
34	34.025	-75.827	115	733	26.5	36.65	1.29	nan	nan	0.0099	0.0018	3.29	0.61	0.27	
34	34.029	-75.824	299	733	14.6	35.88	1.51	19.52	1.15	0.0022	0.0011	0.78	0.37	0.33	
35	34.007	-76.243	2	192	29.8	35.82	0.54	0.07	0.04	0.0163	0.0048	12.30	3.61	0.81	
35	34.009	-76.241	54	192	24.6	36.30	3.23	0.09	0.04	0.0007	0.0000	0.87	0.01	0.80	
36	34.006	-77.367	2	26	29.9	35.86	0.69	0.07	0.04	0.0116	0.0010	11.71	1.00	0.90	
36	34.006	-77.368	18	26	29.0	35.77	0.92	0.07	0.04	0.0087	0.0022	8.42	2.18	0.83	
36	34.006	-77.367	23	26	25.9	36.44	2.23	0.07	0.04	0.0089	0.0023	12.45	3.21	1.19	
37	34.539	-76.397	2	20	29.5	35.92	0.55	0.07	0.04	nan	nan	nan	nan	1.07	
37	34.538	-76.398	9	20	28.3	36.07	0.69	0.07	0.04	0.0130	0.0049	12.85	4.85	0.82	
37	34.539	-76.398	18	20	22.4	36.38	10.30	0.24	0.04	0.0067	0.0013	17.69	3.46	2.17	
39	34.577	-75.456	119	1870	25.8	36.75	1.46	0.39	0.04	0.0043	0.0003	3.20	0.20	0.26	
39	34.569	-75.458	223	1870	20.1	36.72	0.47	7.83	0.34	0.0062	0.0017	1.50	0.42	0.10	
39	34.599	-75.452	301	1870	13.9	35.79	0.95	nan	nan	0.0008	0.0002	0.27	0.07	0.12	
39	34.607	-75.452	473	1870	8.5	35.07	0.60	28.22	1.78	0.0012	0.0004	0.41	0.15	0.17	
41	34.536	-74.544	2	3000	30.0	36.40	0.41	0.07	0.04	0.0239	0.0076	9.36	2.98	0.41	
41	34.535	-74.543	81	3000	26.1	36.52	0.84	0.07	0.04	0.0092	0.0003	4.41	0.16	0.23	
41	34.532	-74.541	106	3000	23.7	36.71	1.12	nan	nan	0.0047	0.0005	2.35	0.23	0.23	

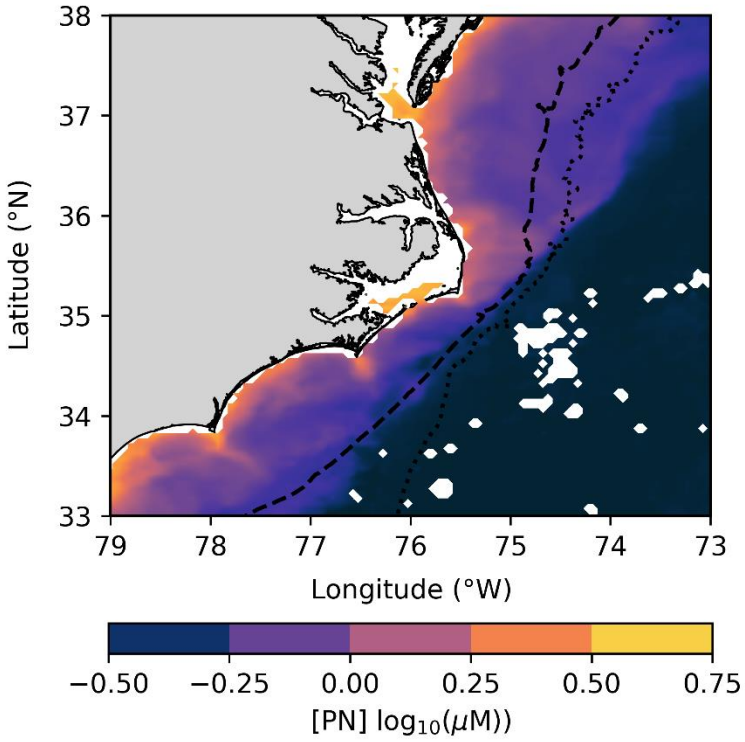

Suppl. Figure 4. PN concentration predicted across the study region from MODIS particulate carbon concentration (NASA Goddard Space Flight Center 2018 Reprocessing), assuming a linear relationship derived from direct measurements ([PN] = 0.0795*[PC] + 0.118, df = 253, R^2 = 0.859, $p < 10^{-6}$).

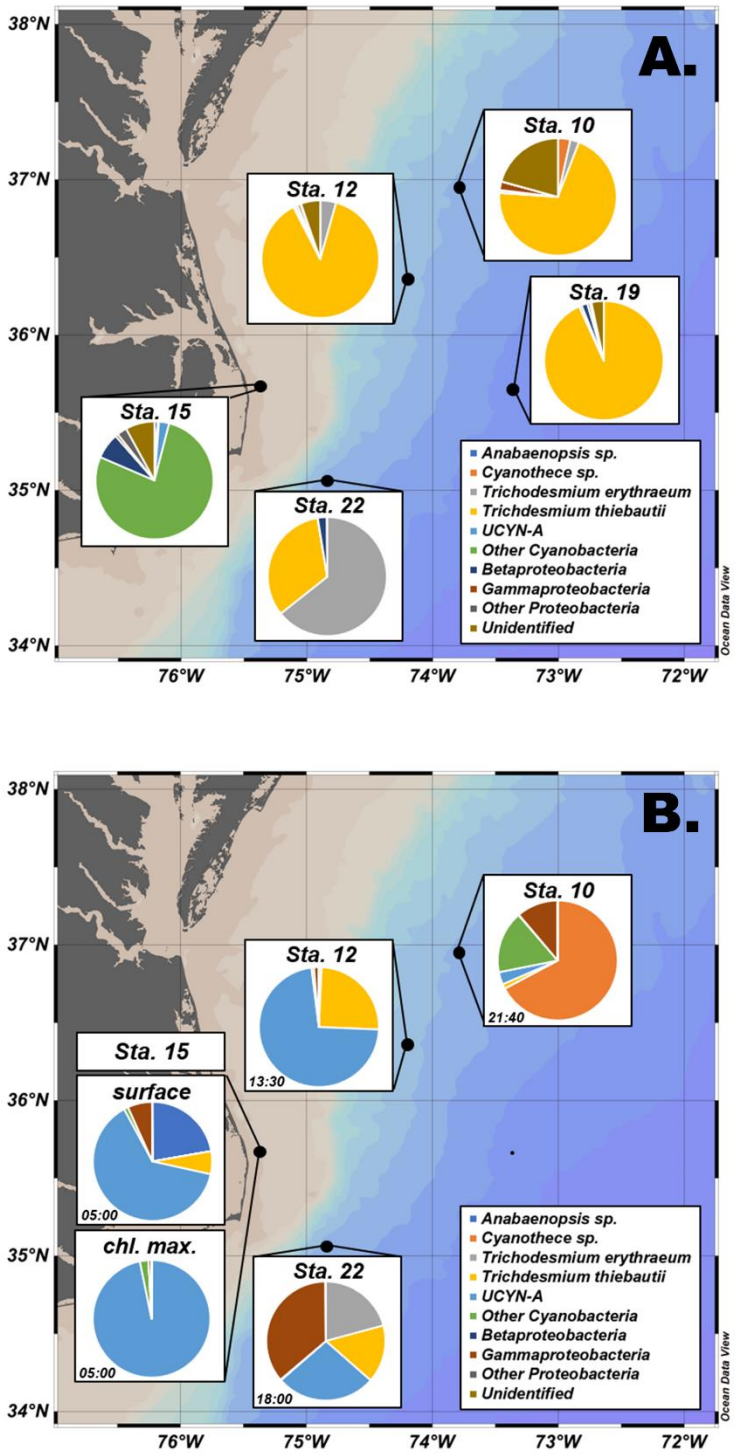

Suppl. Figure 5. *nifH* relative abundance (A) and expression (B) based on amplicon sequencing (Ilumina MiSeq platform) using nested degenerate primers (Zehr and Turner 2001).

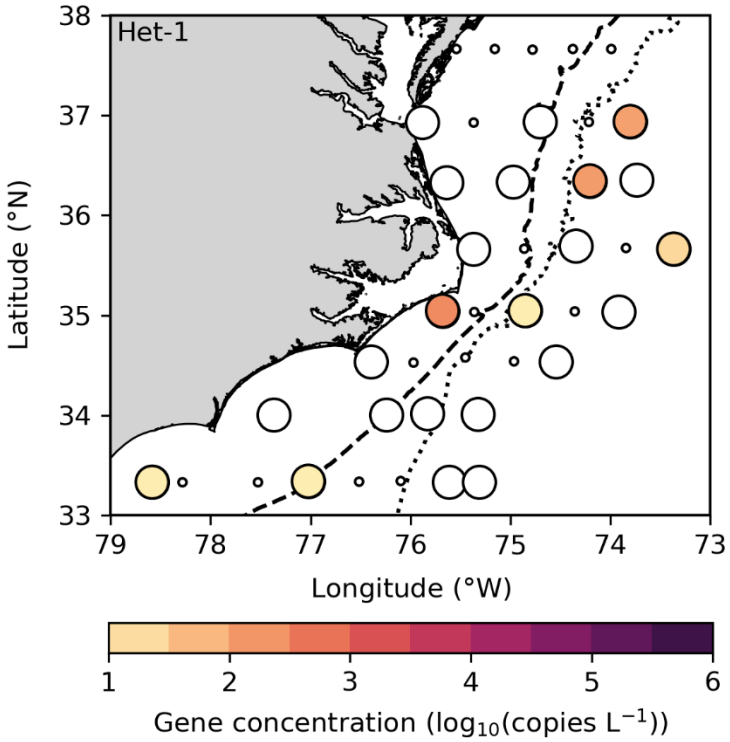

Suppl. Figure 6. Abundance of *nifH* genes associated with the *Rhizosolenia* sp. symbiont *Richelia intracellularis* (Het-1). Large open circles indicate stations where sequences were not detected.

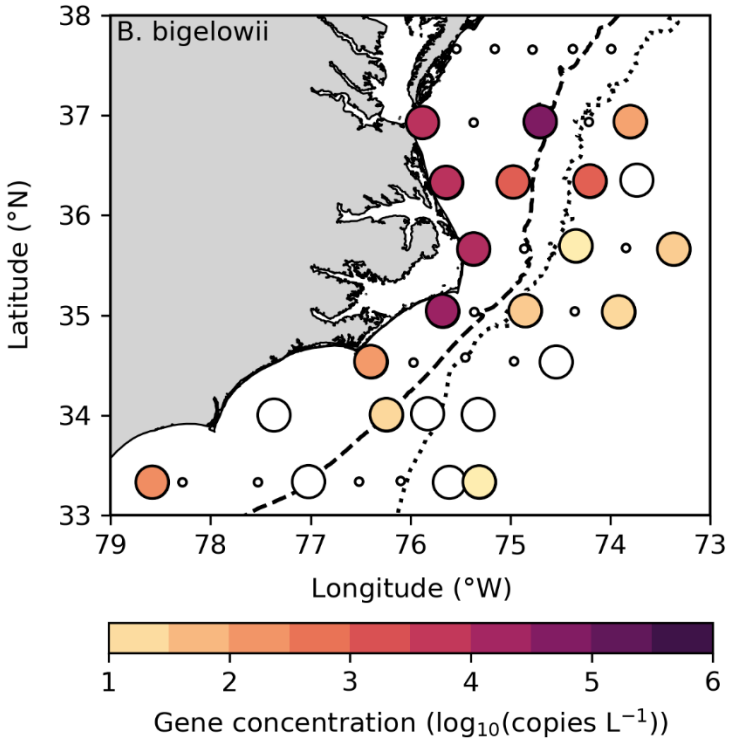

Suppl. Figure 7. Abundance of 18S rRNA genes diagnostic of a potential UCYN-A host, *Braarudosphaera bigelowii*. Large open circles indicate stations where sequences were not detected.

VITA

Corday R. Selden
PhD Candidate
Dept. of Ocean and Earth Sciences
Old Dominion University
4600 Elkhorn Ave.
Norfolk VA 23529-0276

EDUCATION

PhD, Oceanography, Old Dominion University, 2017 – 2020
MS, Ocean and Earth Sciences, Old Dominion University, 2015 – 2017
BS, Biology (minor in Chemistry), Eckerd College, 2011 – 2014

PUBLICATIONS

Selden, C., Mulholland, M., Bernhardt, P., Widner, B., Jayakumar, A. N_2 fixation in the Eastern Tropical South Pacific oxygen deficient zone: Implications for the range of marine diazotrophs. Limnol. Oceanogr., submitted.

Oliver, H., Zhang, W., Smith, W., Alatalo, P., Chappell, P.D., Hirzel, A., **Selden, C.**, Sosik, H., Stanley, R., Zhu, Y., McGillicuddy, D. Extraordinary diatom blooms driven by Eastern boundary current instability. PNAS, in review.

Selden, C., Chappell, P.D., Clayton, S., Macías-Tapia, A., Bernhardt, P., Mulholland, M. A coastal N_2 fixation hotspot at the Cape Hatteras front: Elucidating spatial heterogeneity in diazotroph activity via supervised machine learning. Limnol. Oceanogr., in review.

White, A., Granger, J., **Selden, C.**, Gradoville, M.R., Potts, L., Bourbonnais, A., Fulweiler, R.W., Knapp, A., Mohr, W., Moisander, P., Tobias, C., Wilson, S., Benavides, M., Bonnet, S., Mulholland, M., Chang, B. 2020. A critical review of the $^{15}N_2$ tracer method to measure diazotrophic production in pelagic ecosystems. Limnol. Oceanogr.: Methods. DOI: 10.1002/lom3/10353

Selden, C., Mulholland, M., Bernhardt, P., Widner, B., Macías-Tapia, A., Ji, Q., Jayakumar, A. 2019. Dinitrogen fixation across physico-chemical gradients of the Eastern Tropical North Pacific oxygen deficient zone. Global Biogeoch. Cycles 33. DOI: 10.1029/2019GB006242

Mulholland, M., Bernhardt, P., Widner, B., **Selden, C.**, Chappell, D., Mannino, A., Hyde, K., Clayton, S. 2019. High rates of N_2 fixation in temperate, Western North Atlantic coastal waters expands the realm of marine N_2 fixation. Global Biogeochem. Cycles 33. DOI: 10.1029/2018GB006130

PUBLICATIONS IN PREPARATION

Selden, C., Chappell, P.D., Macías-Tapia, A., Clayton, S., Bernhardt, P., Zhang, W., McGwellicuddy, D., Mulholland, M. Frontal zone mixing enhances diazotroph activity at the New England shelf-break. In prep., for submission to PNAS.